Erosion Characteristics and Optical Properties of State-of-the-Art, Erosion-Resistant Coatings on Infrared Windows: Boron Phosphide, Gallium Phosphide, and Zinc Sulfide on Multispectral Zinc Sulfide

by
Daniel C. Harris
Research and Technology Division

MAY 1996

NAVAL AIR WARFARE CENTER WEAPONS DIVISION
CHINA LAKE, CA 93555-6001

DISCLAIMER NOTICE

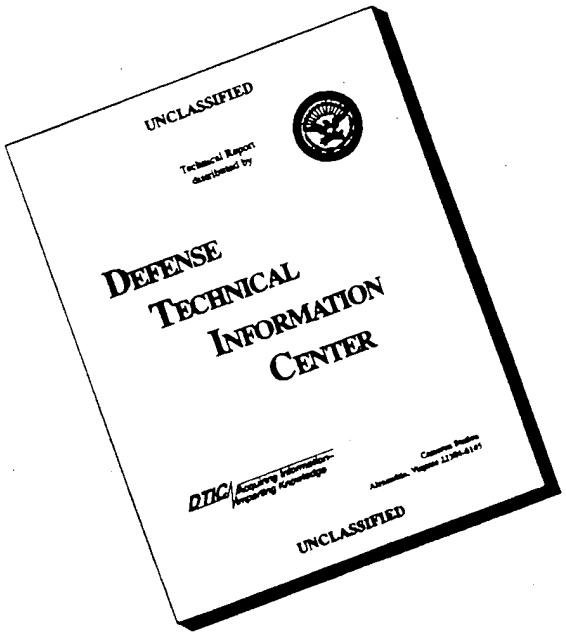

THIS DOCUMENT IS BEST QUALITY AVAILABLE. THE COPY FURNISHED TO DTIC CONTAINED A SIGNIFICANT NUMBER OF PAGES WHICH DO NOT REPRODUCE LEGIBLY.

Naval Air Warfare Center Weapons Division

FOREWORD

This report summarizes sand and rain erosion studies and infrared transmission and emission measurements for infrared optical windows with state-of-the-art erosion-resistant coatings. Windows of multispectral zinc sulfide were coated with boron phosphide, gallium phosphide, or compressively stressed zinc sulfide. For comparison, hot pressed magnesium fluoride, bulk gallium phosphide, and silicon were also studied.

Work was carried out in the Chemistry and Materials Branch of the Research and Technology Division with support from the Office of Naval Research. The report was reviewed for technical accuracy by Linda Johnson and Mark Moran.

Approved by
R. L. DERR, *Head*
Research & Technology Division
1 May 1996

Under authority of
D. B. McKINNEY
RAdm., U.S. Navy
Commander

Released for publication by
S. HAALAND
Director for Research and Engineering

NAWCWPNS Technical Publication 8292

Published by ..... Scientific and Technical Documentation
Collation ..... Cover, 32 leaves
First printing ..... 125 copies

REPORT DOCUMENTATION PAGE

Form Approved
OMB No. 0704-0188

1. AGENCY USE ONLY *(Leave blank)*	2. REPORT DATE	3. REPORT TYPE AND DATES COVERED
	May 1996	Summary Oct 1994-Aug 1995

4. TITLE AND SUBTITLE
Erosion Characteristics and Optical Properties of State-of-the-Art, Erosion-Resistant Coatings on Infrared Windows: Boron Phosphide, Gallium Phosphide, and Zinc Sulfide on Multispectral Zinc Sulfide (U)

5. FUNDING NUMBERS
PE 62234N
Work Unit RS34W54

6. AUTHOR(S)
Daniel C. Harris

7. PERFORMING ORGANIZATION NAME(S) AND ADDRESS(ES)
Naval Air Warfare Center Weapons Division
China Lake, CA 93555-6001

8. PERFORMING ORGANIZATION REPORT NUMBER
NAWCWPNS TP 8292

9. SPONSORING/MONITORING AGENCY NAME(S) AND ADDRESS(ES)
Office of Naval Research
800 North Quincy
Arlington, VA 22207-5660

10. SPONSORING/MONITORING AGENCY REPORT NUMBER

11. SUPPLEMENTARY NOTES

12A. DISTRIBUTION/AVAILABILITY STATEMENT
A Statement; public release; distribution unlimited.

12B. DISTRIBUTION CODE

13. ABSTRACT *(Maximum 200 words)*

(U) Optical properties and rain and sand erosion resistance of the following infrared window materials were measured: (1) Barr & Stroud boron phosphide coating on multispectral zinc sulfide, (2) Barr & Stroud gallium phosphide coating (with a thin outer layer of boron phosphide) on multispectral zinc sulfide, (3) Raytheon zinc sulfide coating on multispectral zinc sulfide, (4) Texas Instruments bulk gallium phosphide, (5) polycrystalline magnesium fluoride, and (6) single-crystal silicon. ZnS-coated ZnS has low optical emission for operation at 500°C in both the 3-5 and 8-10 μm regions. Bulk GaP and bare MgF_2 have low emission only in the 3-5 μm region. BP/ZnS and BP/GaP/ZnS have prohibitive optical emission at 500°C in both the 3-5 and 8-10 μm regions. In whirling arm rain erosion experiments, none of the coated materials was as durable as bare MgF_2. BP/ZnS is more durable than ZnS/ZnS, but subsurface damage preceded damage to the BP coating in BP/ZnS. GaP fractured easily on orthogonal crystal planes upon raindrop impact. In sand erosion experiments, BP and BP/GaP/ZnS were best and MgF_2 was second most durable.

14. SUBJECT TERMS
Erosion, Rain Erosion, Sand Erosion, Optical Coating, Coatings, Boron Phosphide, Gallium Phosphide, Zinc Sulfide, Magnesium Fluoride, Infrared Window, Optical Materials, Infrared Emittance

15. NUMBER OF PAGES
62

16. PRICE CODE

17. SECURITY CLASSIFICATION OF REPORT	18. SECURITY CLASSIFICATION OF THIS PAGE	19. SECURITY CLASSIFICATION OF ABSTRACT	20. LIMITATION OF ABSTRACT
UNCLASSIFIED	UNCLASSIFIED	UNCLASSIFIED	UL

CONTENTS

ACKNOWLEDGMENTS

We are grateful to the following people who supplied test materials: Andy Sijan and Des Gibson of Barr & Stroud (Glasgow, Scotland), Lee Goldman and Randy Tustison of Raytheon (Lexington, Massachusetts), and Paul Klocek of Texas Instruments (Dallas, Texas). Optical measurements were made by Alan Harker at Rockwell Science Center (Thousand Oaks, California) and by Phil Archibald, Mel Nadler and Karl Klemm at China Lake. Rain erosion experiments were carried out at the Wright Laboratory/University of Dayton Research Institute facility (Dayton, Ohio) by John Detrio, Dale Grant, and John Buhrmaster with support from Bob Ondercin of the Air Force Materials Laboratory. Sand erosion experiments were carried out at Wright Laboratory under the supervision of Richard Smith. Additional microscopy was conducted by Karl Klemm at China Lake.

EXECUTIVE SUMMARY

Optical properties and rain and sand erosion resistance of the following infrared window materials were measured: (1) Barr & Stroud boron phosphide (BP) coating on multispectral zinc sulfide (ms-ZnS), (2) Barr & Stroud gallium phosphide (GaP) coating (with a thin outer layer of BP) on ms-ZnS, (3) Raytheon zinc sulfide coating on ms-ZnS, (4) Texas Instruments antireflection-coated gallium phosphide (the coating was not intended for erosion resistance), and (5) uncoated polycrystalline magnesium fluoride (MgF_2). ZnS-coated ms-ZnS has low optical emission for operation at 500°C in both the 3-5 and 8-10 micrometer (μm) regions. Bulk GaP and bare MgF_2 have low emission only in the 3-5 μm region. BP/ms-ZnS and BP/GaP/ms-ZnS have prohibitive optical emission at 500°C in both the 3-5 and 8-10 μm regions. Erosion resistance was characterized in side-by-side exposure in the whirling arm rainfield and sand erosion test facilities at the Air Force Wright Laboratory. In a 25.4-millimeter/hour (mm/h) rain field of 2-mm-diameter drops at 210 meters/second (m/s) and 252 m/s at perpendicular incidence, none of the coated materials was as durable as bare MgF_2. BP/ms-ZnS is more durable than ZnS/ms-ZnS, but subsurface damage preceded damage to the BP coating in BP/ms-ZnS. Antireflection-coated GaP fractured easily on orthogonal crystal planes upon raindrop impact. In sand erosion experiments with 149- to 177-μm-diameter sand particles at an impact speed of 75 m/s at normal incidence, BP/ms-ZnS was the most durable coating. The relative loss in transmittance (T/T_o) after a loading of 300 milligram/square centimeter (mg/cm^2) was: BP/ms-ZnS, -6%; bare MgF_2, -25%; ZnS/ms-ZnS (with DAR-1 antireflection coating), -40%; ZnS/ms-ZnS (with DAR-3 antireflection coating), -56%; bare silicon, -58%; antireflection-coated GaP, -72%. In erosion experiments with <38-μm-diameter sand particles at 210 m/s, BP/ms-ZnS was most durable and BP/GaP/ms-ZnS was second best. Other samples behaved in a similar manner to the 75 m/s run.

LIST OF ABBREVIATIONS

AR	antireflection coated
BP	boron phosphide
DAR	Raytheon proprietary "Durable AntiReflection coating," DAR-1 and DAR-3 were evaluated in the present work
DLC	diamond-like carbon
GaP	gallium phosphide
MgF_2	magnesium fluoride
ms-ZnS	multispectral zinc sulfide
PMMA	poly(methylmethacrylate), also called Plexiglas®
REP	Raytheon designation for "Rain Erosion Protection" coating referring to compressively stressed zinc sulfide deposited as a window coating
ZnS	zinc sulfide

INTRODUCTION

The purpose of this study was to compare the erosion resistance of protective coatings on multispectral zinc sulfide. Multispectral zinc sulfide was chosen as the substrate material because of its ability to transmit in both the midwave (3-5 μm) and long wave (8-10 μm) infrared regions.

Recently developed durable coatings include boron phosphide (from Barr & Stroud, Reference 1), gallium phosphide (from Barr and Stroud, Reference 1) and from Texas Instruments (References 2 and 3), and compressively stressed zinc sulfide (ZnS, from Raytheon (Reference 4)). Boron phosphide (BP) provides good erosion resistance (Reference 5), but is visibly black and has an infrared absorption of 0.7% per μm of thickness in the 8-12 μm wavelength region. Boron phosphide also absorbs in the 3-5 μm region. Gallium phosphide (GaP) is a less durable, but more transparent coating (References 1 through 3, and 6). The compressive ZnS coating has good erosion resistance and it retains the same optical properties as bulk ZnS.

The only material combinations in our tests that are potentially capable of 2-color (midwave and long wave) operation are GaP on multispectral ZnS and compressively stressed ZnS on multispectral ZnS. However, for comparison, BP coatings on multispectral ZnS, bulk GaP, hot pressed MgF_2, and single crystal Si were also examined.

MATERIALS

Magnesium Fluoride (2.54-mm thick x 25-mm-diameter disk). Light gray, uncoated, polycrystalline material was used. The origin is uncertain, but it is probably Kodak IRTRAN 1® from ~1970. For whirling arm rain erosion tests, an identical piece of MgF_2 was placed behind the test specimen so the total thickness was 5.1 mm.

Raytheon ZnS-Coated Multispectral ZnS (5.2-mm thick x 25-mm-diameter disk). The compressive ZnS rain erosion protective coating (designated REP by Raytheon) on the front (impact) surface was 20-μm thick. Some samples also had a 40-μm thick REP coating on the back surface. The outside front surface had one of two proprietary antireflection coatings, designated DAR-1 or DAR-3, designed for 8-10 μm operation.

Barr & Stroud BP-Coated Cleartran® ZnS (5.0-mm thick x 25-mm-diameter disk). This material was coated on one side only with ~18 μm of BP covered by a thin antireflection (AR) layer of diamondlike carbon designed for the 8-10 μm region. Cleartran is the trade name for multispectral ZnS manufactured by Morton International. Cleartran is referred to as multispectral ZnS in most of this paper.

Barr & Stroud GaP-Coated Cleartran® ZnS (5.0-mm thick). This material was coated on one side with 10-11 μm of gallium phosphide (GaP). On the outside of the gallium phosphide was 2.0 μm of boron phosphide overcoated with a diamond-like carbon antireflection layer optimized for the 8-10 μm region. Samples were received as 25-mm x 25-mm squares that were ground into 25-mm-diameter disks at China Lake. Minor edge chipping occurred during grinding.

Texas Instruments Antireflection-Coated GaP (5.5-mm thick x 22-mm-diameter disk). Bulk gallium phosphide grown from a melt was coated on both sides with a thin, antireflection coating designed for the 3-5 μm region. The coating was not intended to provide erosion resistance.

Silicon. A single crystal (6.5-mm thick x 25-mm-diameter disk) with no special orientation was used for sand erosion studies. For infrared transmission, polycrystalline material (resistivity > 10 Ω·cm) with a thickness of 3.0 mm was employed.

OPTICAL CHARACTERISTICS

Infrared transmittance and emittance were measured with a Perkin Elmer 983 spectrophotometer at Rockwell Science Center using graphite as a reference emitter with an assumed emissivity of 0.97. Samples were held in an evacuated, electrically heated furnace. For emission measurements, the rear transparent window of the furnace was covered by a water cooled back flange. At 500°C, the long wave emittance measurements have an estimated relative accuracy of ±5%. At short wavelengths, where the emittance is ~0.01-0.02, the relative accuracy may be ±50%. Nominal spectral resolution was 11 cm^{-1} at 4000 cm^{-1}, 5.6 cm^{-1} at 2000 cm^{-1}, and 3.6 cm^{-1} at 1000 cm^{-1}.

Total integrated optical scatter at 3.39-μm and 10.59-μm wavelengths was measured with a Coblentz sphere collecting all light between 2.5 and 70° from the incident laser direction in either the forward or backward hemispheres (Reference 7). Table 1 shows that the infrared optical scatter at 3.39 μm is very low for Raytheon coated ZnS and low for Barr & Stroud BP-coated ms-ZnS and for Texas Instruments bulk GaP. The forward scatter of bulk MgF_2 is representative of seeker domes in operational missiles. In the long-wave region at 10.59 μm, ZnS and GaP have extremely low optical scatter and MgF_2 is opaque.

TABLE 1. Total Integrated Infrared Optical Scatter in Forward Hemisphere.[a]

Sample	3.39 μm		10.59 μm	
	Forward	Backward	Forward	Backward
Raytheon:				
Uncoated ms-ZnS	0.28	0.06	0.10	0.03
DAR-1/REP/ms-ZnS	0.35, 0.39	0.10, 0.13	0.09, 0.11	0.05, 0.06
Barr & Stroud:				
Uncoated ms-ZnS	0.40	0.05	0.21	0.05
BP/ms-ZnS	1.00, 0.60	0.54, 0.33	0.14, 0.12	0.07, 0.03
Texas Instruments GaP	0.93, 1.43	0.03, 0.04	0.14, 0.22	0.06, 0.15
MgF_2	1.4, 1.8	0.38, 0.35	...	...

[a] Pairs of numbers give scatter for two different samples. Measurements were made with a Coblentz sphere collecting all light between 2.5 and 70° from the incident laser direction (Reference 7). Each measurement is an average of several points in the specimen.

Infrared transmittance and emittance up to 500°C for each material studied are shown in Figures 1-8. Figure 9 is an enlargement of the midwave region of the transmission spectrum of MgF_2. Figure 10 compares the transmittance of the materials at 20 and 500°C. Figure 11 compares emission spectra at 500°C. Observations on optical performance are summarized as follows:

- Magnesium Fluoride. Transmission in the 3-5 μm region is excellent (Figure 1) but decreases toward short wavelength as optical scatter increases. Emittance is low ($\lesssim$ 2%) between 4 and 5 μm, but rises to ~6% at 3 μm. Part of this rise might be an artifact from optical scatter. However, part probably arises from a broad OH impurity absorption band centered near 3450 cm^{-1} (Figure 9). There is a strong, sharp OH impurity band near 3615 cm^{-1}.
- Uncoated Multispectral ZnS. Transmission is excellent in both the 3-5 and 8-10 μm regions at 20°C (Figures 2 and 4). Emittance at 500°C is very low (~2%) from 3 to 9 μm, but increases to ~10% at 10 μm.
- ZnS-Coated Multispectral ZnS. This has higher emittance in the 8-10 μm region than does uncoated multispectral ZnS (Figure 11, upper spectrum). The extra emittance probably arises from the oxide antireflection coating.
- BP-Coated Multispectral ZnS. The coating reduces the transmission (Figure 10) and increases the emittance (Figure 11), relative to uncoated material. Optical emission is prohibitive for high temperature applications. Even though the sample cell was evacuated, there was enough oxygen present for combustion.
- BP/GaP-Coated Multispectral ZnS. Although not as high as that of BP-coated material (Figure 11), the optical emission is still probably too great for high temperature applications. Changes in the 20°C transmission spectrum after heating the sample to 500°C in the evacuated sample cell suggest that the outer diamond-like carbon burned off during heating for the emittance measurement.
- Antireflection-Coated GaP. This is an excellent optical material for the 3-5 μm region (Figure 7). At 8-10 μm, transmittance is low and emittance is prohibitively high for most applications.

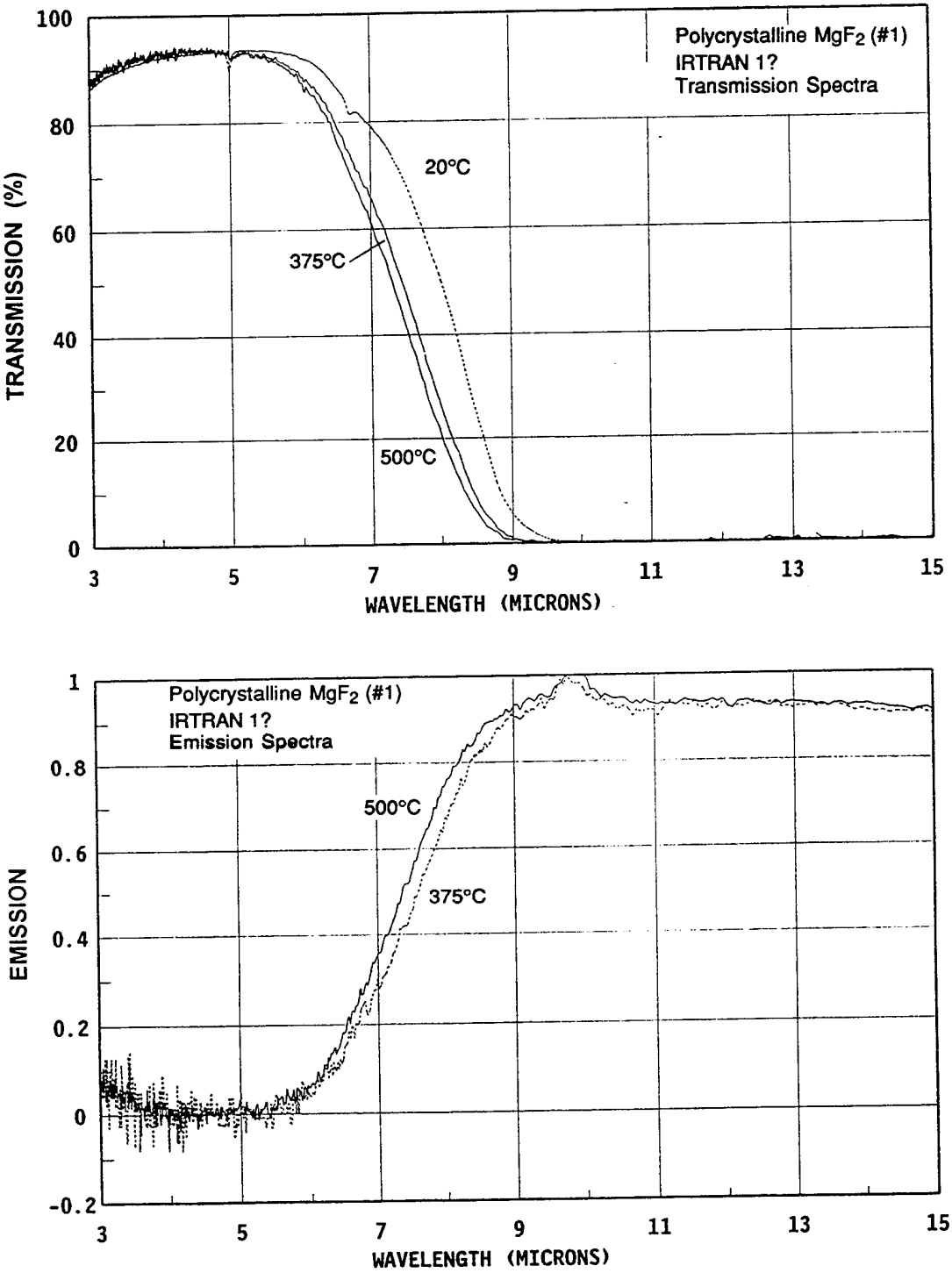

FIGURE 1. Infrared Transmission (Upper) and Emission (Lower) of Polycrystalline Magnesium Fluoride (2.54-mm Thick) as a Function of Temperature.

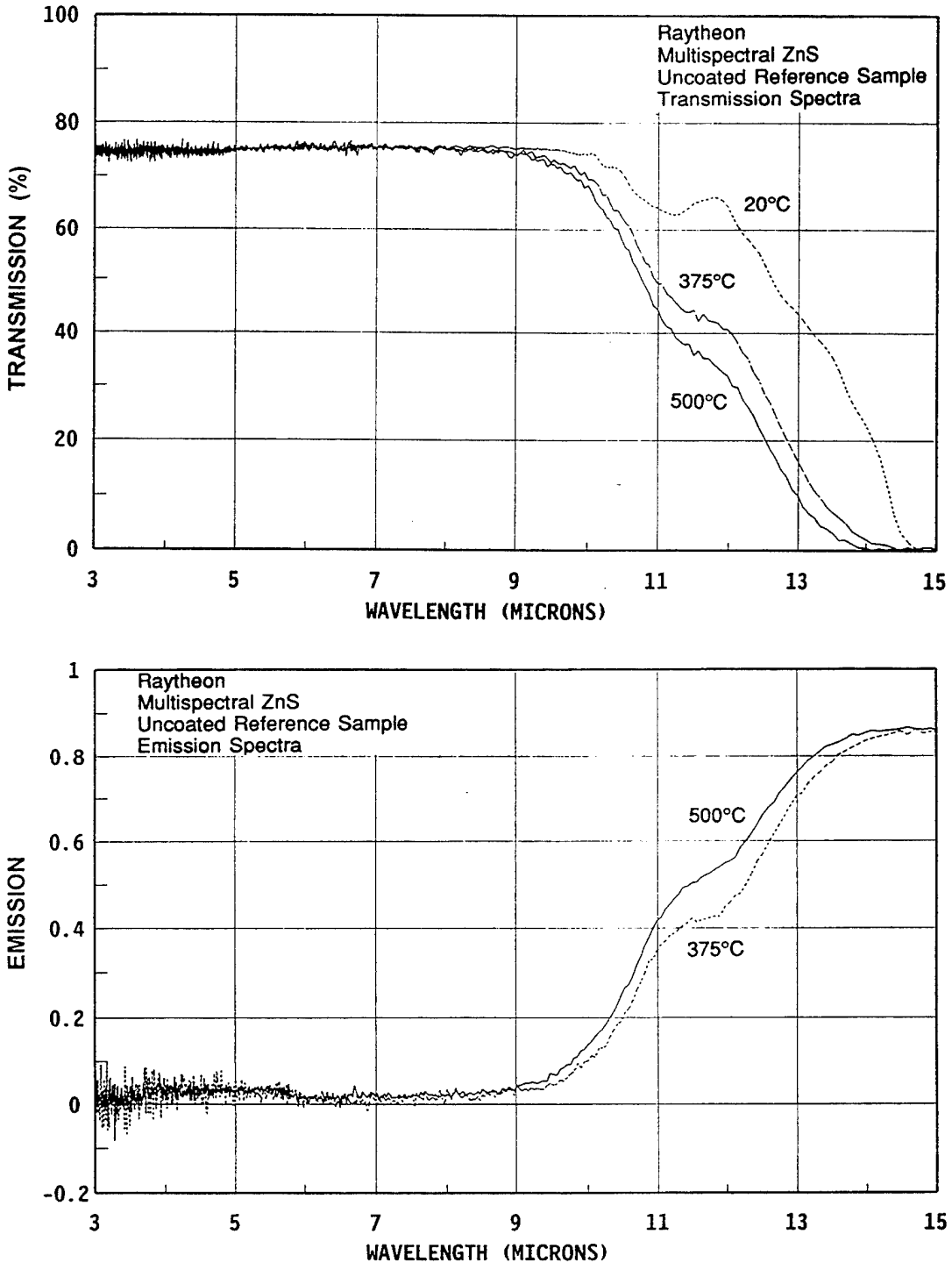

FIGURE 2. Infrared Transmission (Upper) and Emission (Lower) of Raytheon Uncoated Multispectral Zinc Sulfide (5.2-mm Thick) as a Function of Temperature.

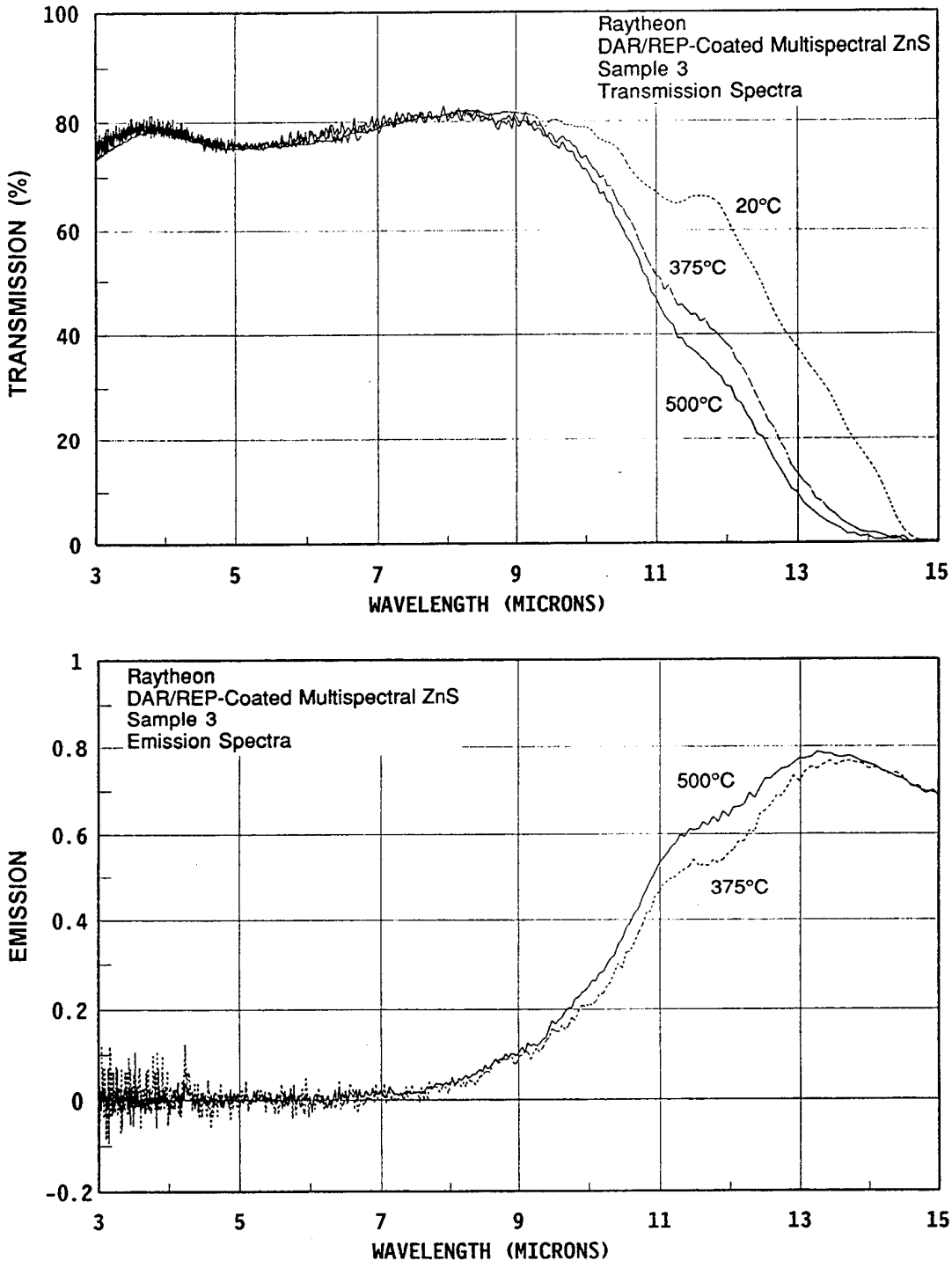

FIGURE 3. Infrared Transmission (Upper) and Emission (Lower) of Raytheon DAR-1/ REP-Coated Multispectral Zinc Sulfide (5.2-mm Thick) as a Function of Temperature.

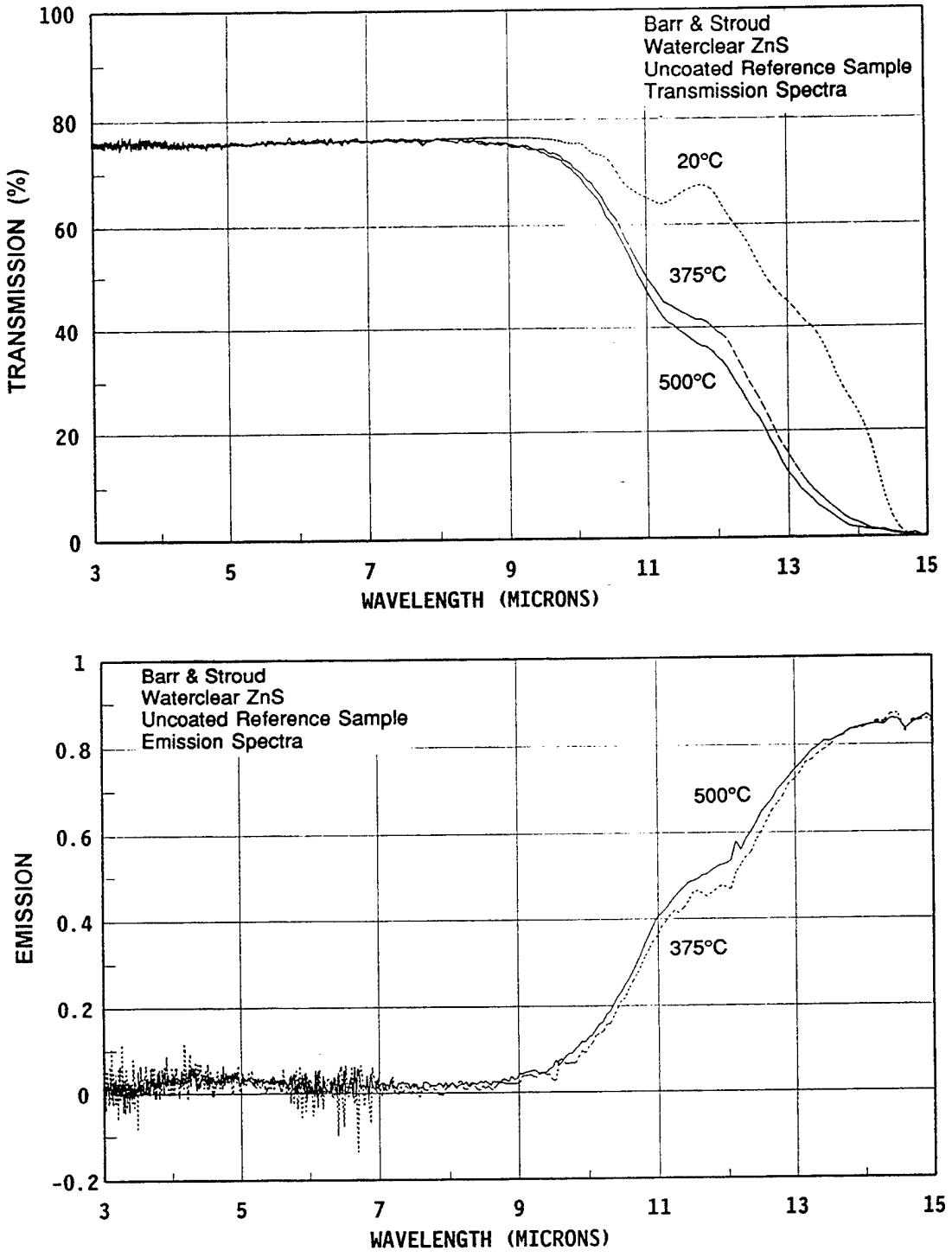

FIGURE 4. Infrared Transmission (Upper) and Emission (Lower) of Barr & Stroud Uncoated Cleartran Zinc Sulfide (5.0-mm Thick) as a Function of Temperature.

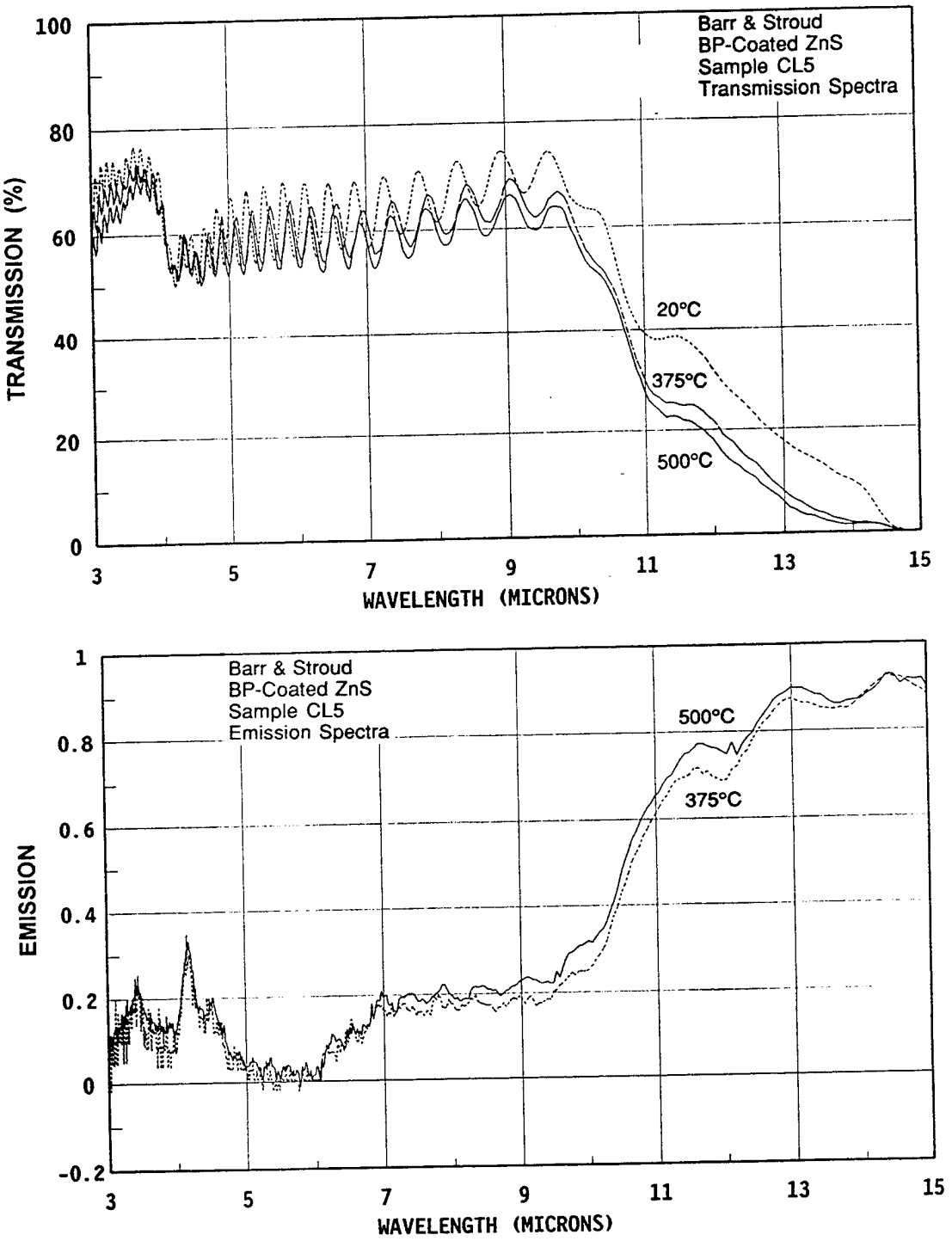

FIGURE 5. Infrared Transmission (Upper) and Emission (Lower) of Barr & Stroud DLC/BP-Coated Cleartran Zinc Sulfide (5.0-mm Thick) as a Function of Temperature.

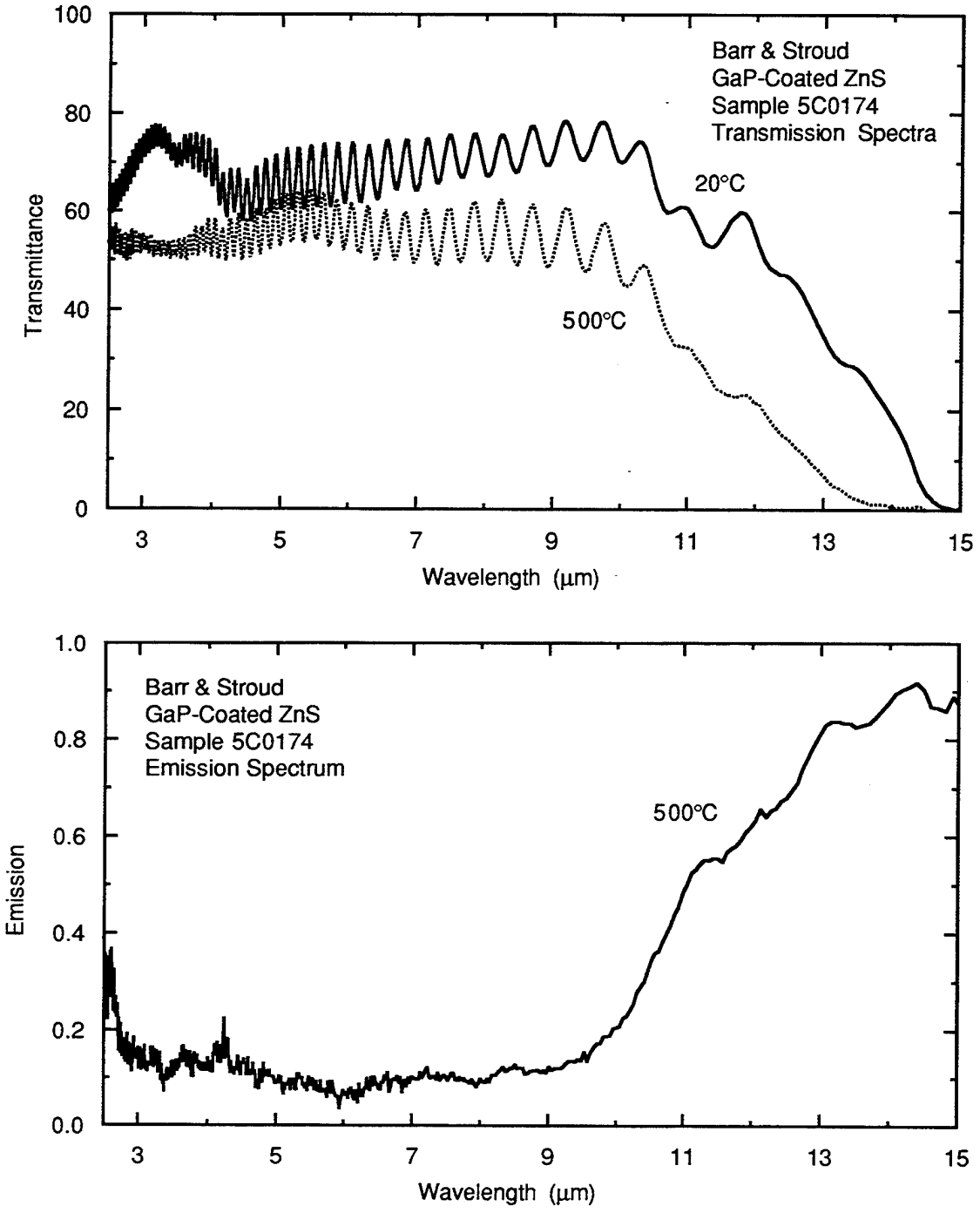

FIGURE 6. Infrared Transmission (Upper) and Emission (Lower) of Barr & Stroud DLC/BP/GaP-Coated Cleartran Zinc Sulfide (5.0-mm Thick) as a Function of Temperature.

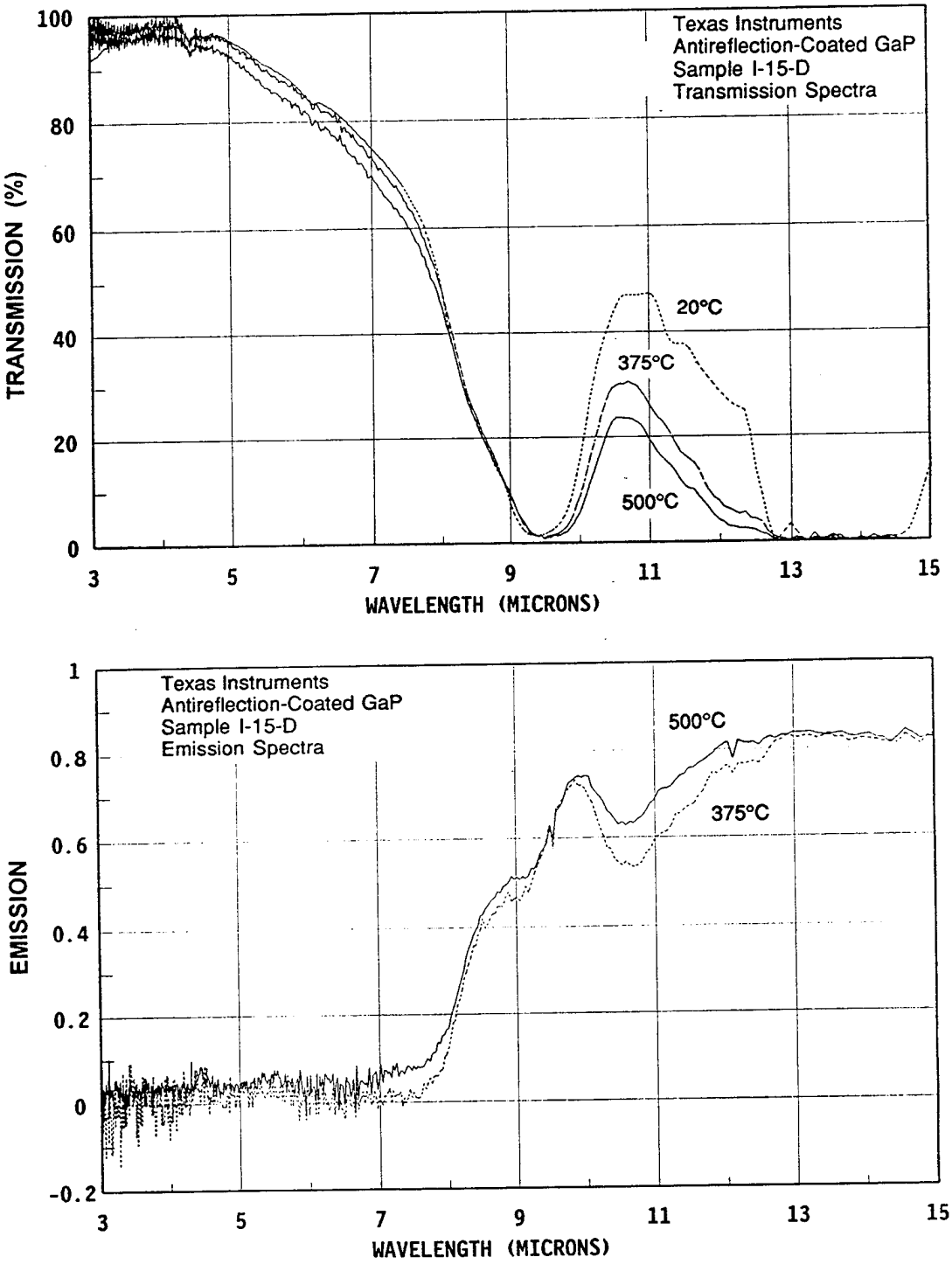

FIGURE 7. Infrared Transmission (Upper) and Emission (Lower) of Texas Instruments Antireflection-Coated Gallium Phosphide (5.5-mm Thick) as a Function of Temperature.

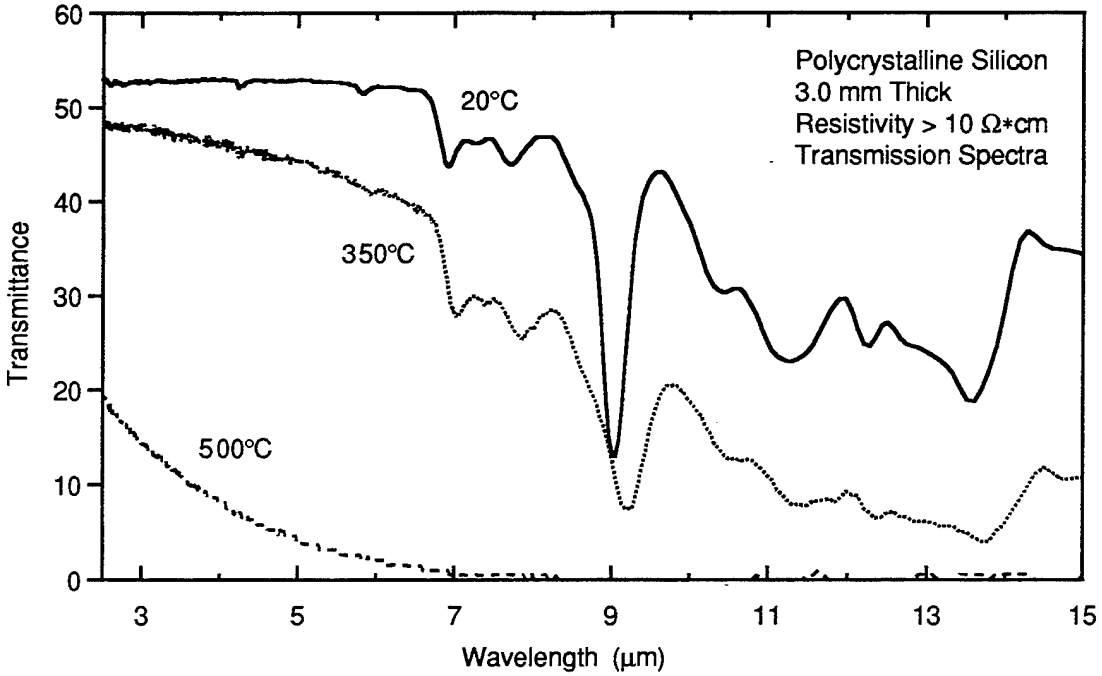

FIGURE 8. Infrared Transmission of Polycrystalline Silicon (3.0-mm Thick).

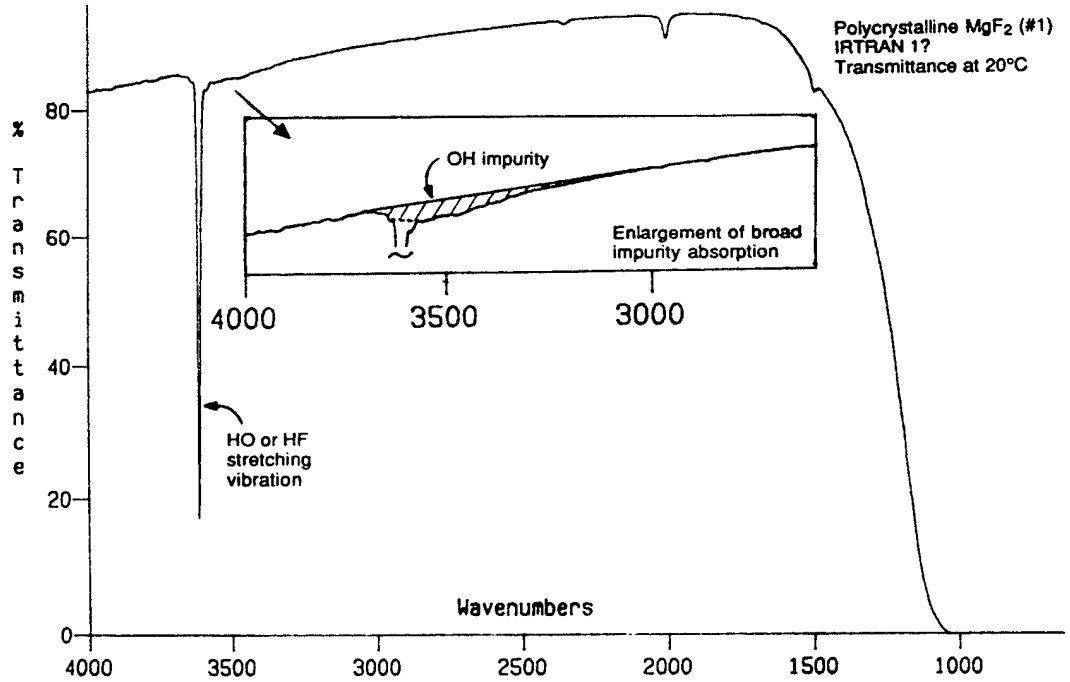

FIGURE 9. Expanded Spectrum of MgF_2 (2.54-mm Thick) Showing Sharp Absorption Band at 3615 cm^{-1} (2.766 μm) and Weak, Broad Band Centered Near 3450 cm^{-1} (2.9 μm).

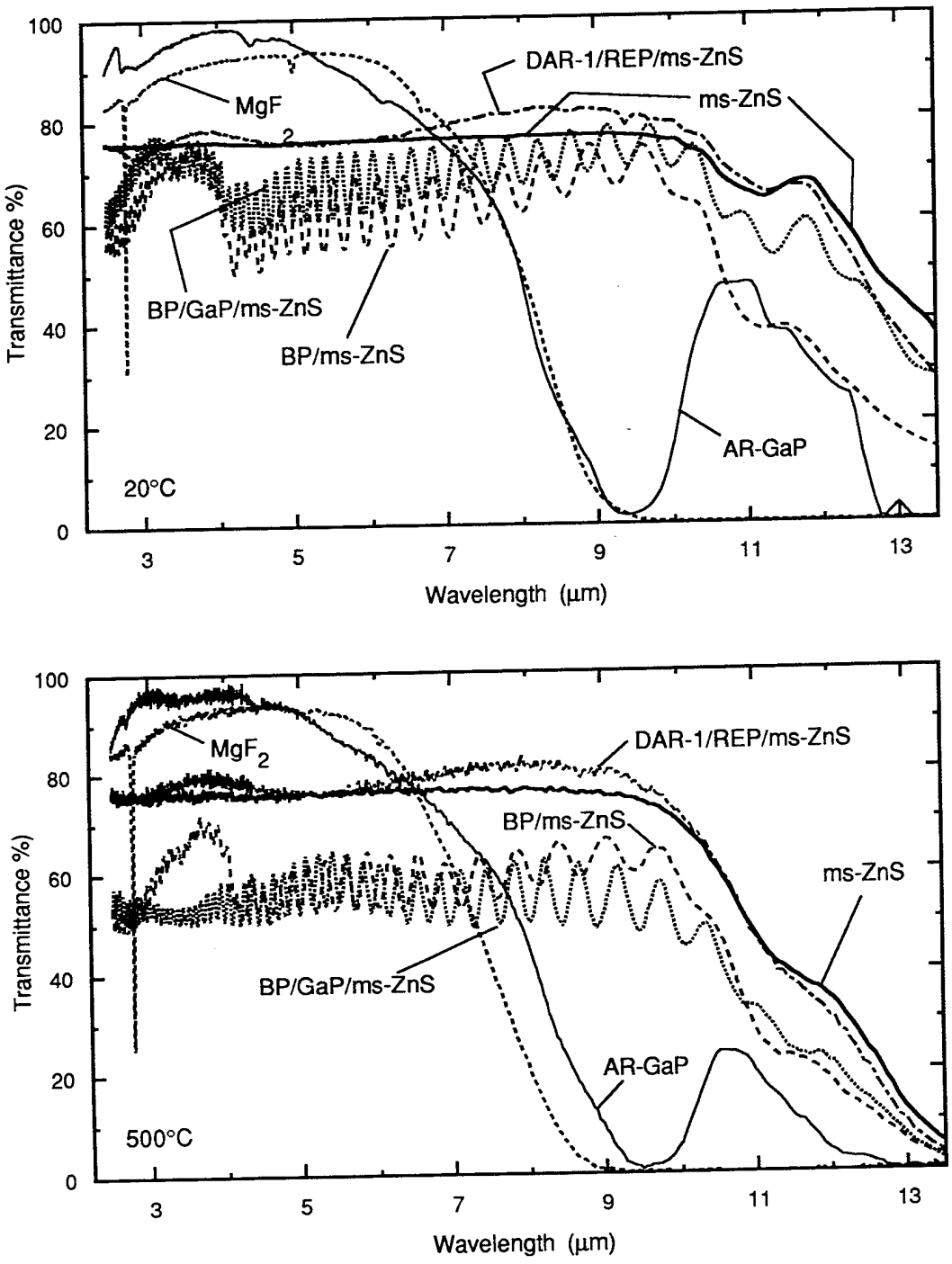

FIGURE 10. Comparison of Transmission Spectra at 20°C (Upper) and 500°C (Lower).

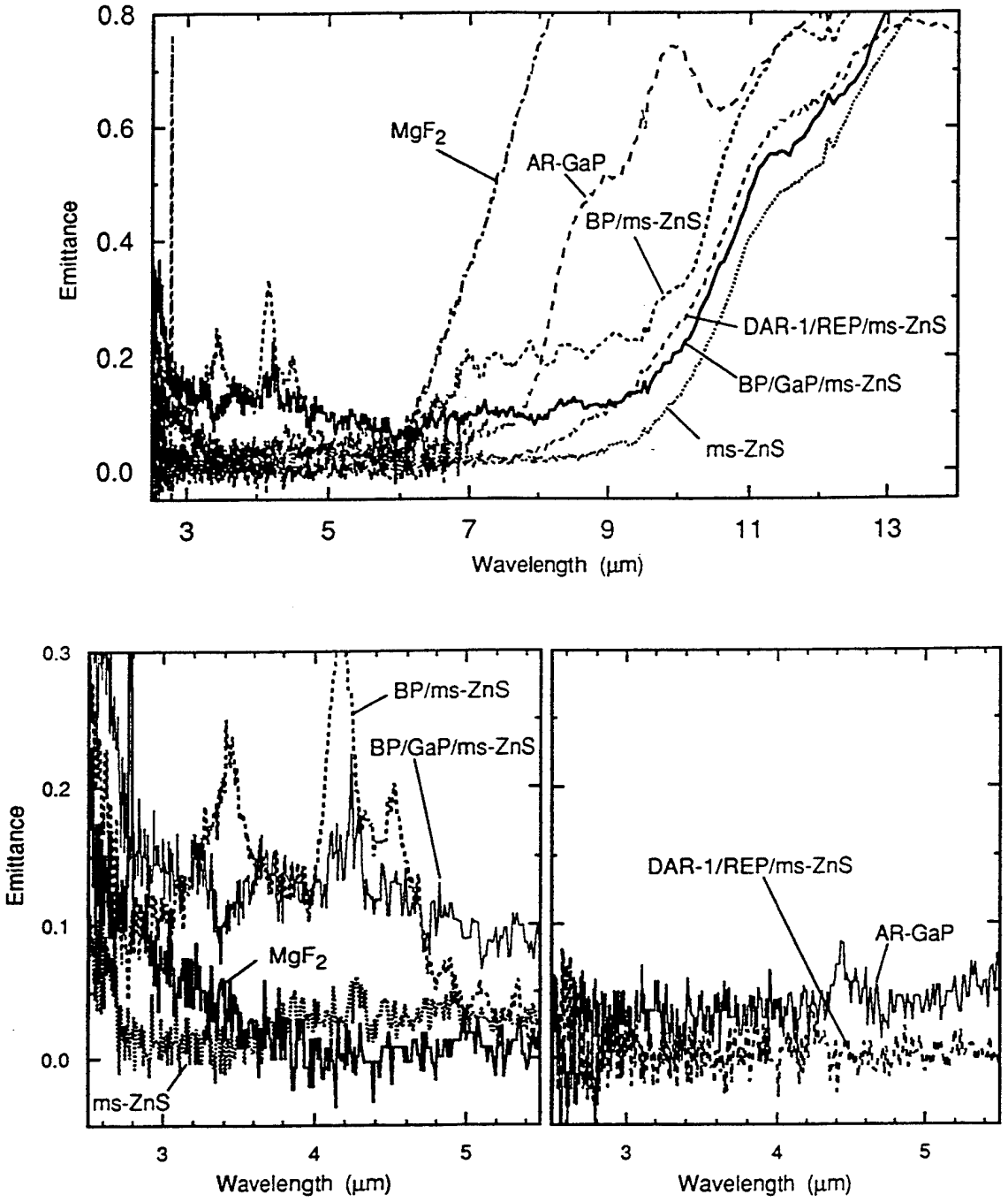

FIGURE 11. Comparison of Infrared Emission Spectra at 500°C. The diamond-like carbon outer antireflection layer burned off the BP/GaP/ms-ZnS sample at 500°C prior to the measurement and probably also burned off the BP/ms-ZnS sample.

RAIN EROSION

Samples were tested at the Whirling Arm facility at Wright Laboratory on 13 March 1995. All tests were run in a 2-mm-diameter drop rainfield with a rainfall rate of 25.4 mm/h at perpendicular incidence. All samples except GaP were backed by a rubber disk in the sample holder and tightened with a torque wrench set to 3 inch-lbs. The GaP sample (which had a smaller diameter, 22 mm instead of 25 mm) was backed by a Teflon disk. Each sample was photographed at 3x magnification prior to testing and at several intervals during testing. Samples were illuminated at a low angle (~60° from normal) by two lights 180° apart for photography.

For each run, one sample was placed in position A on the whirling arm and a second sample in position B 180° away. The test was run for a desired time while observing the disks through a video camera. Table 2 lists conditions for each run and observations of sample condition by the naked eye and by a skilled observer using a magnifying glass. Runs 1, 2, 7, and 8 were calibration trials to record the number and types of raindrop impacts. Figures 12 through 25 show the 3x photographs of each run. The exposed surface of the sample in each picture is approximately 20 mm in diameter. Figures 26 through 33 show micrographs of representative damage sites.

Figures 34 and 35 summarize results from rain erosion tests. No damage to MgF_2 exposed at 210 m/s (470 miles/h) was visible to the naked eye, but impact and ring fractures were observed with a microscope. A sample of MgF_2 exposed at 252 m/s fractured after 8 minutes (min). Antireflection-coated bulk GaP readily cleaved along weak crystal planes when impacted at 210 m/s. In addition to bulk fracture of GaP along the right edge in Figure 34, Figure 35 shows a distinctive pattern of orthogonal surface fractures characteristic of a (100) crystal plane. Previous work with GaP-coated germanium (Ge) demonstrated that the (100) crystal planes suffered much more damage than (111) planes (Reference 6). It is likely that (111) GaP would be more durable than the samples we studied. A possibly better performance by GaP than we observed has been reported for single drop impact studies (Reference 8).

Two samples of ZnS-coated ms-ZnS in Figure 34 suffered extensive internal and surface damage. The micrograph of ZnS-coated ms-ZnS in Figure 35 shows internal and surface damage, as well as coating delamination. In general, delamination was not common in ZnS-coated ms-ZnS. Results for ZnS-coated ms-ZnS in Figure 34 stand in marked contrast with the previously reported performance of ZnS-coated standard grade ZnS, which suffered no gross damage in a 10-min exposure at 210 m/s in the whirling arm (Reference 4).

Two samples of BP-coated ms-ZnS in Figure 34 display less obvious damage than the ZnS-coated ms-ZnS. However, the very durable BP coating is visibly opaque. When viewed from the rear, the transparent ms-ZnS exhibits subsurface damage that is barely evident from the BP-coated surface. The micrograph of an impact site in Figure 35 shows conchoidal fracture and the distinct texture of the undamaged BP coating.

TABLE 2. Whirling Arm Rain Impact Test Results.

Run	Speed m/s, mph	Arm position	Sample	Total elapsed time	Observations
1	210	A	PMMA 940572	10 s	Rainfield calibration run (49.0 impact sites/cm^2 observed after the run). PMMA = poly(methylmethacrylate) = Plexiglas
	(470)	B	PMMA 940573	10 s	Calibration run (51.3 impact sites/cm^2).
2	210	A	PMMA 940574	20 s	Calibration run (69.7 impact sites/cm^2).
	(470)	B	PMMA 940575	20 s	Calibration run (71.0 impact sites/cm^2).
3	210	A	MgF_2-5	2.5 min	No damage.
	(470)			5.0 min	No damage.
				10.0 min	No damage.
				16.0 min	Pitting/erosion damage.
		B	Barr & Stroud	2.5 min	No damage.
			BP/ZnS-CL7	5.0 min	No damage.
				10.0 min	Local coating removal.
				16.0 min	Increased localized coating removal/ subsurface ring fractures/ZnS fracture. Cracked through diameter of the substrate at 14-15 min.
4	210	A	MgF_2-2	5.0 min	No damage.
	(470)			10.0 min	Slight pitting/erosion damage.
		B	Raytheon	5.0 min	Localized DAR coating removal/pitting.
			DAR-1/REP/ZnS-1	10.0 min	Increased DAR localized coating removal/ pitting/REP pitting/cratering/surface microcracks/subsurface ring fractures/ erosion failure.
5	210	A	MgF_2-3	5.0 min	No damage.
	(470)			10.0 min	Slight pitting/erosion damage.
		B	Texas Instruments	5.0 min	Substrate fractures/pitting/subsurface microcracks. Patterns of lines were evident to the naked eye, but not seen in the 3x photograph. Edge of disk beneath mounting cap fractured off into several pieces. There is an obvious problem with weak crystal cleavage planes.
			AR-Coated GaP-I15-D	10.0 min	Pitting/cratering/surface microcracks/ localized coating removal/erosion failure. A dozen obvious craters and hundreds of tiny fracture lines with an orthogonal pattern could be seen by the naked eye. There was increased edge damage beneath the mounting cap.

TABLE 2. (Contd.)

Run	Speed m/s, mph	Arm position	Sample	Total elapsed time	Observations
6	210 (470)	A	Raytheon DAR-1/REP/ZnS-2	2.7 min	Pre-existing surface defects/ coating pitting/subsurface ring fracture/ surface microcracks/subsurface impact damage.
				5.0 min	Increased pitting/cratering.
				10.0 min	Increased subsurface fracture/surface. microcrack/pitting/cratering/local coating removal/erosion failure.
		B	Barr & Stroud BP/ZnS-CL10	2.7 min	Pre-existing surface defects/ slight coating pitting. ~6 tiny craters appear to the eye, but not in the photo.
				5.0 min	Increased pitting.
				10.0 min	Gross surface damage easily seen in the photo Increased pitting/cratering/ subsurface ring fractures/localized coating removal (erosion damage).
7	252	A	PMMA 940576	10 s	Calibration run (40.8 impact sites/cm^2).
	(564)	B	PMMA 940577	10 s	Calibration run (56.1 impact sites/cm^2).
8	252	A	PMMA 940578	20 s	Calibration run (64.6 impact sites/cm^2).
	(564)	B	PMMA 940579	20 s	Calibration run (65.9 impact sites/cm^2).
9	252	A	Raytheon DAR-1/REP/ZnS-3	1.0 min	One easily observed impact mark and several tiny marks.
	(564)			3.0 min	Sample shattered. Increased surface damage.
		B	Barr & Stroud BP/ZnS-CL11	1.0 min	~4 tiny pits—almost imperceptible
				3.0 min	No obvious damage on the surface or inside (when viewed from the transparent back side).
10	252 (564)	A	MgF_2-4	8.4 min	Sample fractured near 8 min and backing disk of MgF_2 broke also. Pitting/cratering/erosion failure.
		B	Sapphire-1	8.4 min	Slight pitting/erosion damage (not evident to casual observer).
11	252 (564)	A	Raytheon DAR-1/REP/ZnS-4	3.0 min	Significant surface and subsurface damage. Major crack in substrate does not go all the way to the edges of the disk. DAR localized coating removal/pitting/cratering/ REP erosion failure/subsurface ring fractures/erosion failure.
		B	Barr & Stroud BP/ZnS-CL12	3.0 min	Sample cracked through its diameter at 2.4 min. Crack continued to grow in the remaining 0.6 min of the run. Numerous small surface pits.

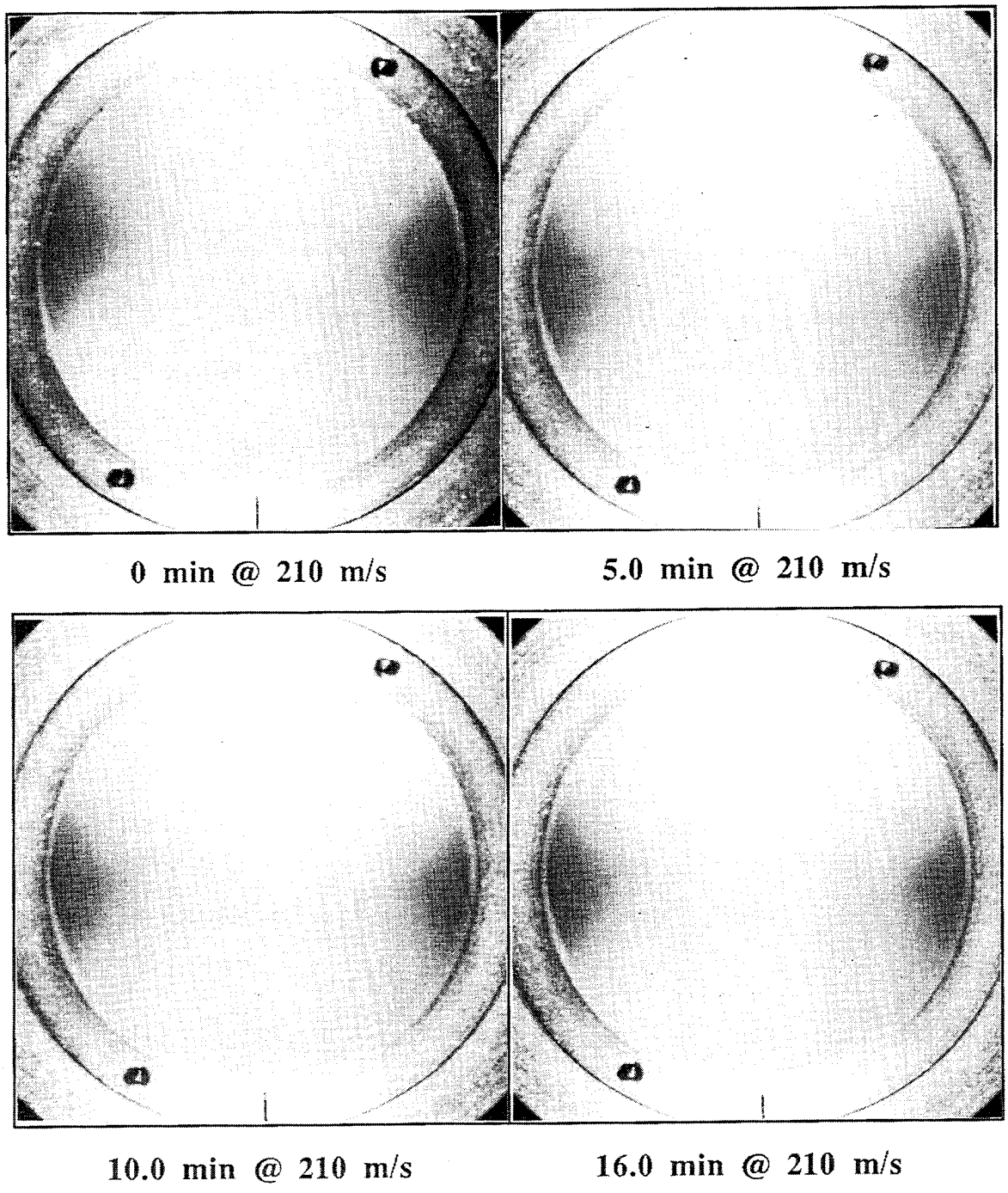

FIGURE 12. Whirling Arm Rain Exposure of MgF_2 (Sample 5) in Run 3 at 210 m/s in a 25.4 mm/h Rainfall of 2-mm-Diameter Drops at Perpendicular Incidence.

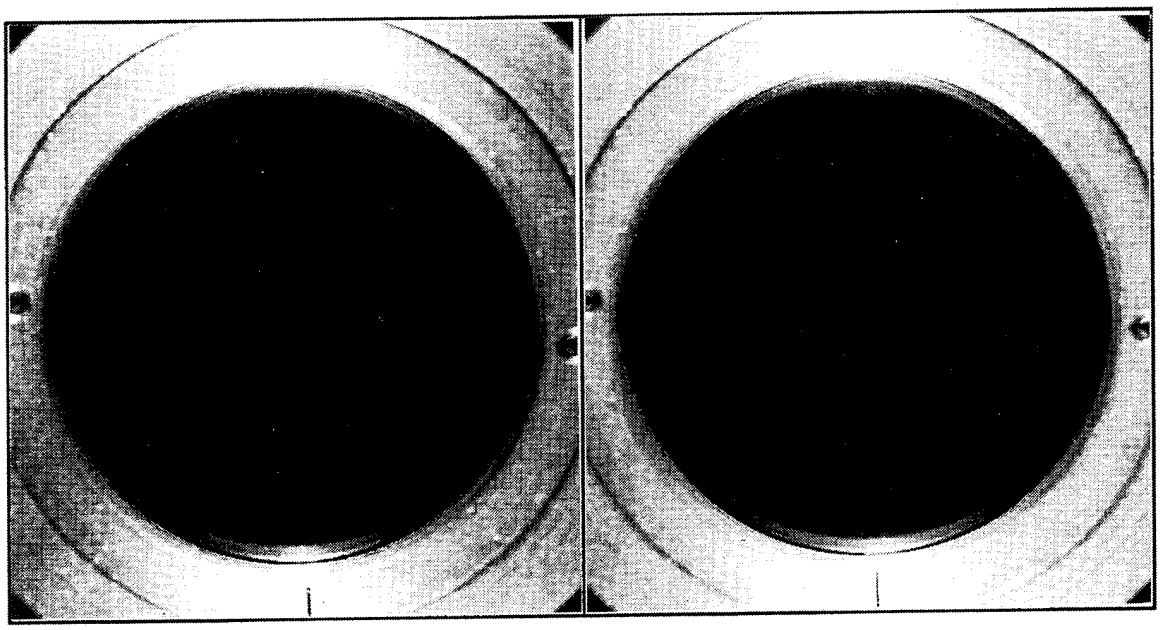

0 min @ 210 m/s

5.0 min @ 210 m/s

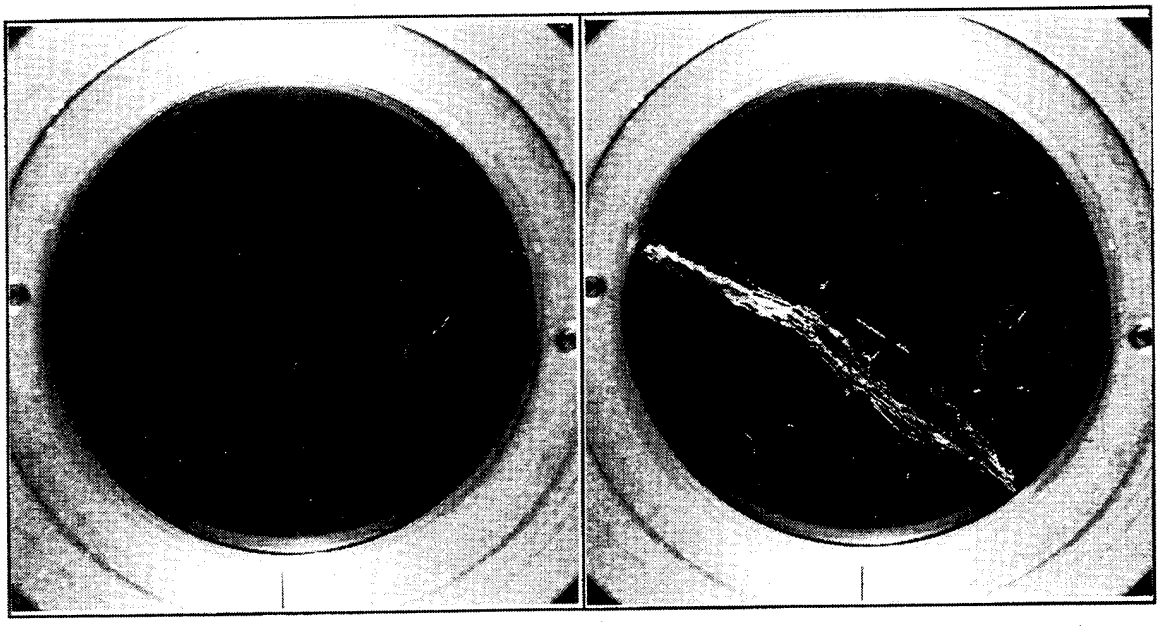

10.0 min @ 210 m/s

16.0 min @ 210 m/s

FIGURE 13. Whirling Arm Rain Exposure of BP/ms-ZnS (Sample CL7) in Run 3 at 210 m/s in a 25.4 mm/h Rainfall of 2-mm-Diameter Drops at Perpendicular Incidence. This sample of BP/ZnS had been exposed to 500°C for measuring optical properties prior to the rain erosion test. The outer diamond-like carbon layer probably burned off.

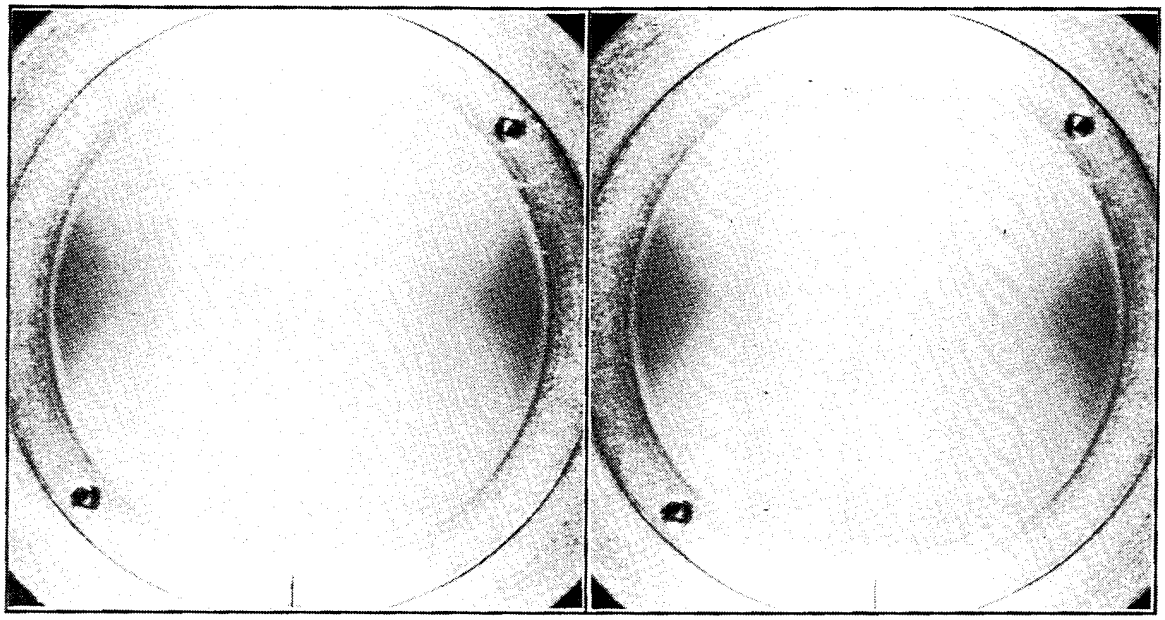

0 min @ 210 m/s

5.0 min @ 210 m/s

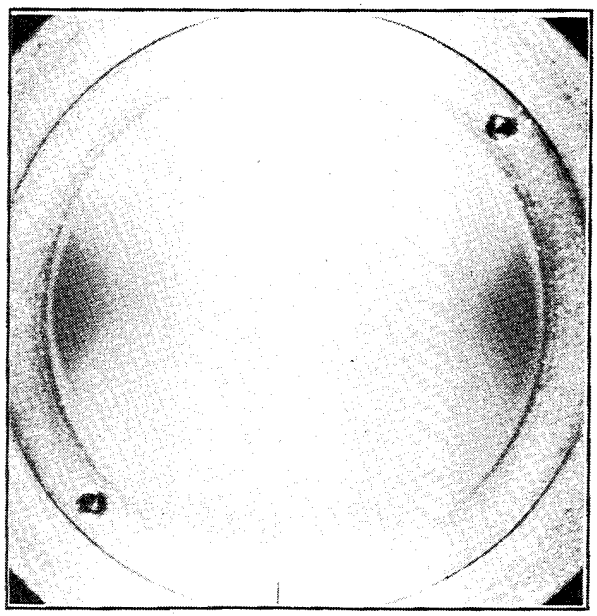

10.0 min @ 210 m/s

FIGURE 14. Whirling Arm Rain Exposure of MgF_2 (Sample 2) in Run 4 at 210 m/s in a 25.4 mm/h Rainfall of 2-mm-Diameter Drops at Perpendicular Incidence.

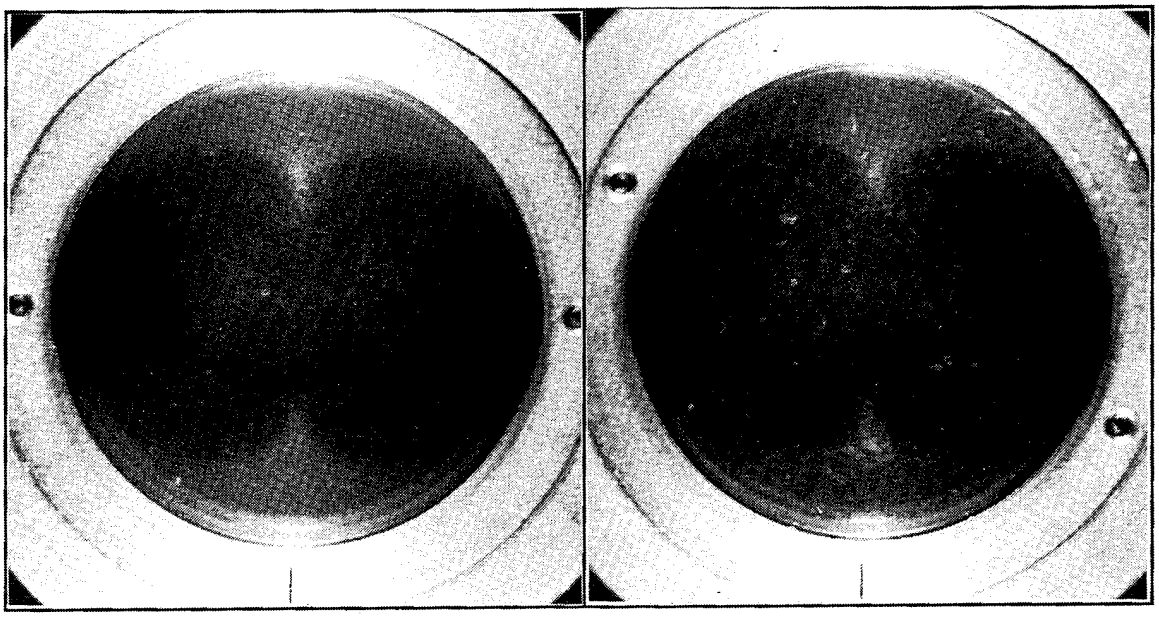

0 min @ 210 m/s

5.0 min @ 210 m/s

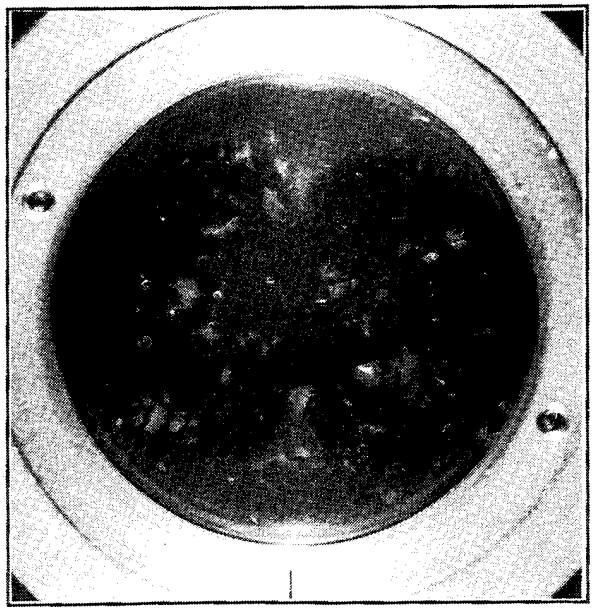

10.0 min @ 210 m/s

FIGURE 15. Whirling Arm Rain Exposure of DAR-1/REP/ms-ZnS (Sample 1) in Run 4 at 210 m/s in a 25.4 mm/h Rainfall of 2-mm-Diameter Drops at Perpendicular Incidence.

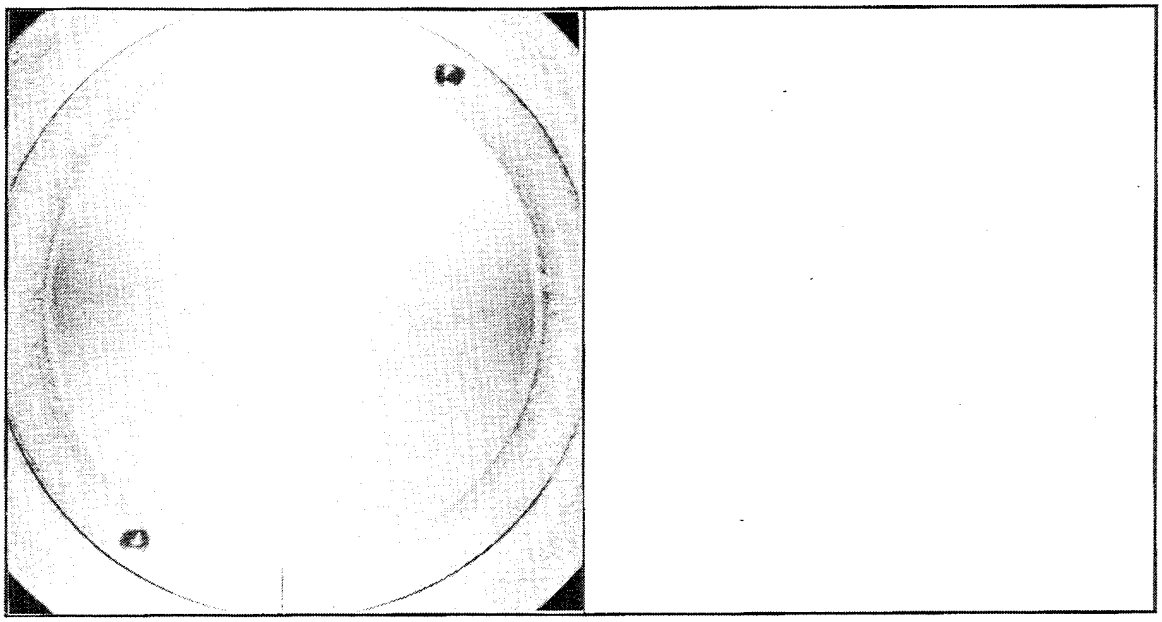

0 min @ 210 m/s

5.0 min @ 210 m/s

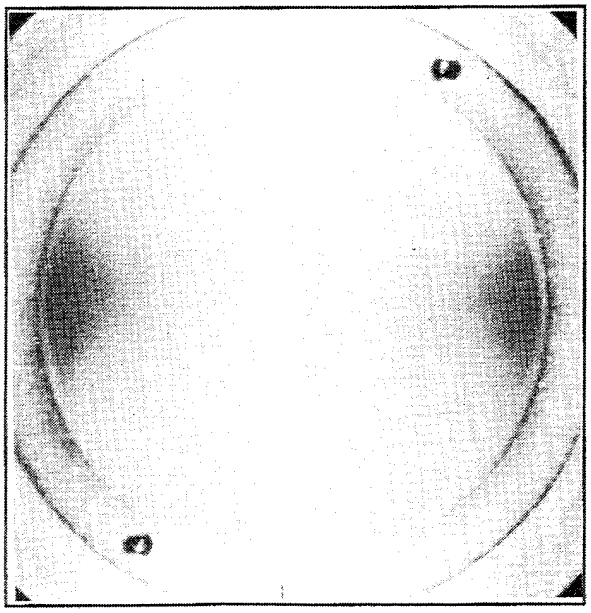

10.0 min @ 210 m/s

FIGURE 16. Whirling Arm Rain Exposure of MgF_2 (Sample 3) in Run 5 at 210 m/s in a 25.4 mm/h Rainfall of 2-mm-Diameter Drops at Perpendicular Incidence.

0 min @ 210 m/s

5.0 min @ 210 m/s

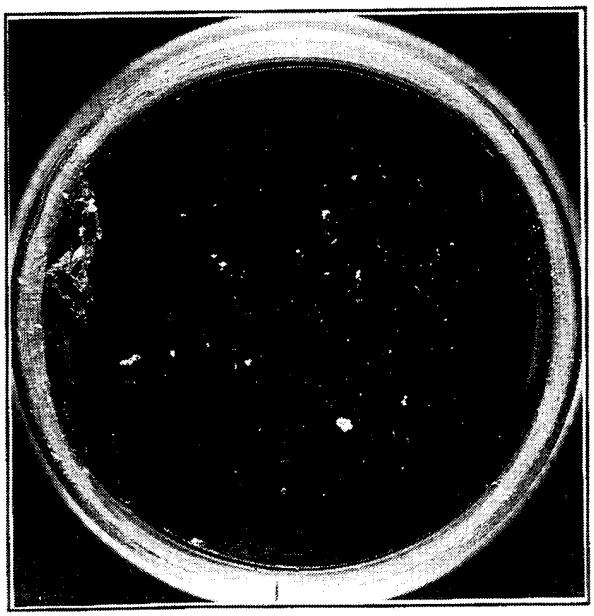

10.0 min @ 210 m/s

FIGURE 17. Whirling Arm Rain Exposure of Antireflection-Coated Bulk GaP (Sample I15-D) in Run 5 at 210 m/s in a 25.4 mm/h Rainfall of 2-mm-Diameter Drops at Perpendicular Incidence. This sample was exposed to 500°C for measuring optical properties prior to the rain erosion test.

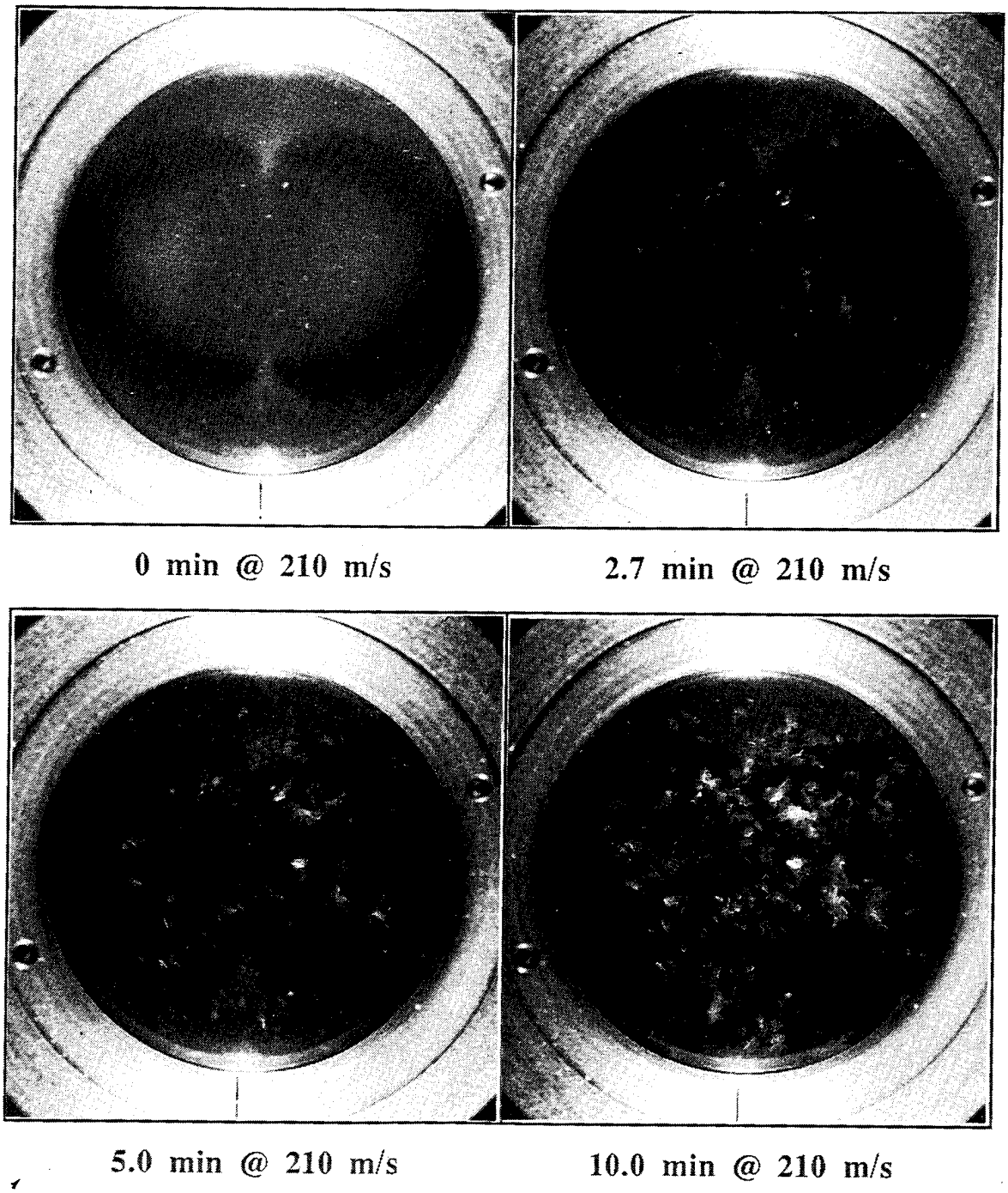

FIGURE 18. Whirling Arm Rain Exposure of DAR-1/REP/ms-ZnS (Sample 2) in Run 6 at 210 m/s in a 25.4 mm/h Rainfall of 2-mm-Diameter Drops at Perpendicular Incidence.

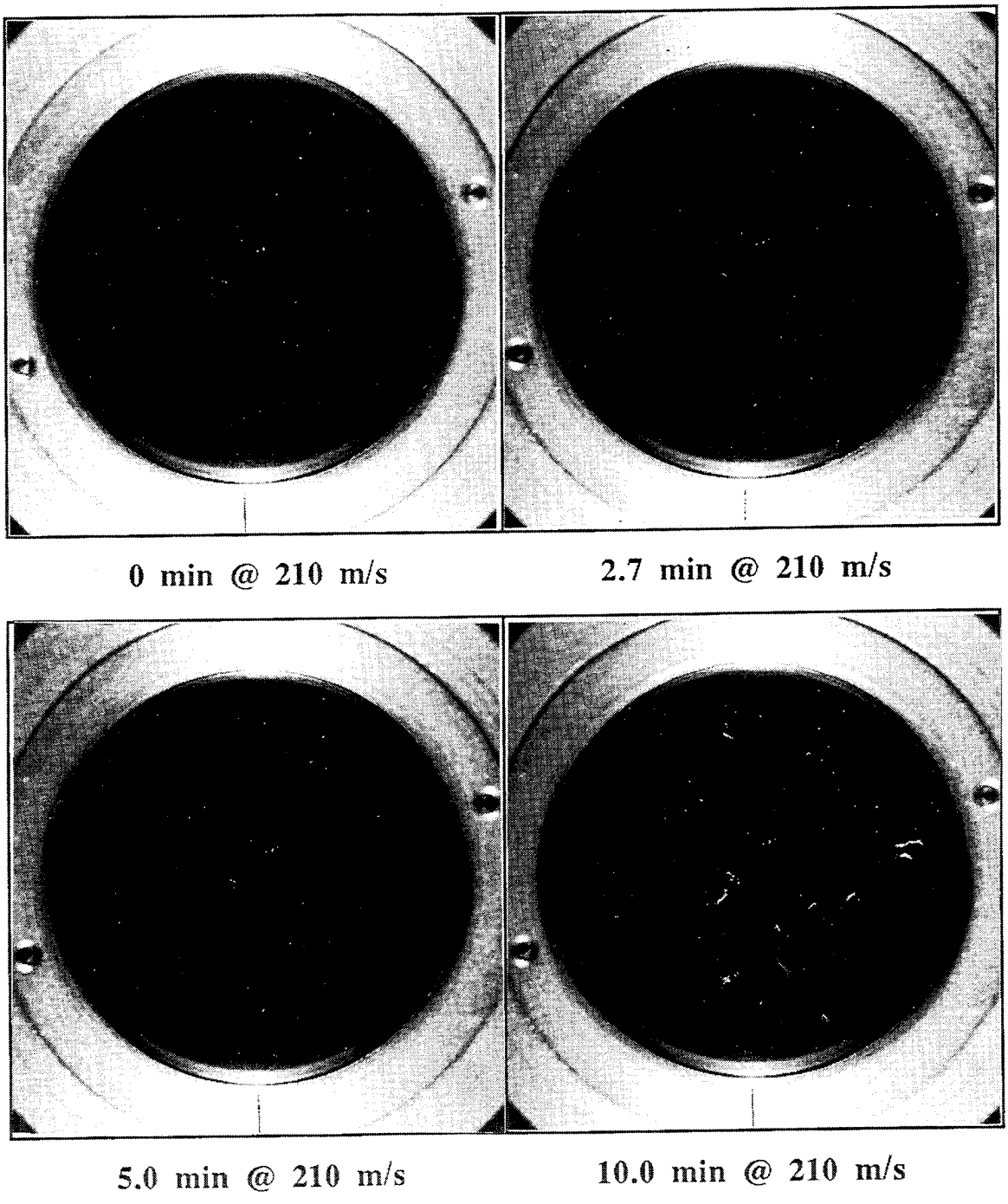

FIGURE 19. Whirling Arm Rain Exposure of BP/ms-ZnS (Sample CL10) in Run 6 at 210 m/s in a 25.4 mm/h Rainfall of 2-mm-Diameter Drops at Perpendicular Incidence.

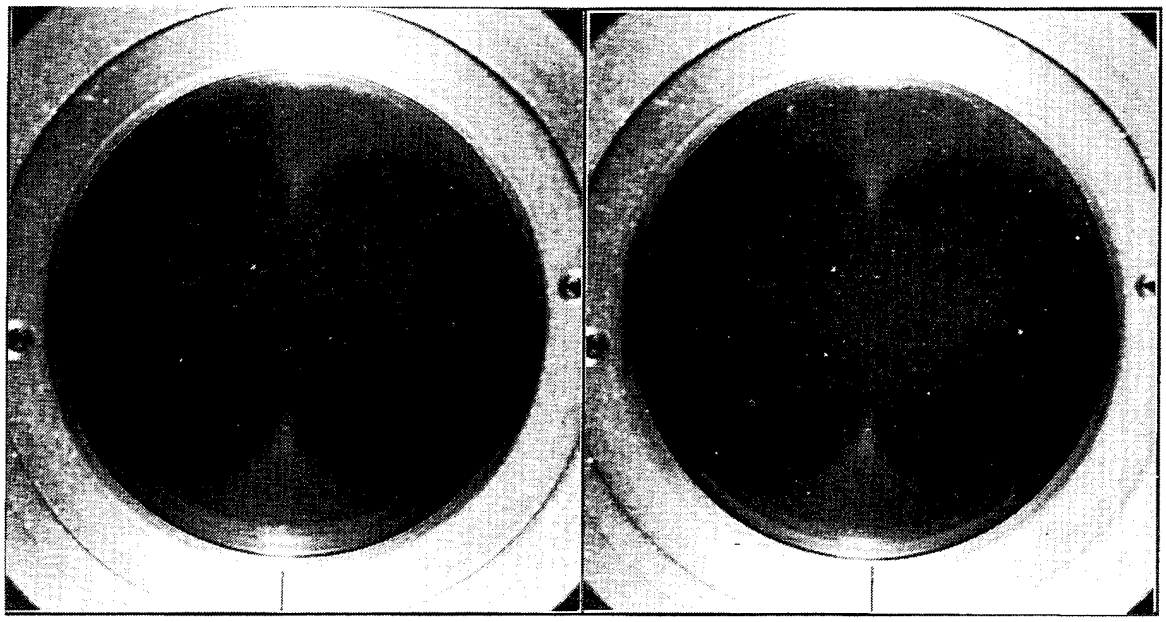

0 min @ 252 m/s

1.0 min @ 252 m/s

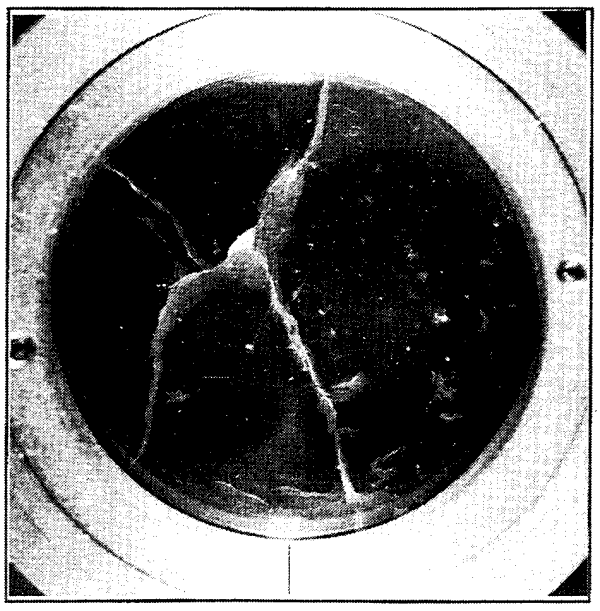

3.0 min @ 252 m/s

FIGURE 20. Whirling Arm Rain Exposure of DAR-1/REP/ms-ZnS (Sample 3) in Run 9 at 252 m/s in a 25.4 mm/h Rainfall of 2-mm-Diameter Drops at Perpendicular Incidence. This sample was exposed to 500°C for measuring optical properties prior to the rain erosion test.

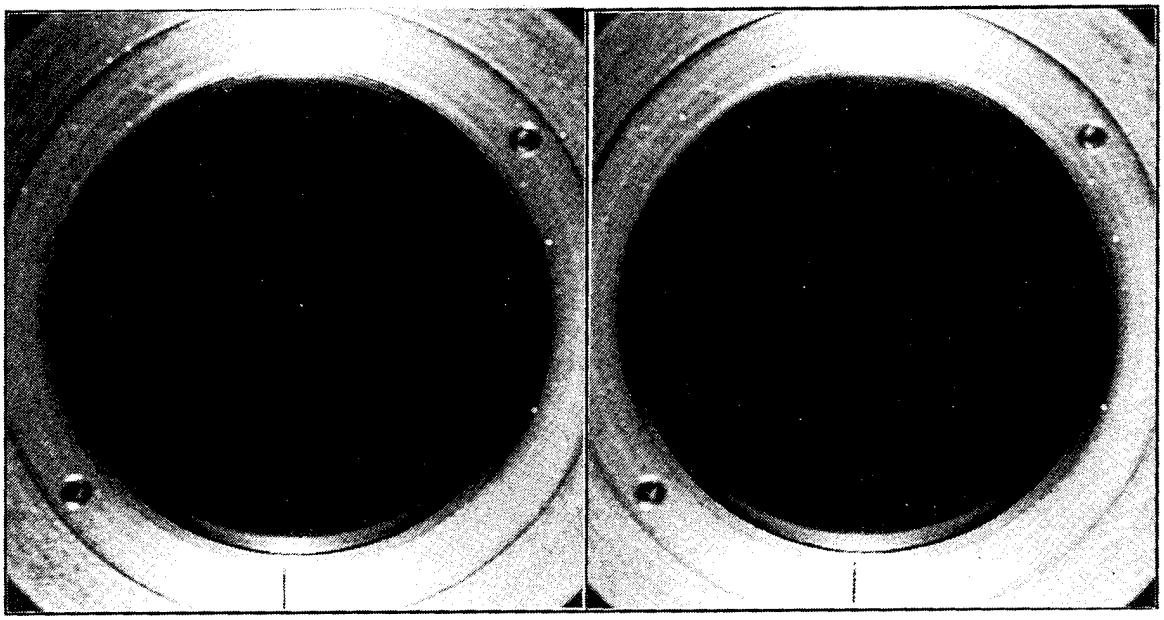

0 min @ 252 m/s

1.0 min @ 252 m/s

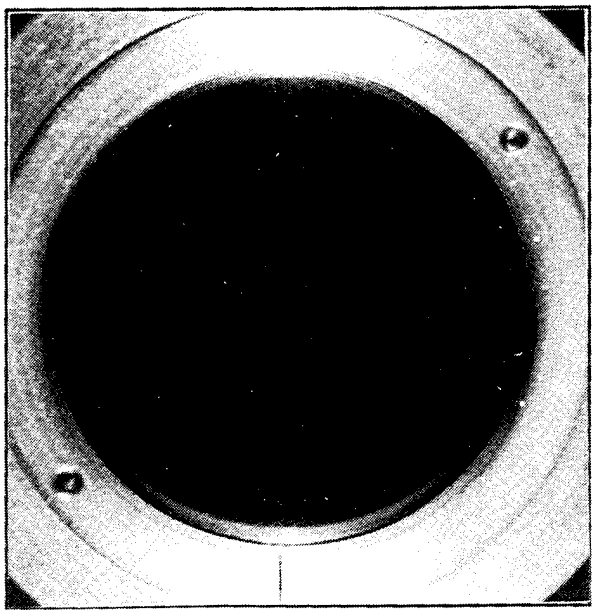

3.0 min @ 252 m/s

FIGURE 21. Whirling Arm Rain Exposure of BP/ms-ZnS (Sample CL11) in Run 9 at 252 m/s in a 25.4 mm/h Rainfall of 2-mm-Diameter Drops at Perpendicular Incidence.

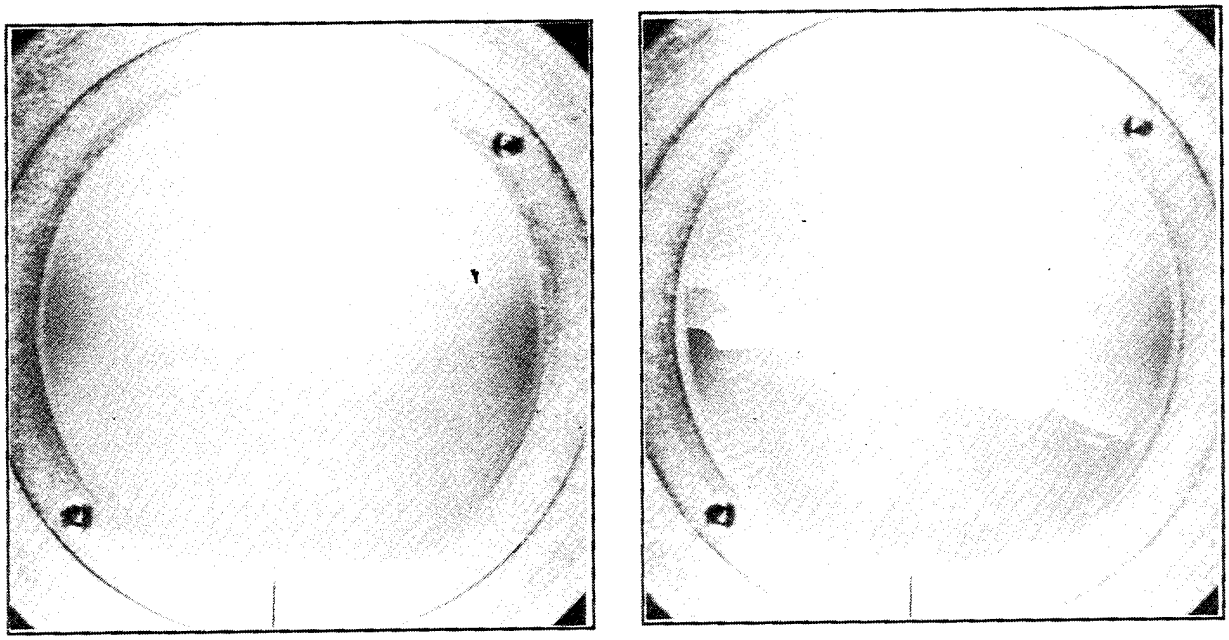

0 min @ 252 m/s 8.4 min @ 252 m/s

FIGURE 22. Whirling Arm Rain Exposure of MgF_2 (Sample 4) in Run 10 at 252 m/s in a 25.4 mm/h Rainfall of 2-mm-Diameter Drops at Perpendicular Incidence.

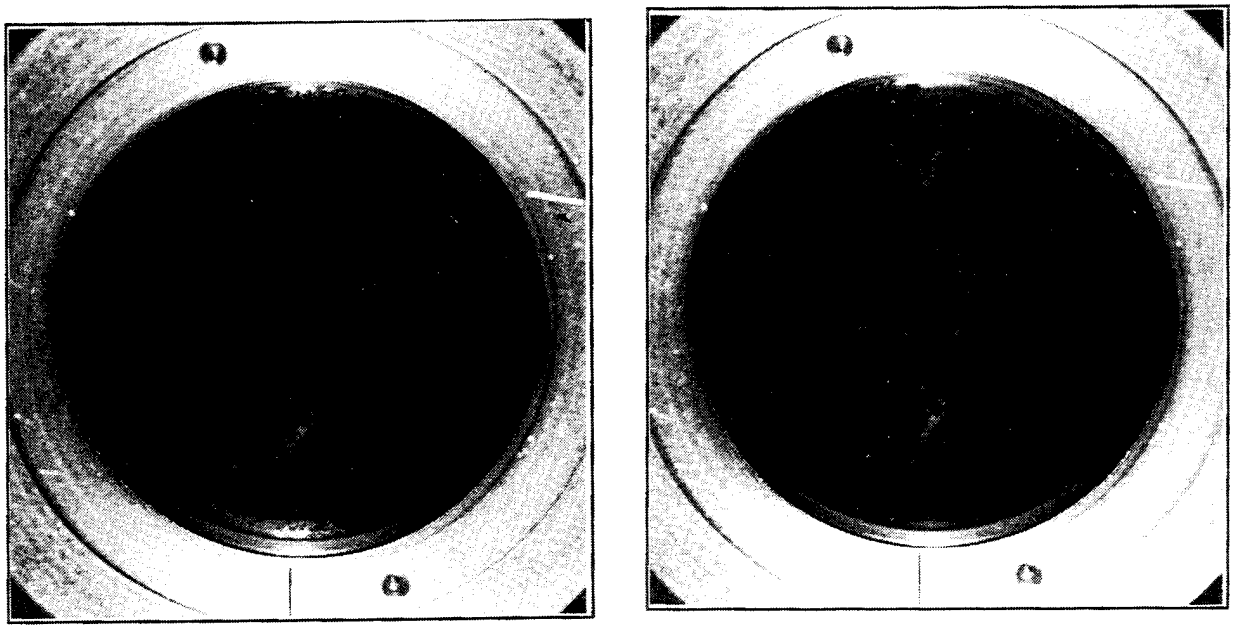

0 min @ 252 m/s 8.4 min @ 252 m/s

FIGURE 23. Whirling Arm Rain Exposure of Single Crystal Sapphire in Run 10 at 252 m/s in a 25.4 mm/h Rainfall of 2-mm-Diameter Drops at Perpendicular Incidence. The Crystal Systems disk (90° cut?, 5.1 mm thick) had been subjected to whirling arm rain erosion testing at the Naval Air Development Center (Warminster, Pennsylvania) for 20 min at a speed of 500 mph at a 13 mm/h rain rate of 2-mm-diameter drops in 1990. The disk had no damage evident to the naked eye from the previous test.

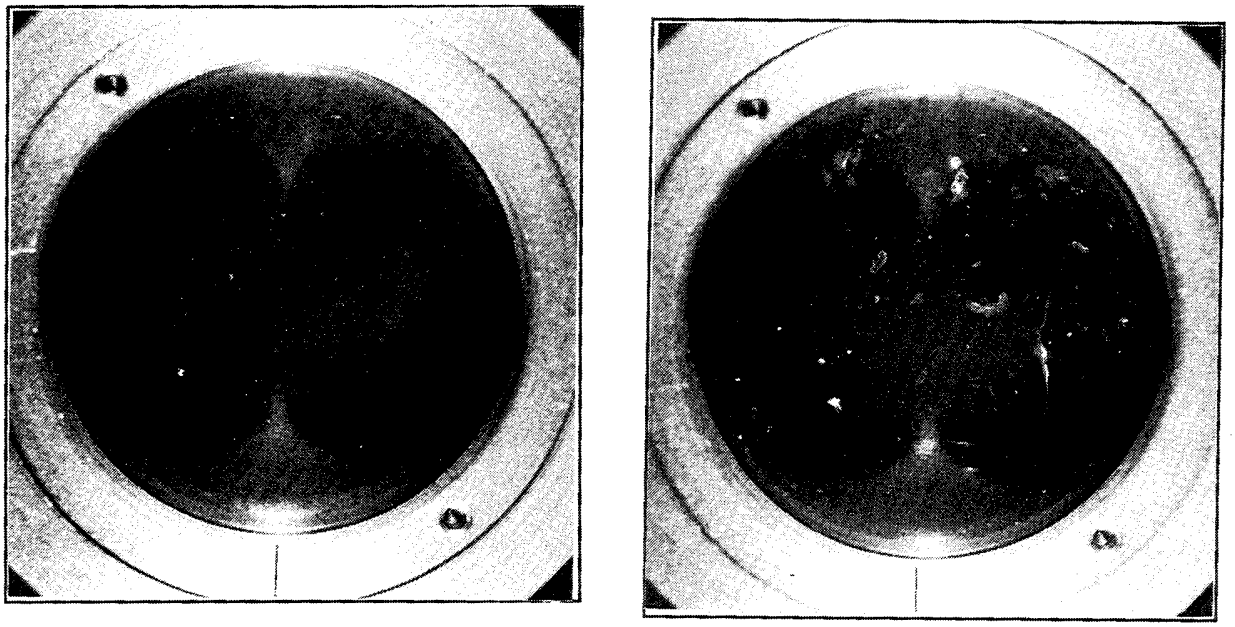

0 min @ 252 m/s 3.0 min @ 252 m/s

FIGURE 24. Whirling Arm Rain Exposure of DAR-1/REP/ms-ZnS (Sample 4) in Run 11 at 252 m/s in a 25.4 mm/h Rainfall of 2-mm-Diameter Drops at Perpendicular Incidence.

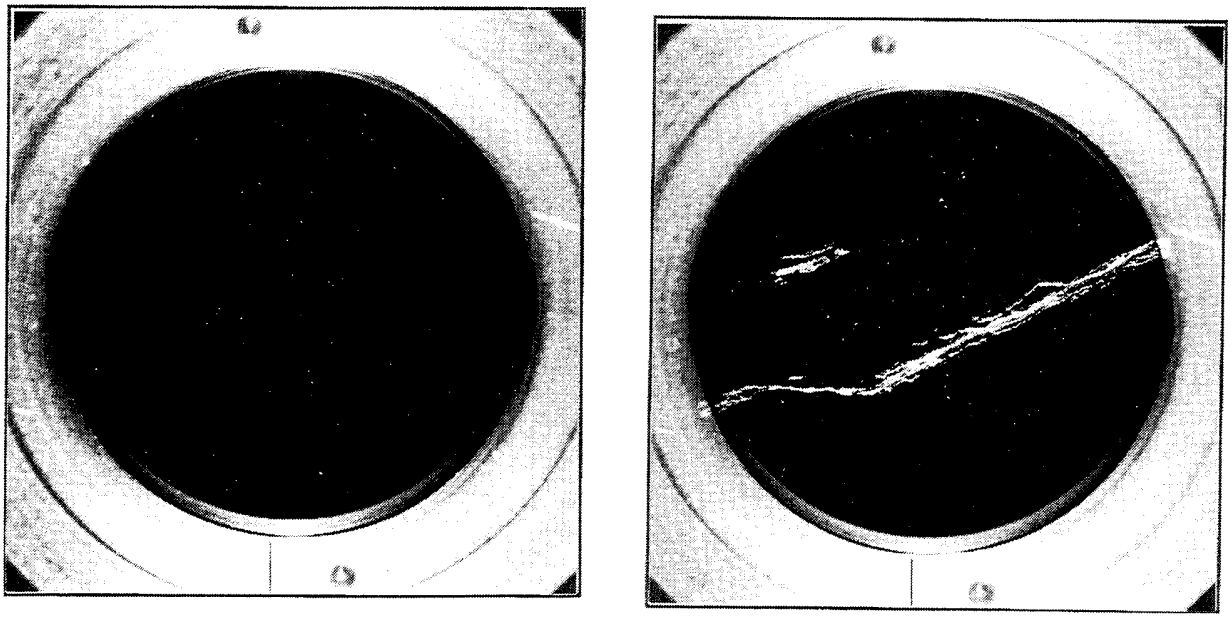

0 min @ 252 m/s 3.0 min @ 252 m/s

FIGURE 25. Whirling Arm Rain Exposure of BP/ms-ZnS (Sample CL12) in Run 11 at 252 m/s in a 25.4 mm/h Rainfall of 2-mm-Diameter Drops at Perpendicular Incidence.

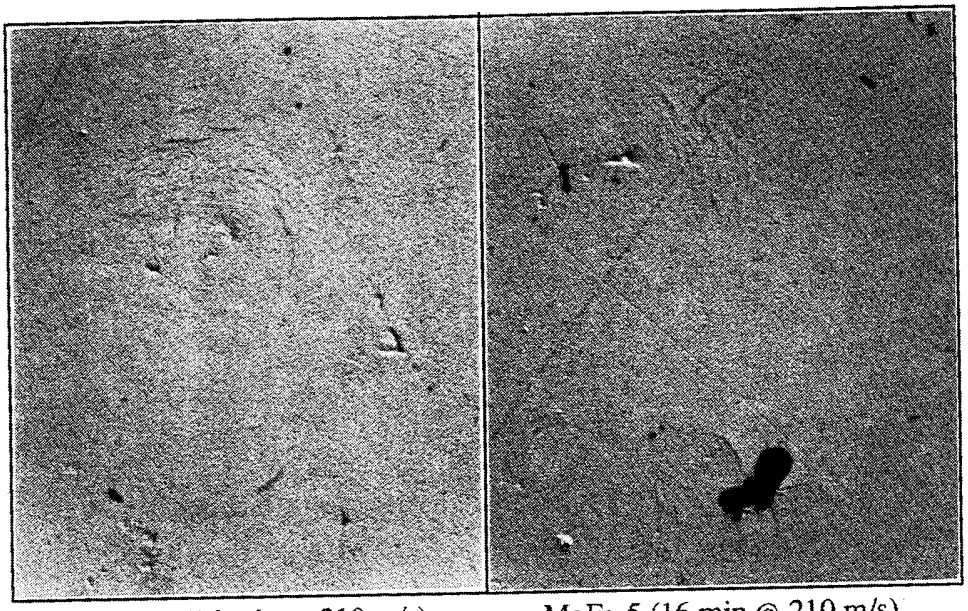

MgF_2-5 (16 min @ 210 m/s)
Nomarski micrograph (93×)
Ring fracture

MgF_2-5 (16 min @ 210 m/s)
Nomarski micrograph (93×)
Material removal

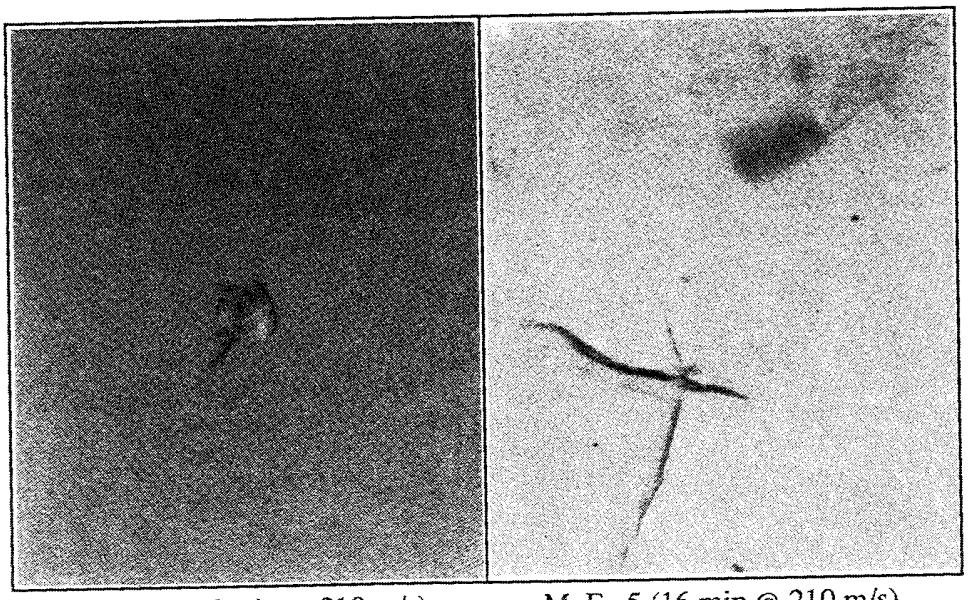

MgF_2-5 (16 min @ 210 m/s)
Transmission micrograph (70×)
Impact fracture

MgF_2-5 (16 min @ 210 m/s)
Transmission micrograph (70×)
Subsurface damage?

FIGURE 26. Micrographs of MgF_2 Showing Rain Impact Damage Sites From Whirling Arm Experiments.

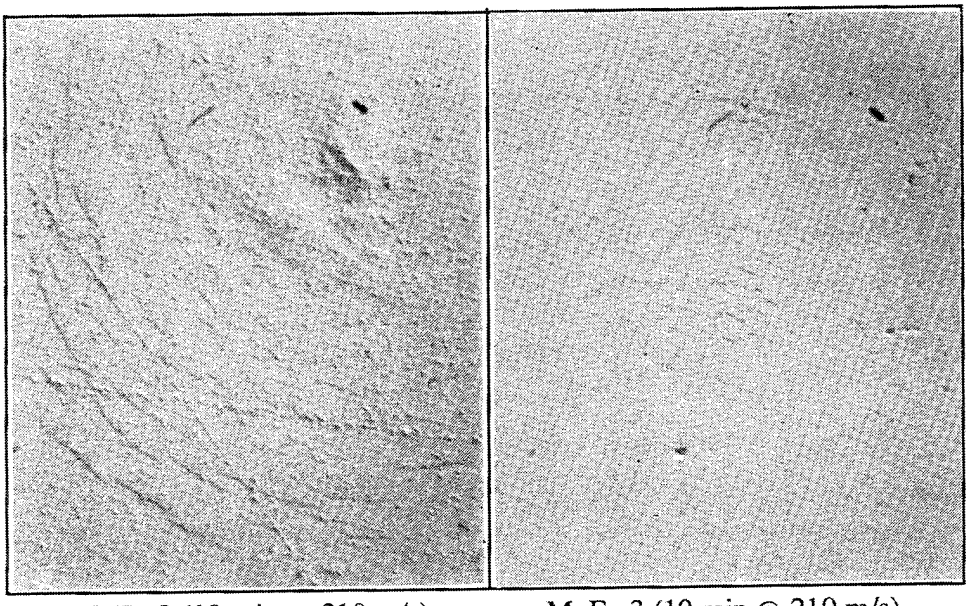

MgF_2-2 (10 min @ 210 m/s)
Nomarski micrograph (360×)
Ring fracture

MgF_2-3 (10 min @ 210 m/s)
Nomarski micrograph (93×)
Ring fracture

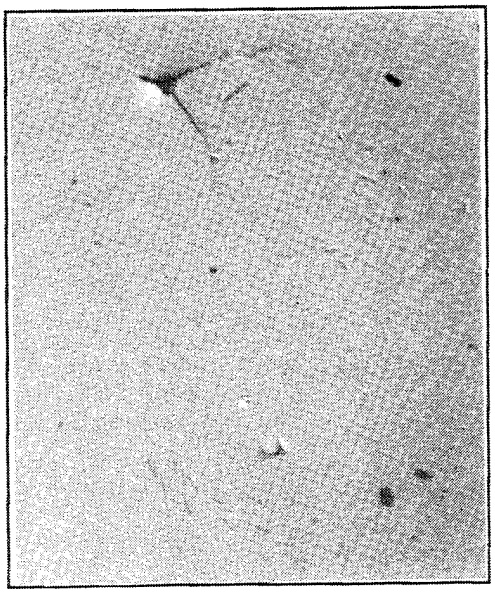

MgF_2-4 (8.4 min @ 252 m/s)
Nomarski micrograph (93×)
Ring and impact fracture

FIGURE 27. Micrographs of MgF_2 Showing Rain Impact Damage Sites From Whirling Arm Experiments.

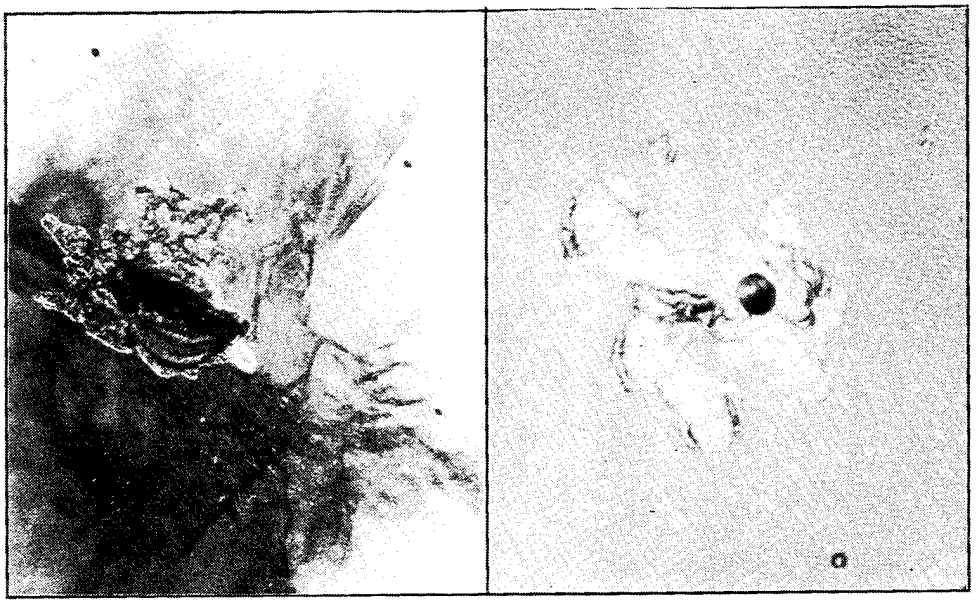

DAR/REP-2 (10 min @ 210 m/s)
Nomarski micrograph (93×)
Surface/subsurface damage/delamination

DAR/REP-2 (10 min @ 210 m/s)
Nomarski micrograph (360×)
Coating delamination

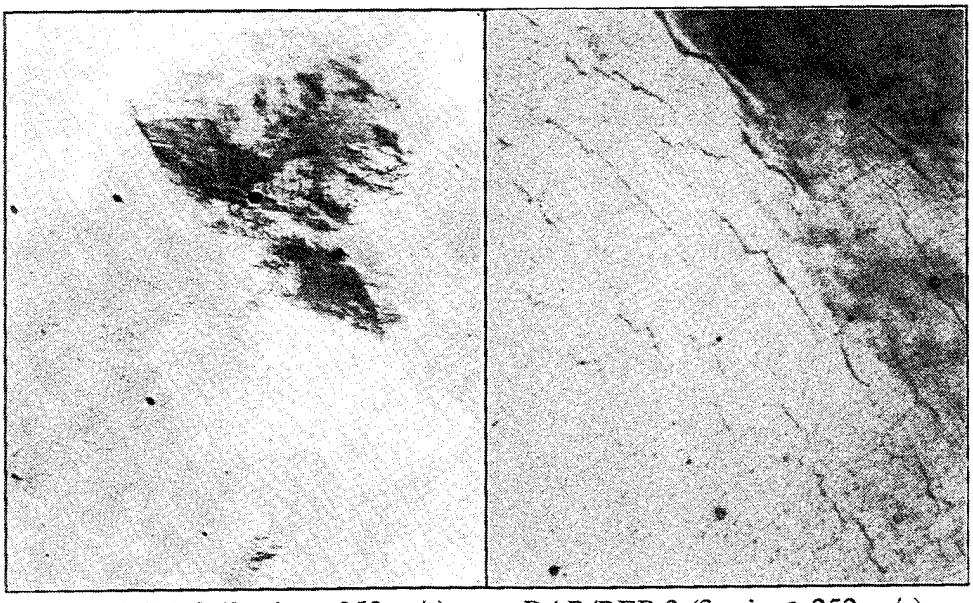

DAR/REP-3 (3 min @ 252 m/s)
Nomarski micrograph (93×)
Surface and subsurface damage

DAR/REP-3 (3 min @ 252 m/s)
Nomarski micrograph (360×)
Surface cracks

FIGURE 28. Micrographs of ZnS-Coated ms-ZnS Showing Rain Impact Damage Sites From Whirling Arm Experiments.

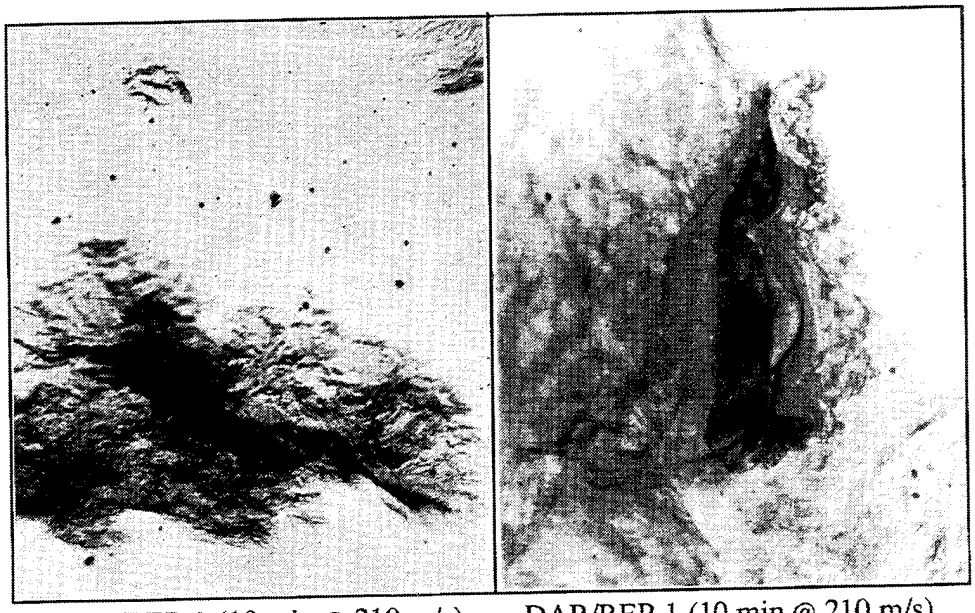

DAR/REP-1 (10 min @ 210 m/s)
Transmission micrograph (50×)
Subsurface damage

DAR/REP-1 (10 min @ 210 m/s)
Nomarski micrograph (93×)
Material removal

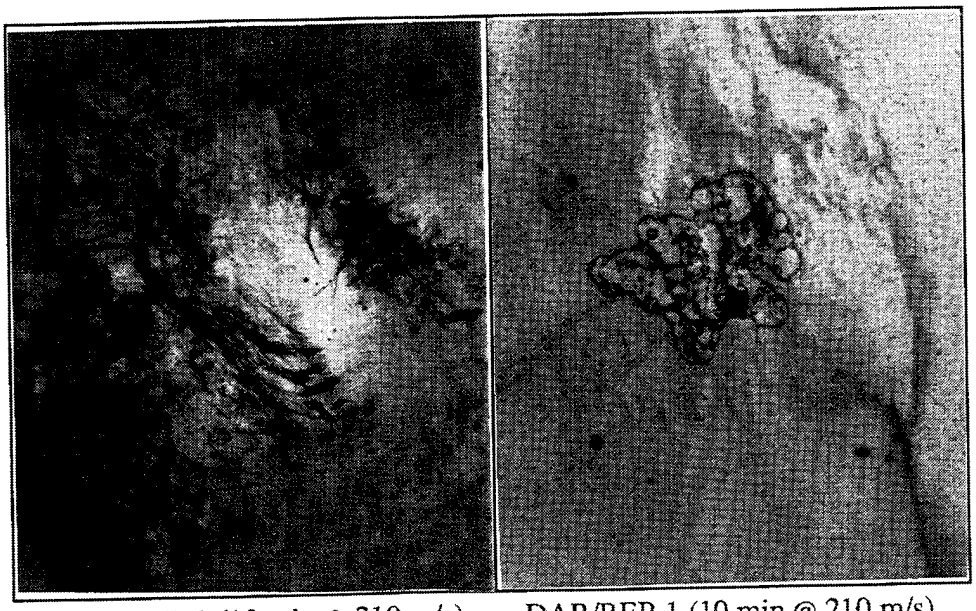

DAR/REP-1 (10 min @ 210 m/s)
Nomarski micrograph (93×)
Surface and subsurface damage

DAR/REP-1 (10 min @ 210 m/s)
Nomarski micrograph (360×)
Coating delamination

FIGURE 29. Micrographs of ZnS-Coated ms-ZnS Showing Rain Impact Damage Sites From Whirling Arm Experiments.

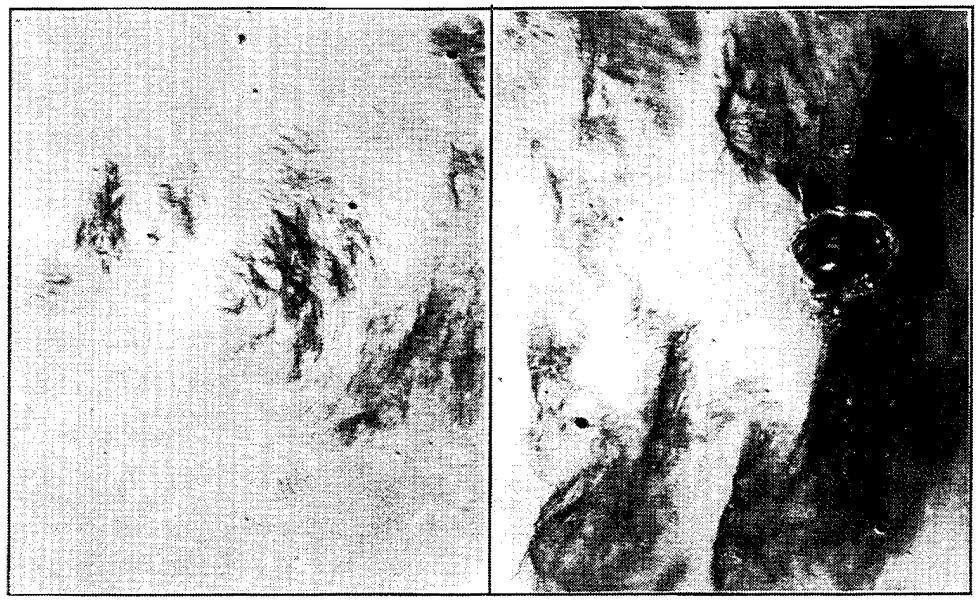

DAR/REP-4 (3 min @ 252 m/s)
Nomarski micrograph (93×)
Surface and subsurface damage

DAR/REP-4 (3 min @ 252 m/s)
Nomarski micrograph (93×)
Surface and subsurface damage

FIGURE 30. Micrographs of ZnS-Coated ms-ZnS Showing Rain Impact Damage Sites From Whirling Arm Experiments.

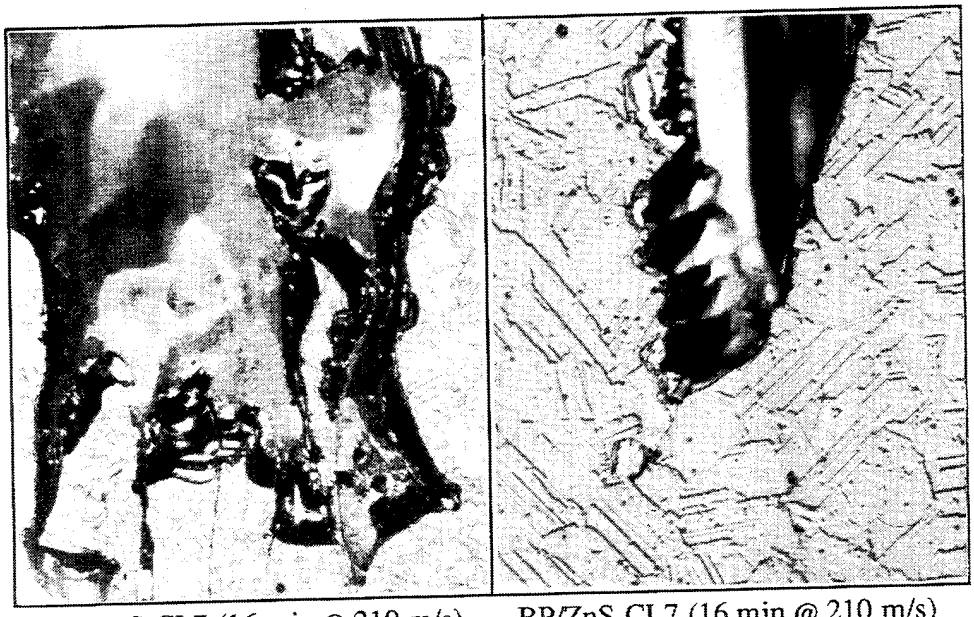

BP/ZnS-CL7 (16 min @ 210 m/s)
Nomarski micrograph (93×)
Material removal/ little delamination

BP/ZnS-CL7 (16 min @ 210 m/s)
Nomarski micrograph (360×)
Material removal

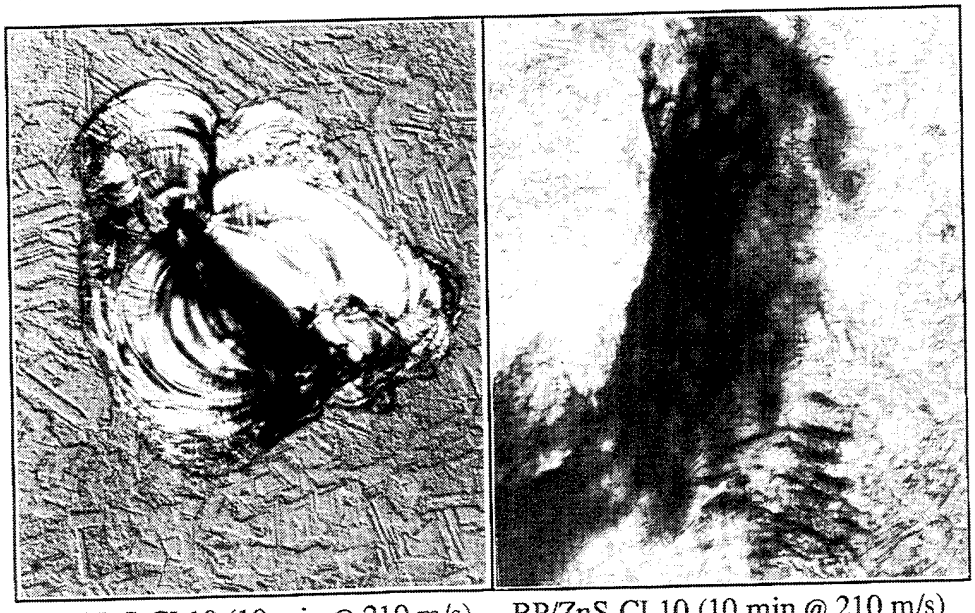

BP/ZnS-CL10 (10 min @ 210 m/s)
Nomarski micrograph (180×)
Impact site

BP/ZnS-CL10 (10 min @ 210 m/s)
Subsurface damage (93×)
viewed through back side

FIGURE 31. Micrographs of BP-Coated ms-ZnS Showing Rain Impact Damage Sites From Whirling Arm Experiments.

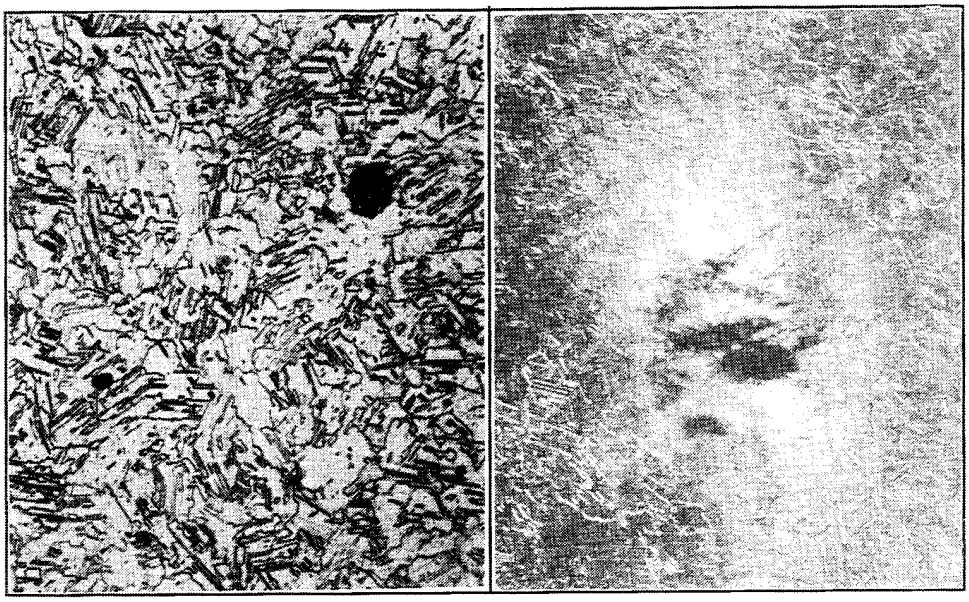

BP/ZnS-CL11 (3 min @ 252 m/s)
Nomarski micrograph (93×)
Impact site

BP/ZnS-CL11 (3 min @ 252 m/s)
Subsurface damage (93×)
viewed through back side

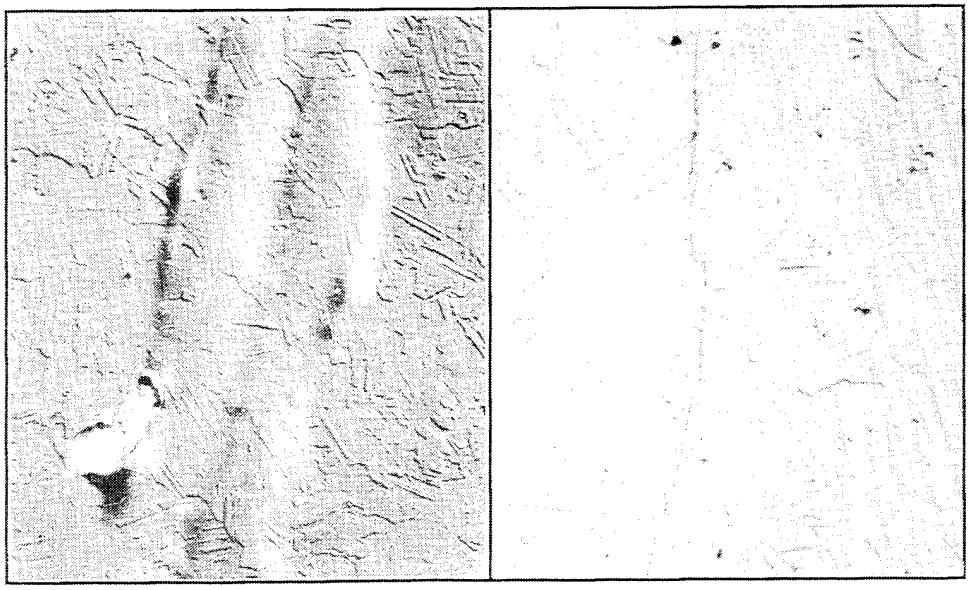

BP/ZnS-CL12 (3 min @ 252 m/s)
Nomarski micrograph (93×)
Subsurface cracking

BP/ZnS-CL12 (3 min @ 252 m/s)
Nomarski micrograph (93×)
Subsurface and surface cracking

FIGURE 32. Micrographs of BP-Coated ms-ZnS Showing Rain Impact Damage Sites From Whirling Arm Experiments.

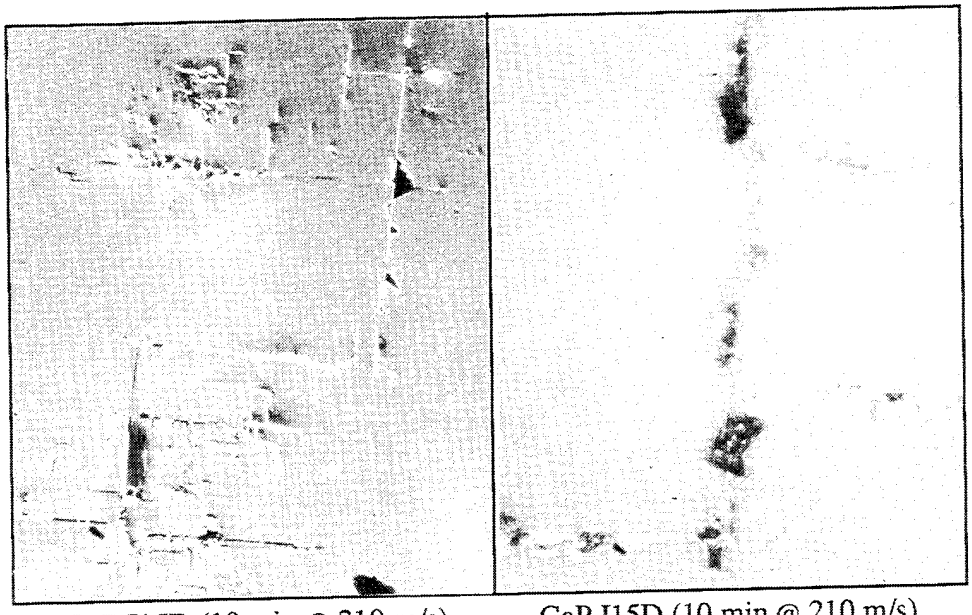

GaP I15D (10 min @ 210 m/s)
Nomarski micrograph (93×)
Orthogonal cracking / material loss

GaP I15D (10 min @ 210 m/s)
Subsurface damage (360×)
Orthogonal cracking / material loss

GaP I15D (10 min @ 210 m/s)
Transmission micrograph (59×)
Subsurface damage

FIGURE 33. Micrographs of Antireflection-Coated Bulk GaP Showing Rain Impact Damage Sites From Whirling Arm Experiments.

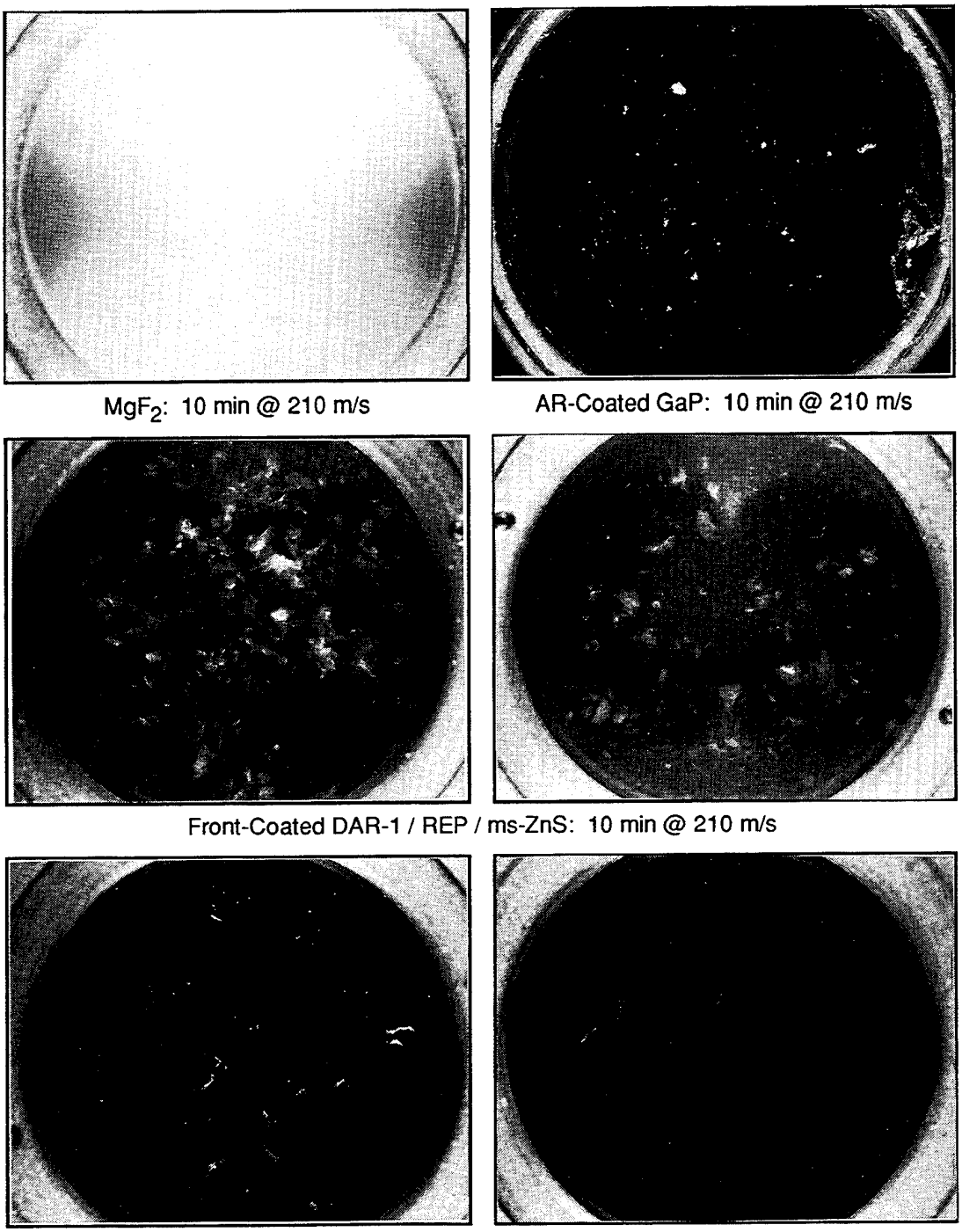

FIGURE 34. Summary of Representative Rain Erosion Results From Whirling Arm Facility at Wright Laboratory Using 2-mm-Diameter Drops at a Rain Rate of 25.4 mm/h.

MgF_2: 10 min @ 210 m/s
Nomarski micrograph (360x)
showing ring fracture

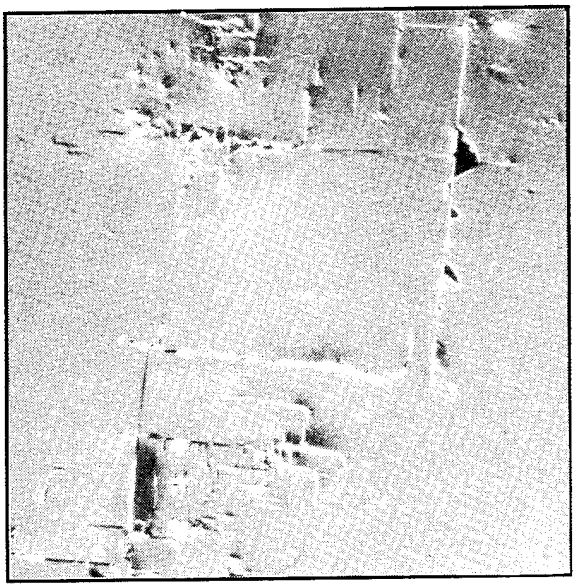

AR-Coated GaP: 10 min @ 210 m/s
Nomarski micrograph (93x) showing
orthogonal cracking and material loss

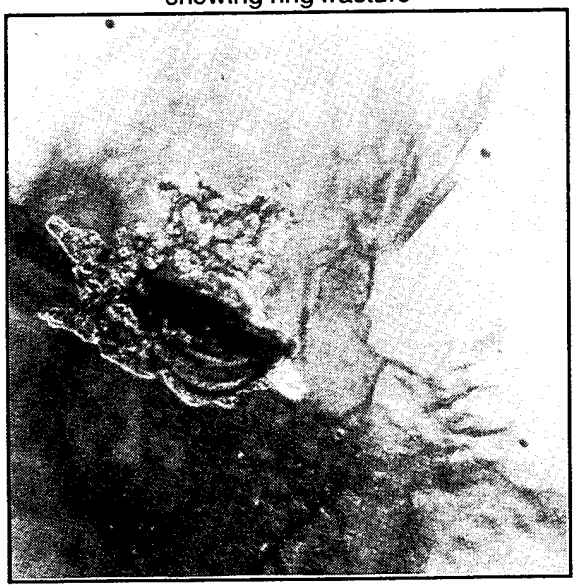

Front DAR-1 / REP / ms-ZnS: 10 min @ 210 m/s
Nomarski micrograph (93x)showing surface
and subsurface ring fracture and delamination

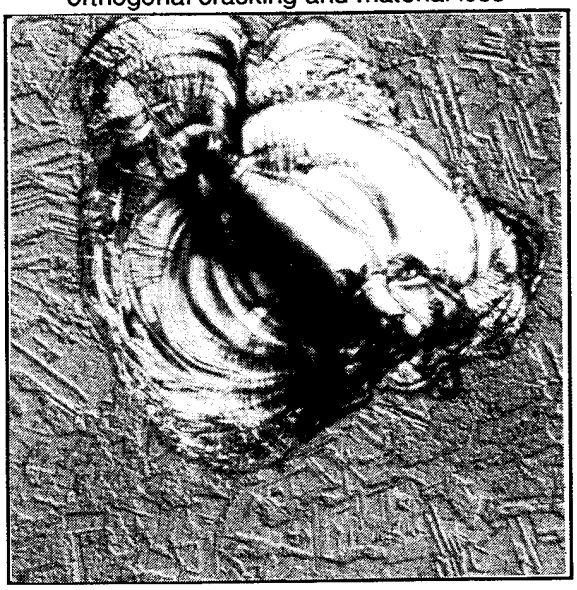

BP / ms-ZnS: 10 min @ 210 m/s
Nomarski micrograph (180x) showing conchoidal
impact site and texture of undamaged coating

FIGURE 35. Representative Micrographs of Samples From Whirling Arm Rain Impact Experiments.

Figure 36 illustrates the variation in material response from run to run. In the two experiments, ZnS-coated ms-ZnS and BP-coated ms-ZnS were run simultaneously in opposite ends of the whirling arm at 252 m/s (564 miles/h). Figure 37 shows that subsurface damage to BP-coated ms-ZnS that is not evident when viewed from the coated side can be seen when viewed through the transparent uncoated side.

The general conclusions from the rain erosion experiments are:

- None of the coated materials was as durable as bare MgF_2.
- BP/ms-ZnS is more durable than ZnS/ms-ZnS, but subsurface damage precedes coating damage in BP/ms-ZnS.
- Bulk GaP fractured on weak crystal planes and was not as durable as the other materials tested.

SAND EROSION

Sand erosion experiments were performed at Wright Laboratory using the equipment formerly located at PDA Engineering (Costa Mesa, California). Sand with a density near 2.75 g/cm^3 (measured by liquid displacement), obtained from Whitehead Brothers Co. (Florham Park, New Jersey), was sieved to obtain particles in the size range of 149 -177 μm, and another fraction with a size range of 0 to 38 μm. Sand from a screw feeder system was accelerated by a 6-mm-diameter compressed air jet and directed at normal incidence (90°) onto a flat specimen holder that could hold as many as 16 25-mm-diameter samples. Sand mass flow rate and velocity were established by prior calibration. The square specimen holder was rastered in a uniform manner such that its full 310 cm^2 area was exposed to the jet twice in 2 minutes. Exposure was measured in terms of milligrams of sand per square centimeter of sample area.

A speed of 75 m/s (148 knots) was chosen for relatively large particles (149-177 μm) to simulate the environment of an aircraft during takeoff and landing. A speed of 210 m/s (413 knots) was chosen for small particles (< 38 μm) to simulate aircraft cruising conditions. One set of samples was exposed simultaneously to the low speed conditions and a second set of samples was exposed to the high speed conditions.

After each exposure, each sample was weighed and its infrared transmission spectrum recorded. A reflection micrograph was recorded with a computer imaging system that printed the result at an effective magnification of 840x. Mass data was not consistent and is not reported. Due to equipment problems, most of the infrared transmission data was lost. We intended to average transmittance over a range of wavelengths (e.g., 3-5 μm) to document the degradation caused by sand erosion. Instead, where the data existed, measurements were made at a single wavelength in a region of the spectrum where there was no absorption band.

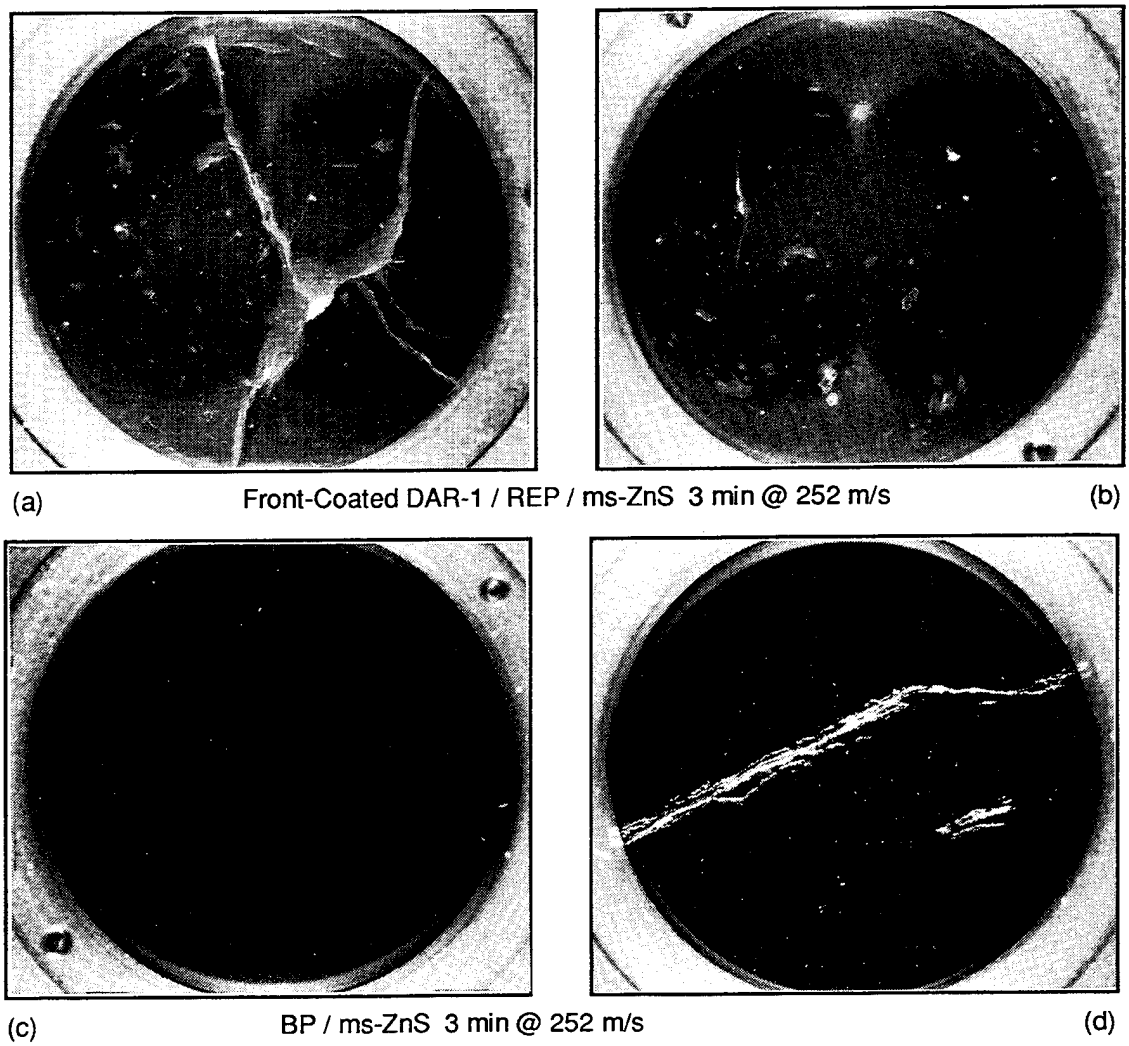

FIGURE 36. Comparison of Behavior of ZnS/ms-ZnS and BP/ms-ZnS in the Whirling Arm at 252 m/s. Samples (a) and (c) were run simultaneously and samples (b) and (d) were run simultaneously.

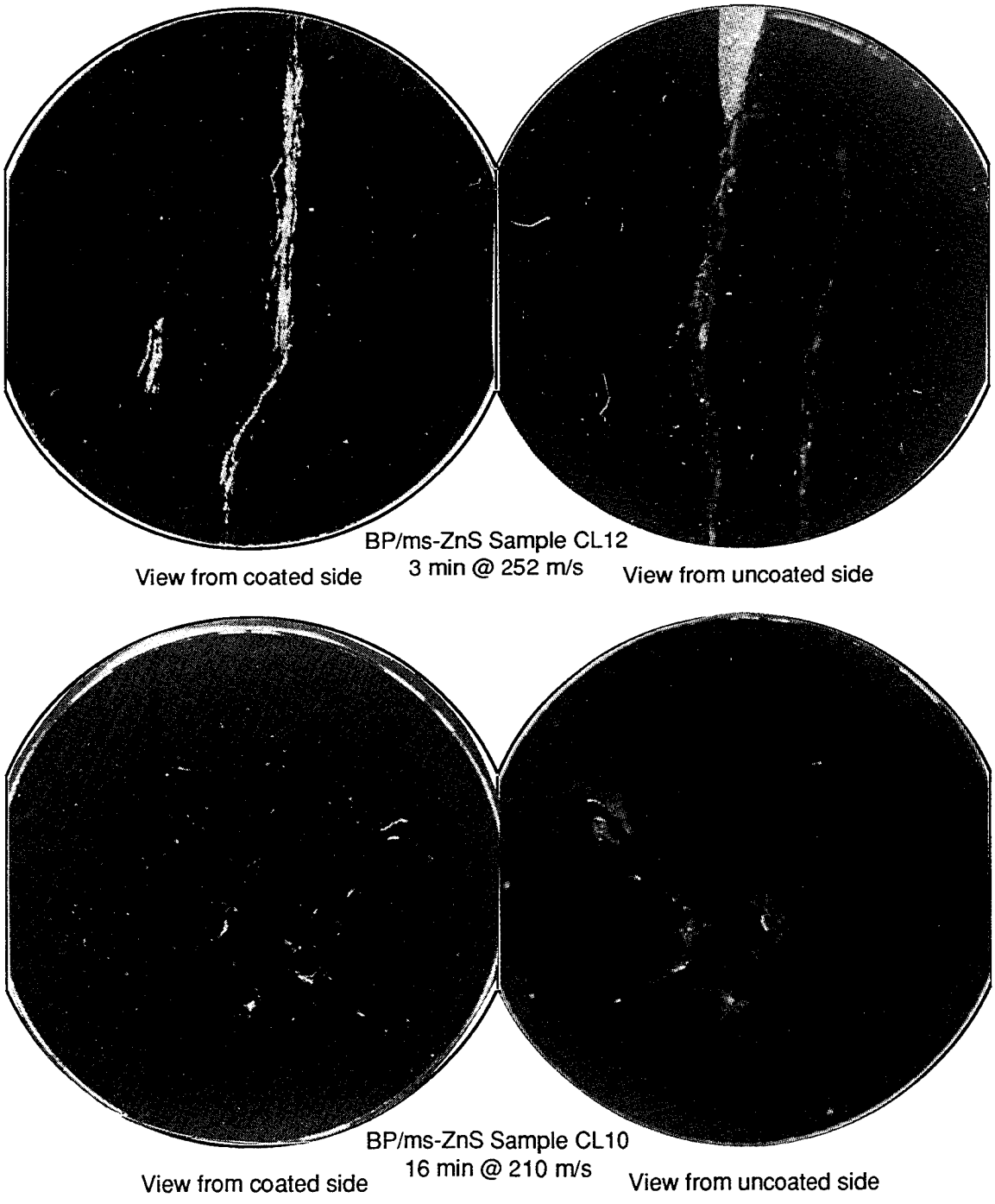

FIGURE 37. Front and Back Views of BP/ms-ZnS Samples After Exposure to Whirling Arm Rain Erosion. The backside view through the transparent ms-ZnS shows subsurface damage that is not evident when viewed through the opaque BP-coated side.

Figure 38 shows the relative loss in transmittance of each material measured in the midwave region in the low speed experiment (149-177 μm particles at 75 m/s). Corresponding data for the high speed experiment were lost. However, previous studies of MgF_2 and other materials indicate that high speed impact by fine particles (< 38 μm particles at 210 m/s) is even more damaging than the low speed conditions (Reference 9).

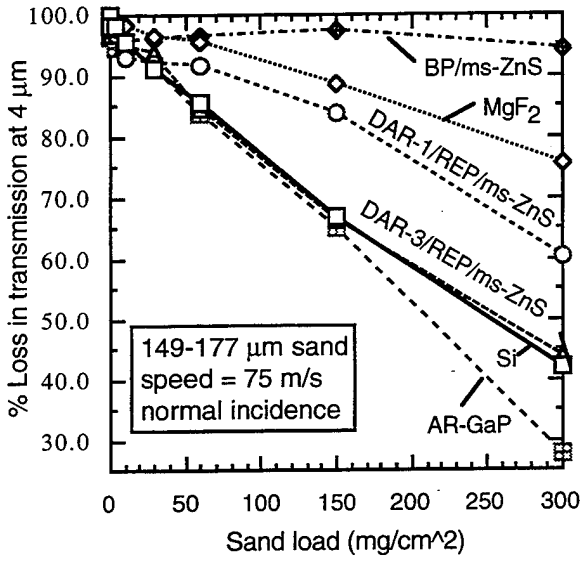

FIGURE 38. Relative Loss of Infrared Transmission vs. Cumulative Sand Loading in Erosion Tests. The ordinate gives the measured transmittance at 4.00-μm wavelength divided by the initial transmittance of the uneroded sample. The BP-coated sample was measured at 3.33 μm to avoid an absorption feature near 4 μm.

Figures 39 and 40 compare the erosion damage under the two sets of conditions on the different materials that were tested. Figures 41 through 52 show the progression of damage in individual samples.

The trends in sand erosion experiments are summarized as follows:

- BP/ZnS is the most durable of the tested materials with respect to sand erosion.
- MgF_2 is the second most durable material.
- The sand erosion durability of Raytheon's REP-coated ZnS depends on the outer antireflection coating. DAR-1 performed better than DAR-3.
- Single crystal silicon performed poorly and bulk GaP was even worse.

To add perspective to these observations, bare MgF_2 missile domes are severely eroded by sand. All of the materials in Figure 37 except BP/ZnS fare even worse than MgF_2.

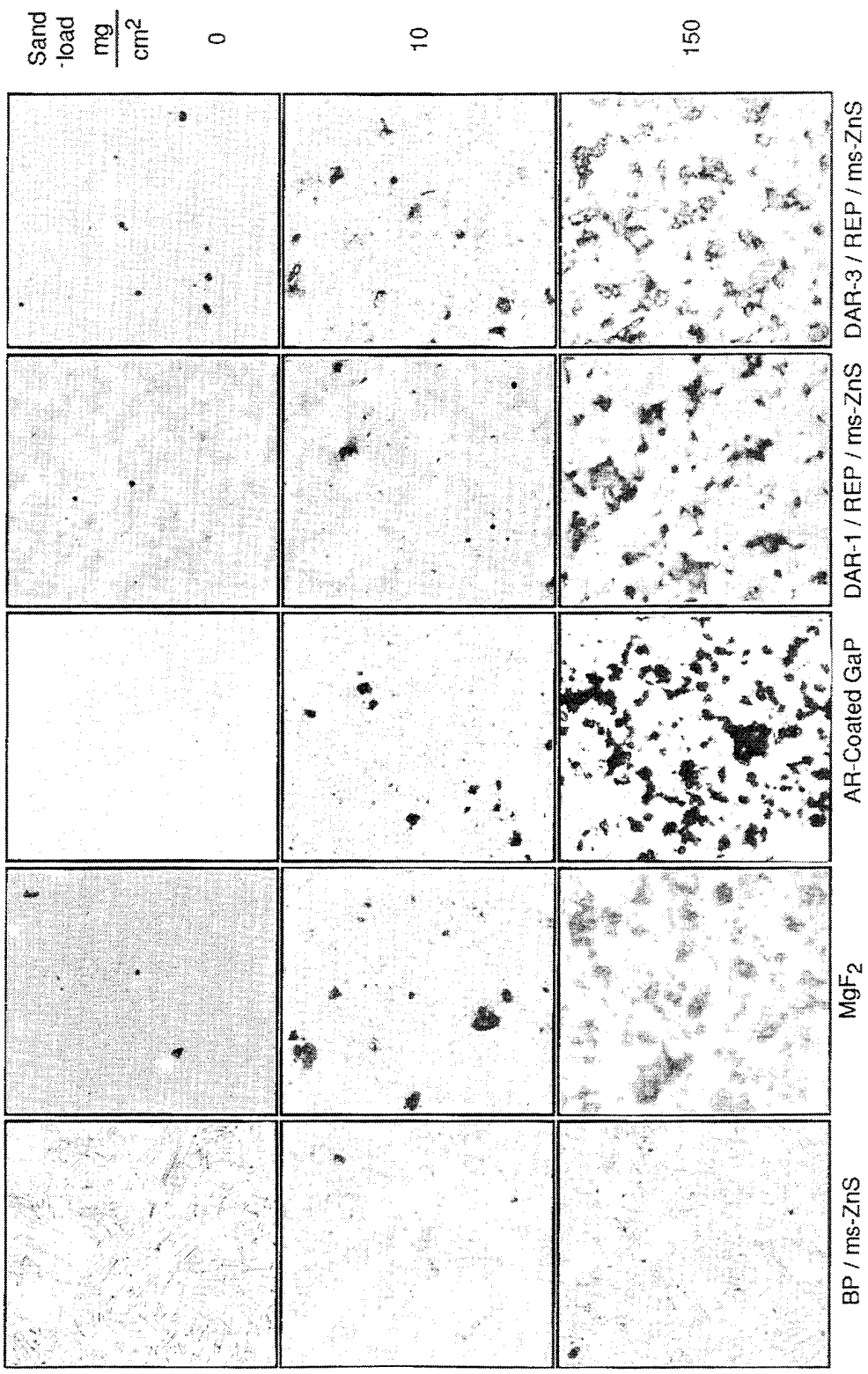

FIGURE 39. Micrographs of Window Materials at Different Stages of Exposure to 149-177 µm Sand Particles at 75 m/s at Normal Incidence.

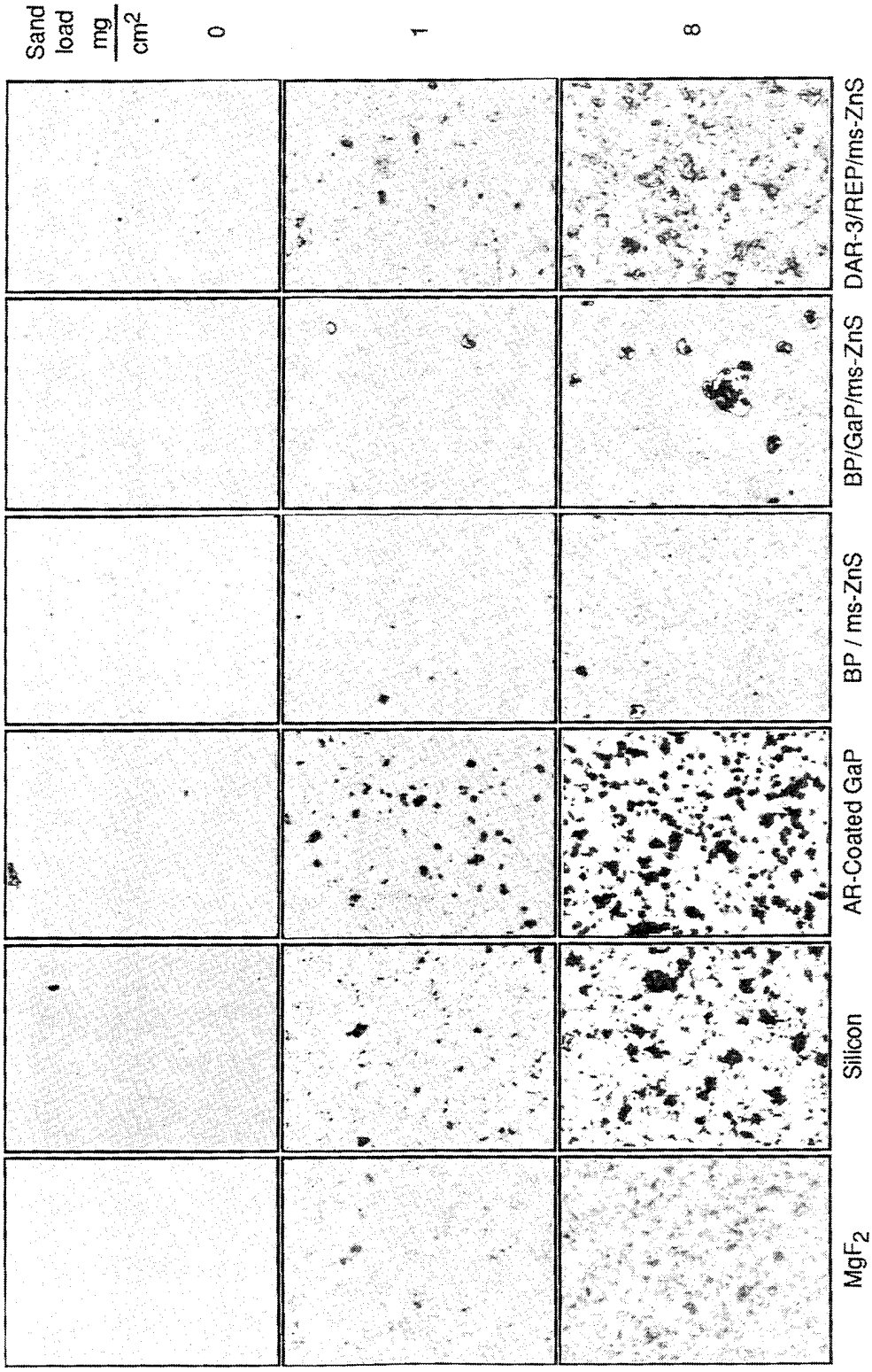

FIGURE 40. Micrographs of Window Materials at Different Stages of Exposure to < 38 µm Sand Particles at 210 m/s at Normal Incidence.

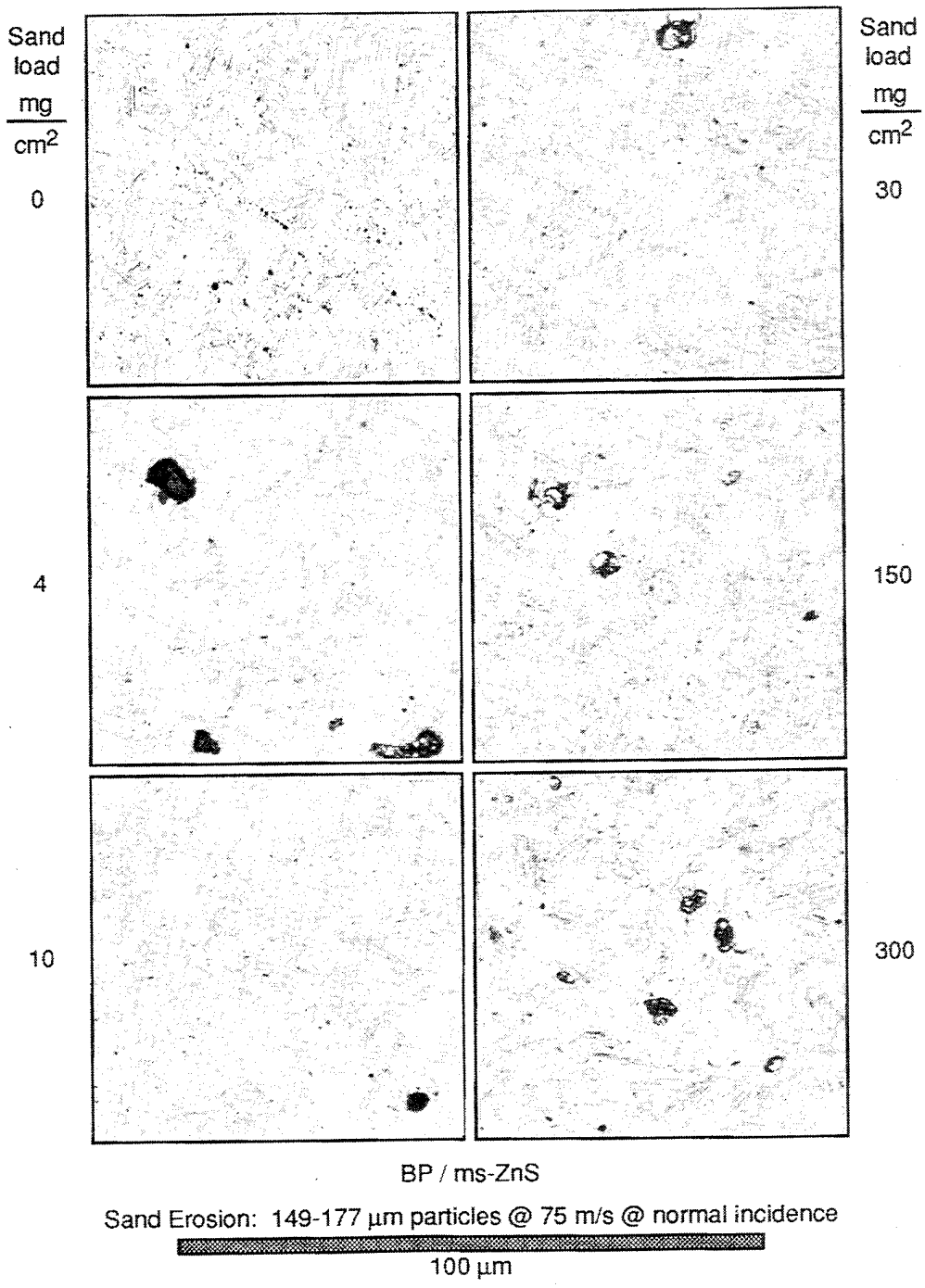

FIGURE 41. Micrographs of BP-Coated ms-ZnS (Sample CL5) at Different Stages of Exposure to 149-177 µm Sand Particles at 75 m/s at Normal Incidence. This sample had been exposed to 500°C for measuring infrared emission prior to the sand erosion test. The outer diamond-like carbon layer has probably burned off.

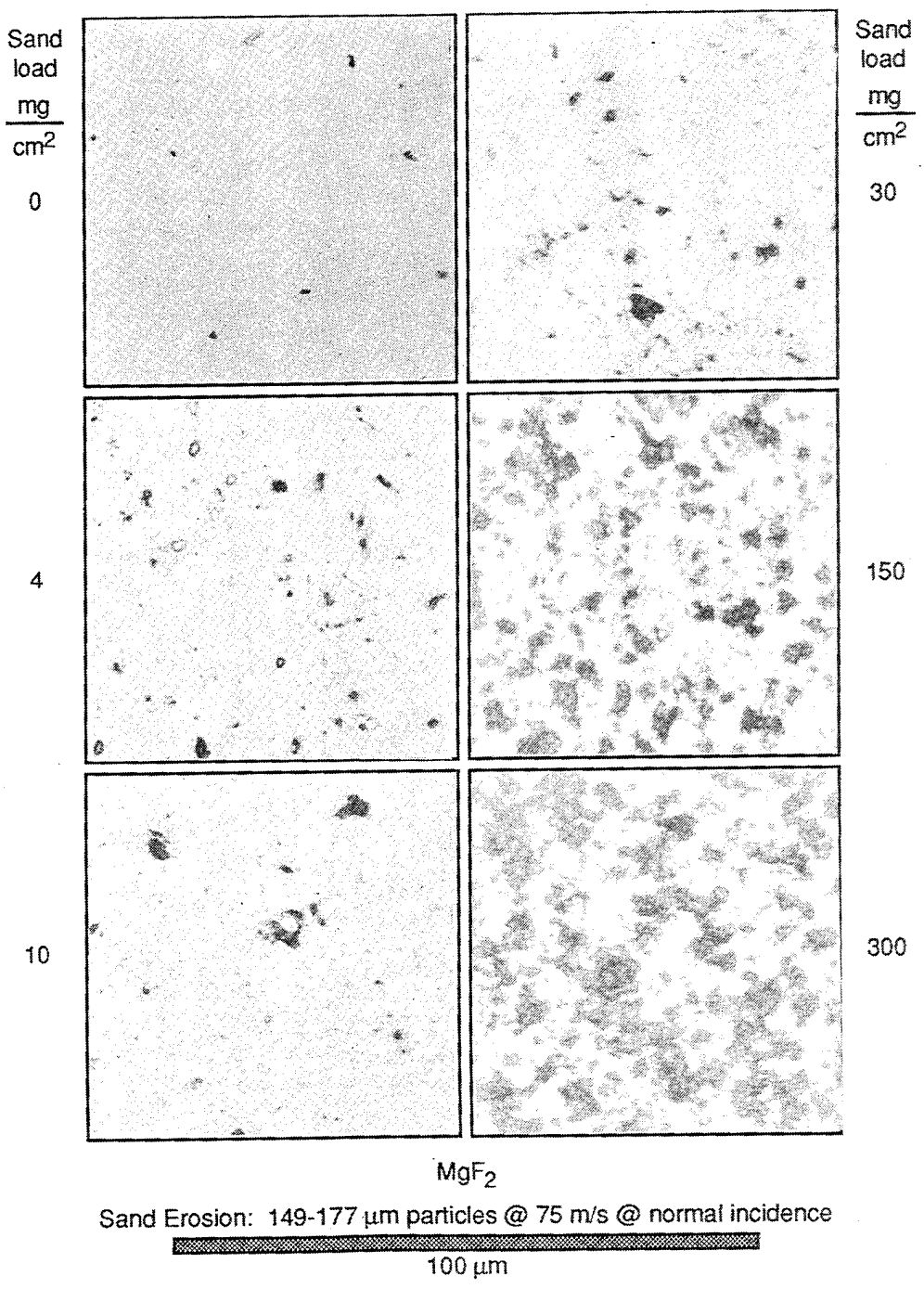

FIGURE 42. Micrographs of MgF_2 (Sample 6) at Different Stages of Exposure to 149-177 µm Sand Particles at 75 m/s at Normal Incidence.

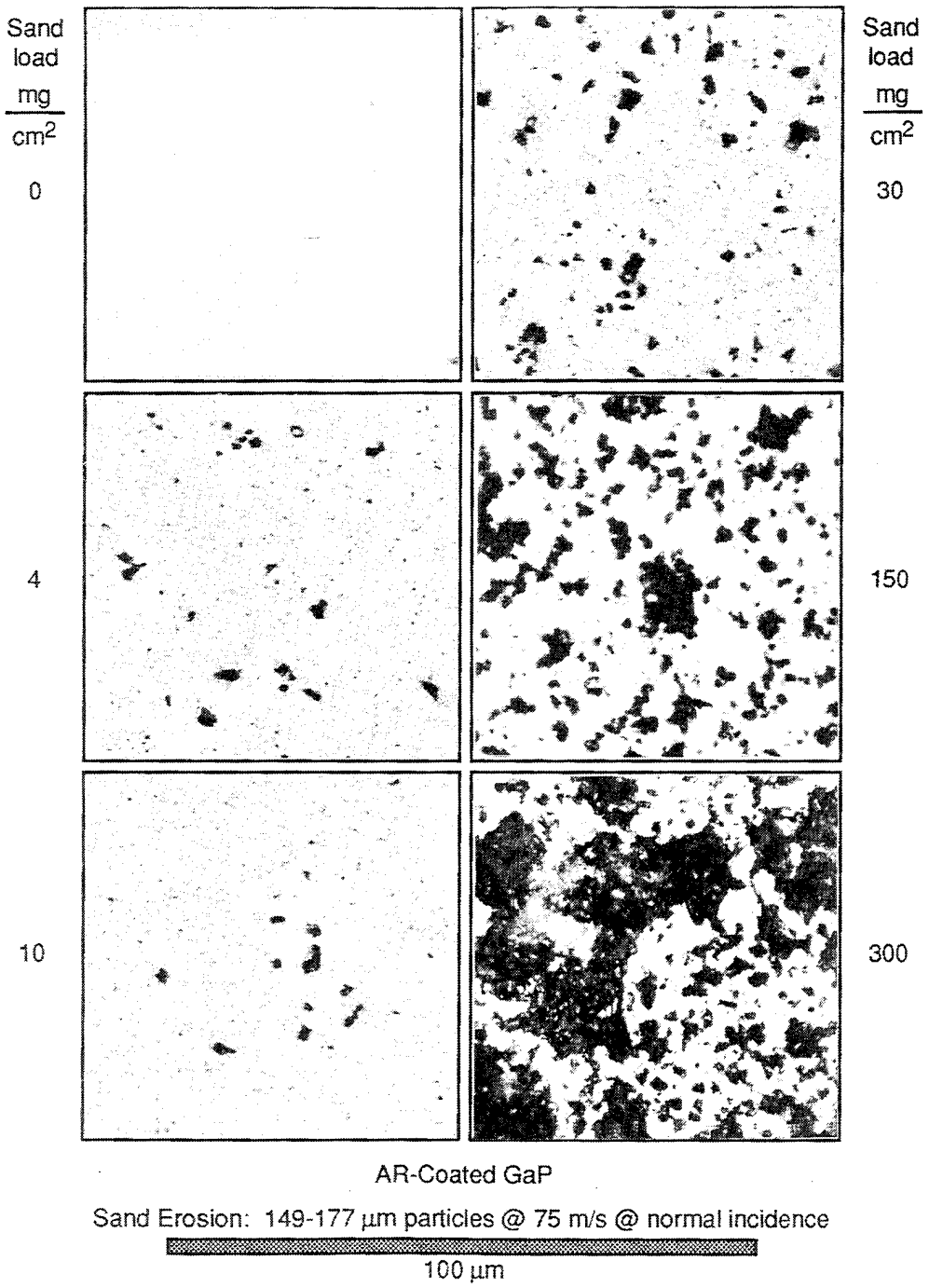

FIGURE 43. Micrographs of AR-Coated Bulk GaP (Sample I15-E) at Different Stages of Exposure to 149-177 μm Sand Particles at 75 m/s at Normal Incidence. This sample was exposed to 500°C for measuring infrared emission prior to the sand erosion test.

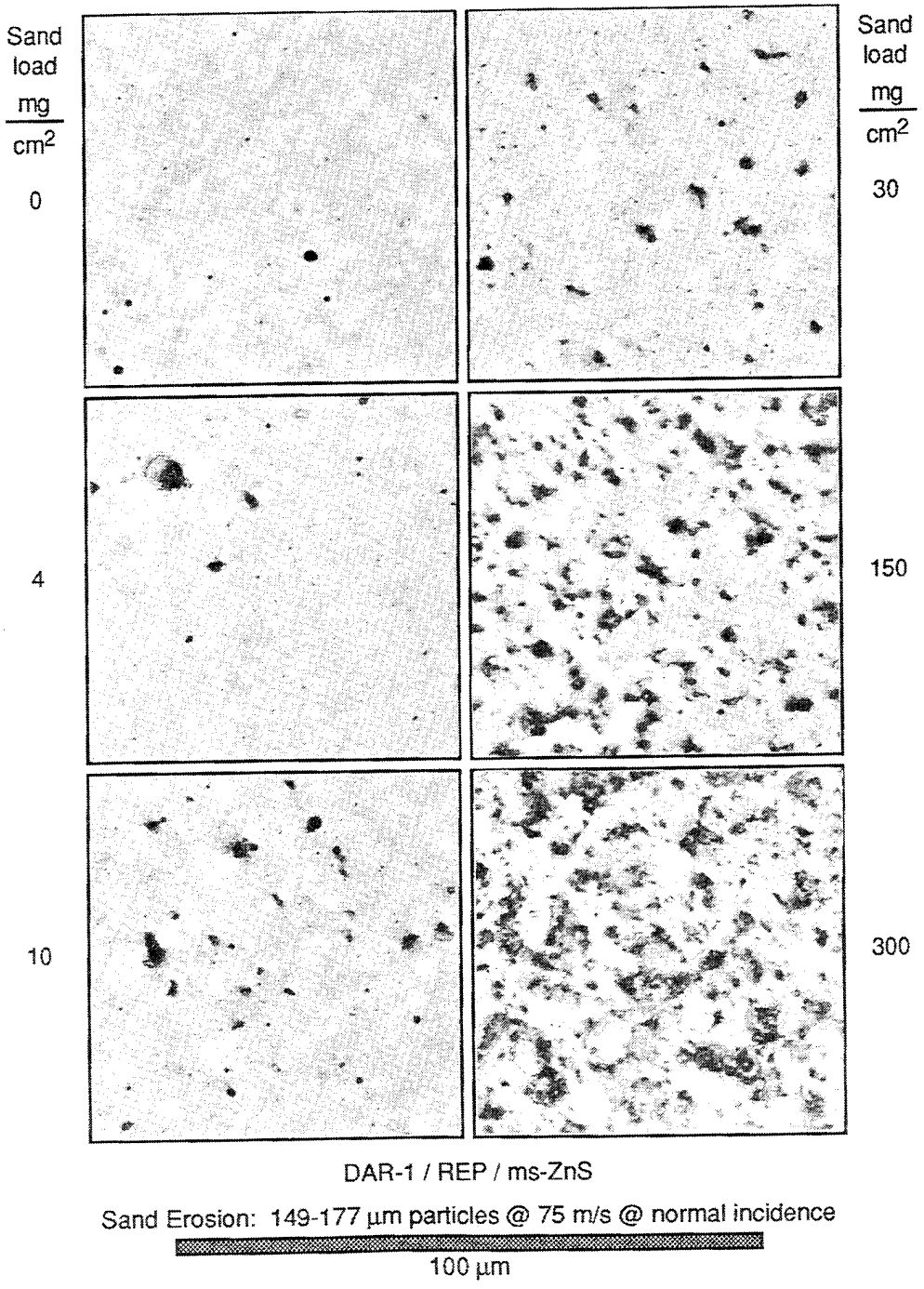

FIGURE 44. Micrographs of ZnS-Coated ms-ZnS (Sample 5) with the Outer Antireflection Coating Designated DAR-1 at Different Stages of Exposure to 149-177 µm Sand Particles at 75 m/s at Normal Incidence.

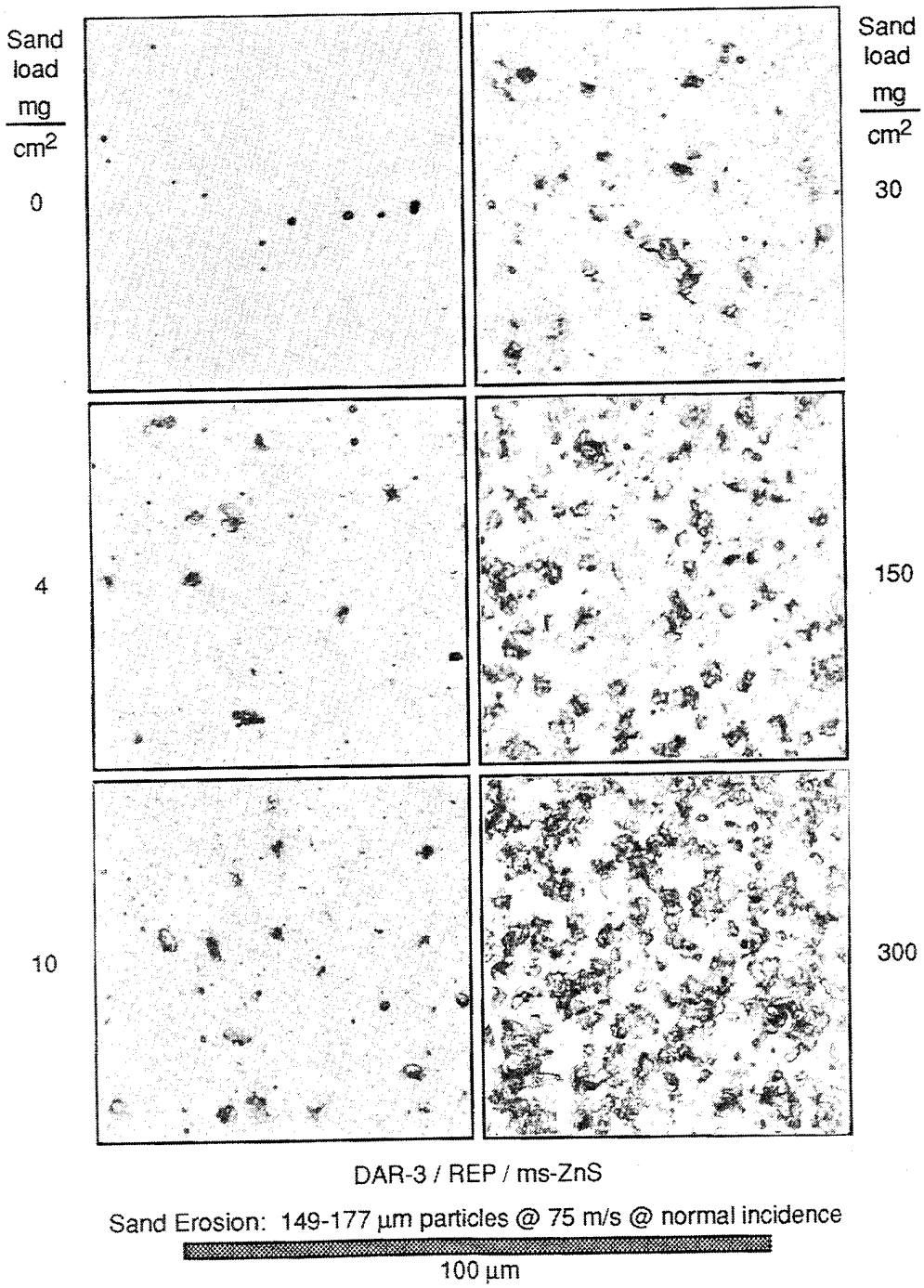

FIGURE 45. Micrographs of ZnS-Coated ms-ZnS (Sample 7) with the Outer Antireflection Coating Designated DAR-3 at Different Stages of Exposure to 149-177 µm Sand Particles at 75 m/s at Normal Incidence.

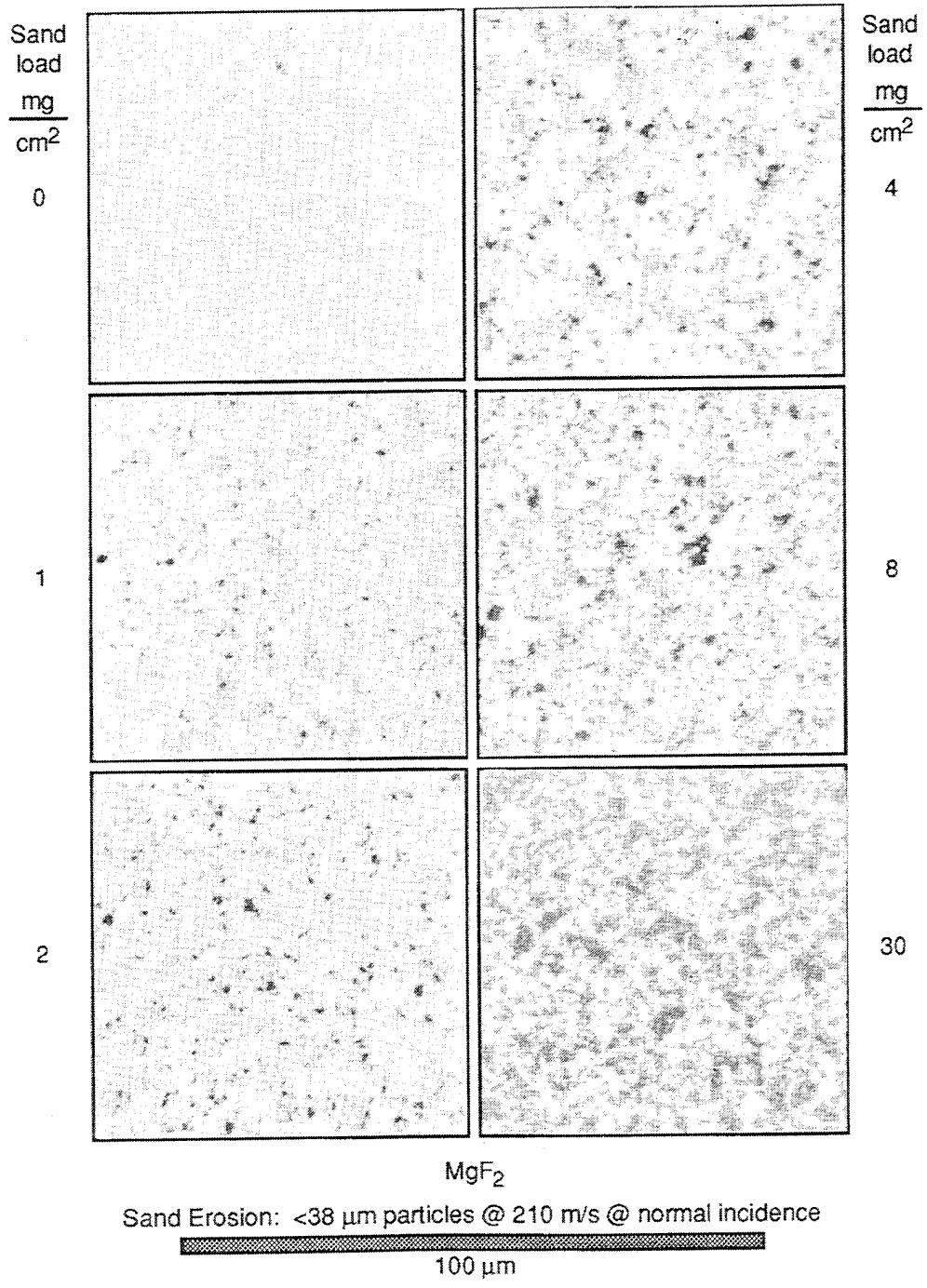

FIGURE 46. Micrographs of MgF_2 (Sample 7) at Different Stages of Exposure to < 38 µm Sand Particles at 210 m/s at Normal Incidence.

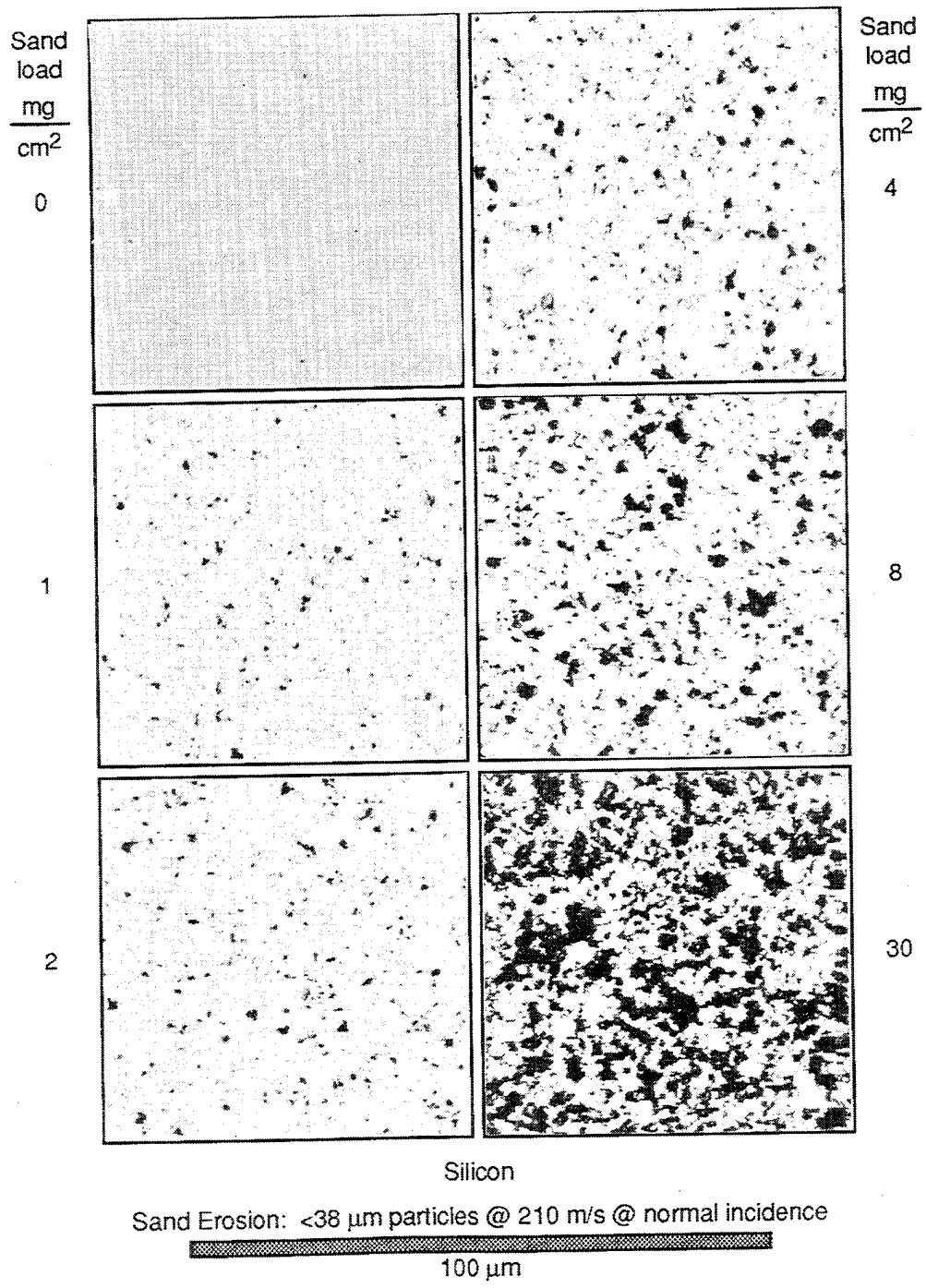

FIGURE 47. Micrographs of Single Crystal Silicon (Sample 1) at Different Stages of Exposure to < 38 µm Sand Particles at 210 m/s at Normal Incidence.

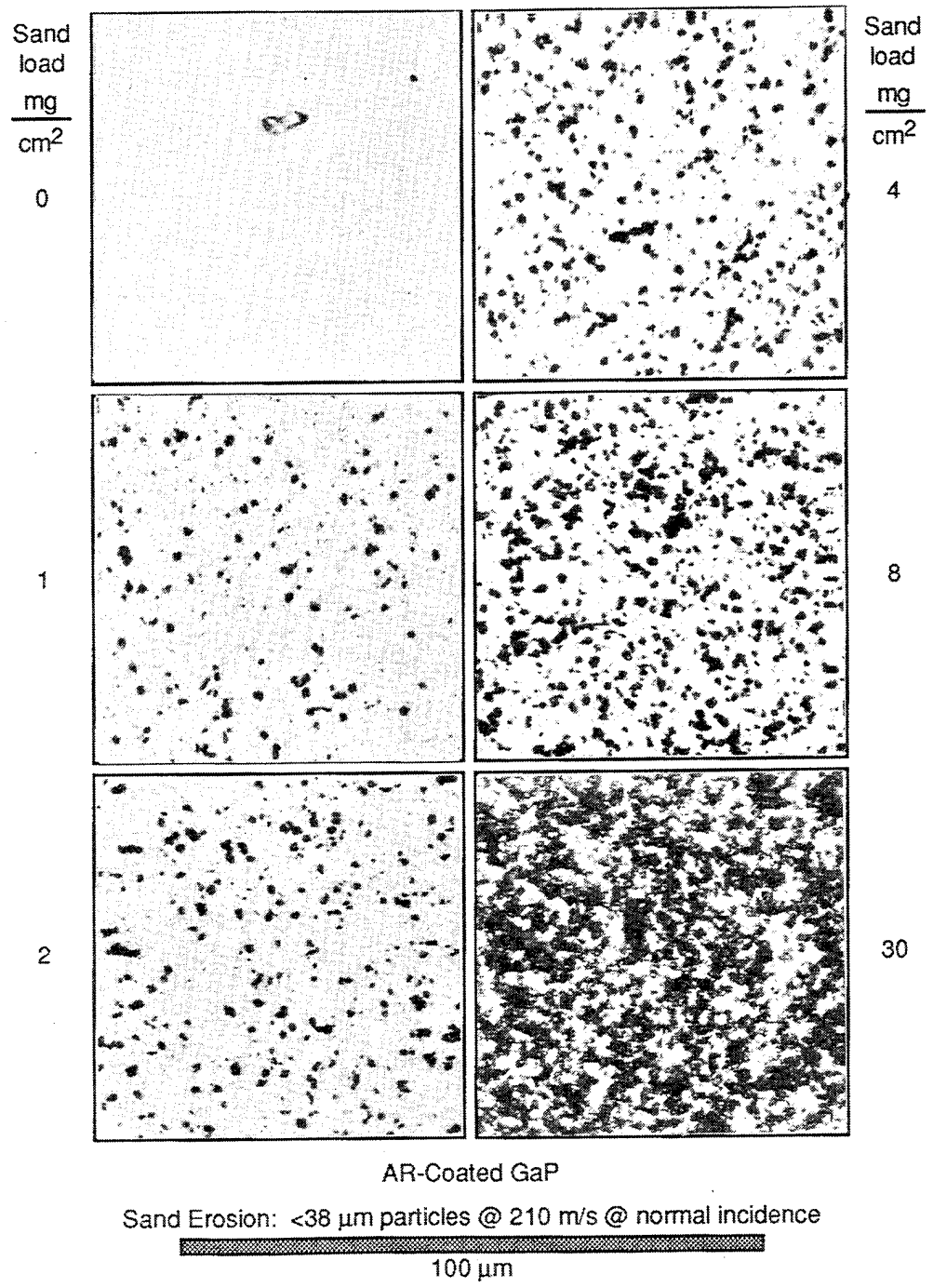

FIGURE 48. Micrographs of AR-Coated Bulk GaP (Sample I15-E) at Different Stages of Exposure to < 38 µm Sand Particles at 210 m/s at Normal Incidence. The other side of the same disk used in Figure 42 was used for this erosion experiment. This sample had been heated to 500°C to measure infrared emission prior to the sand erosion test.

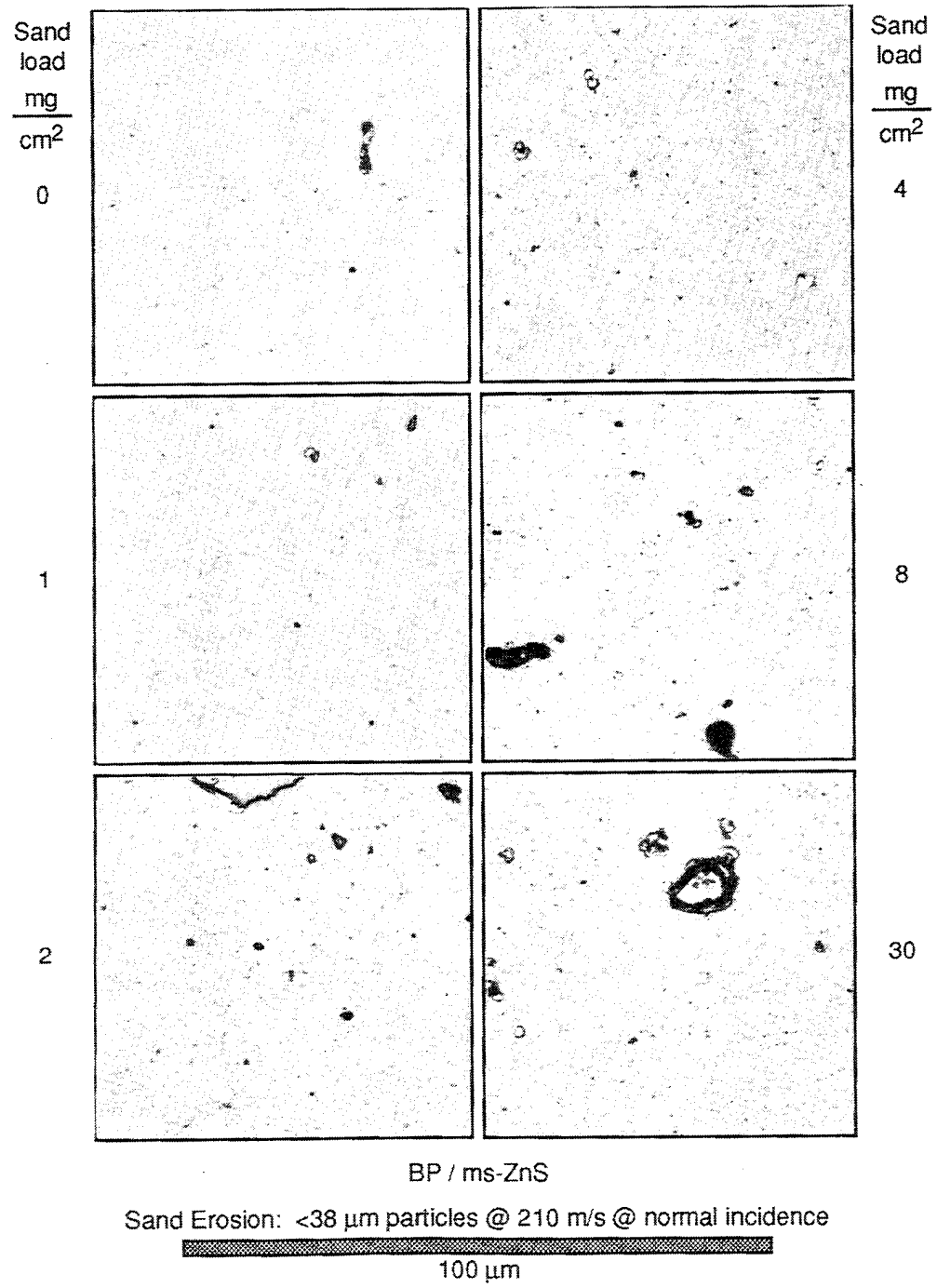

FIGURE 49. Micrographs of BP-Coated ms-ZnS (Sample CL13) at Different Stages of Exposure to < 38 µm Sand Particles at 210 m/s at Normal Incidence.

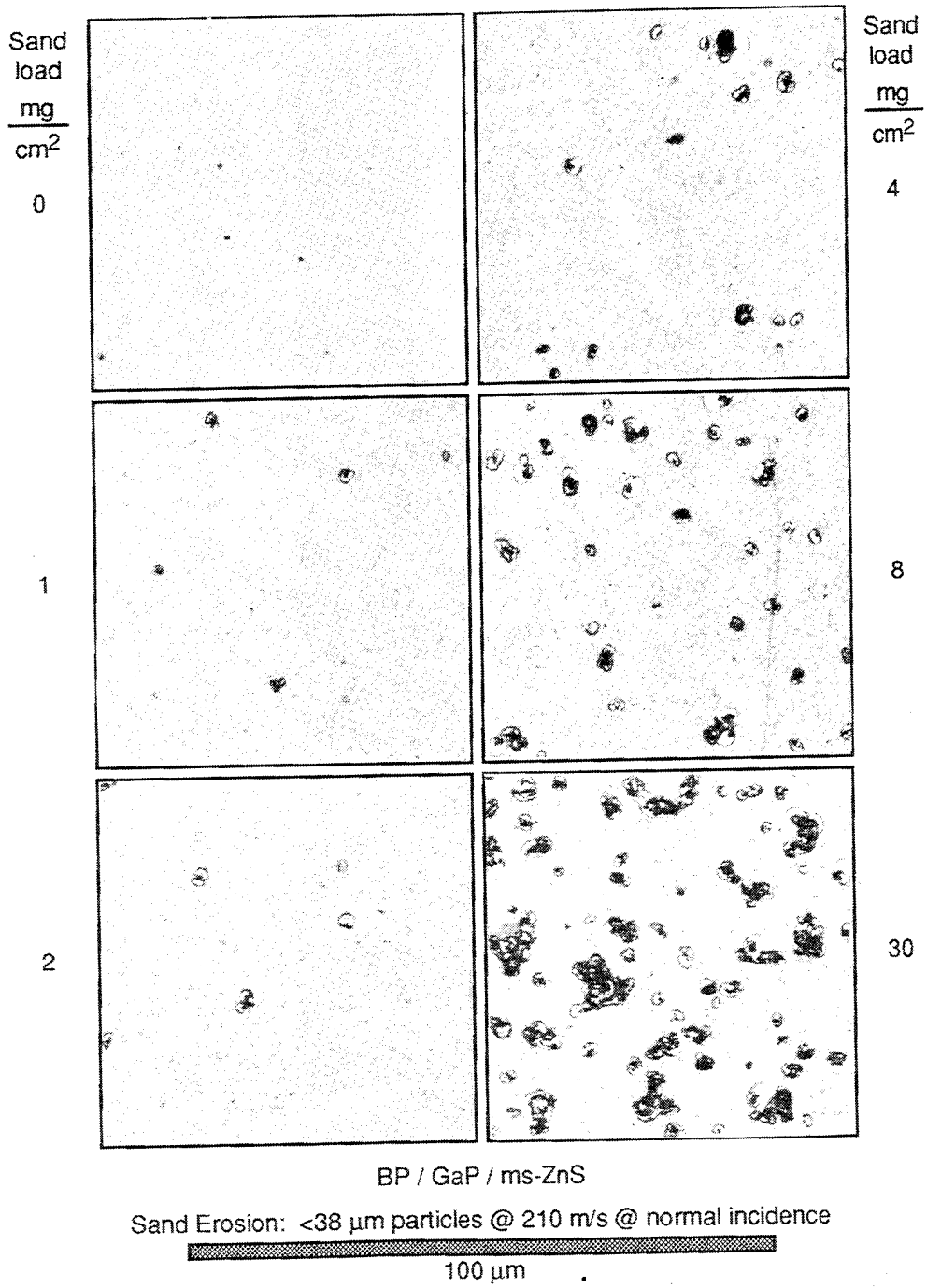

FIGURE 50. Micrographs of BP/GaP/ms-ZnS (Sample 5C0184) at Different Stages of Exposure to < 38 µm Sand Particles at 210 m/s at Normal Incidence.

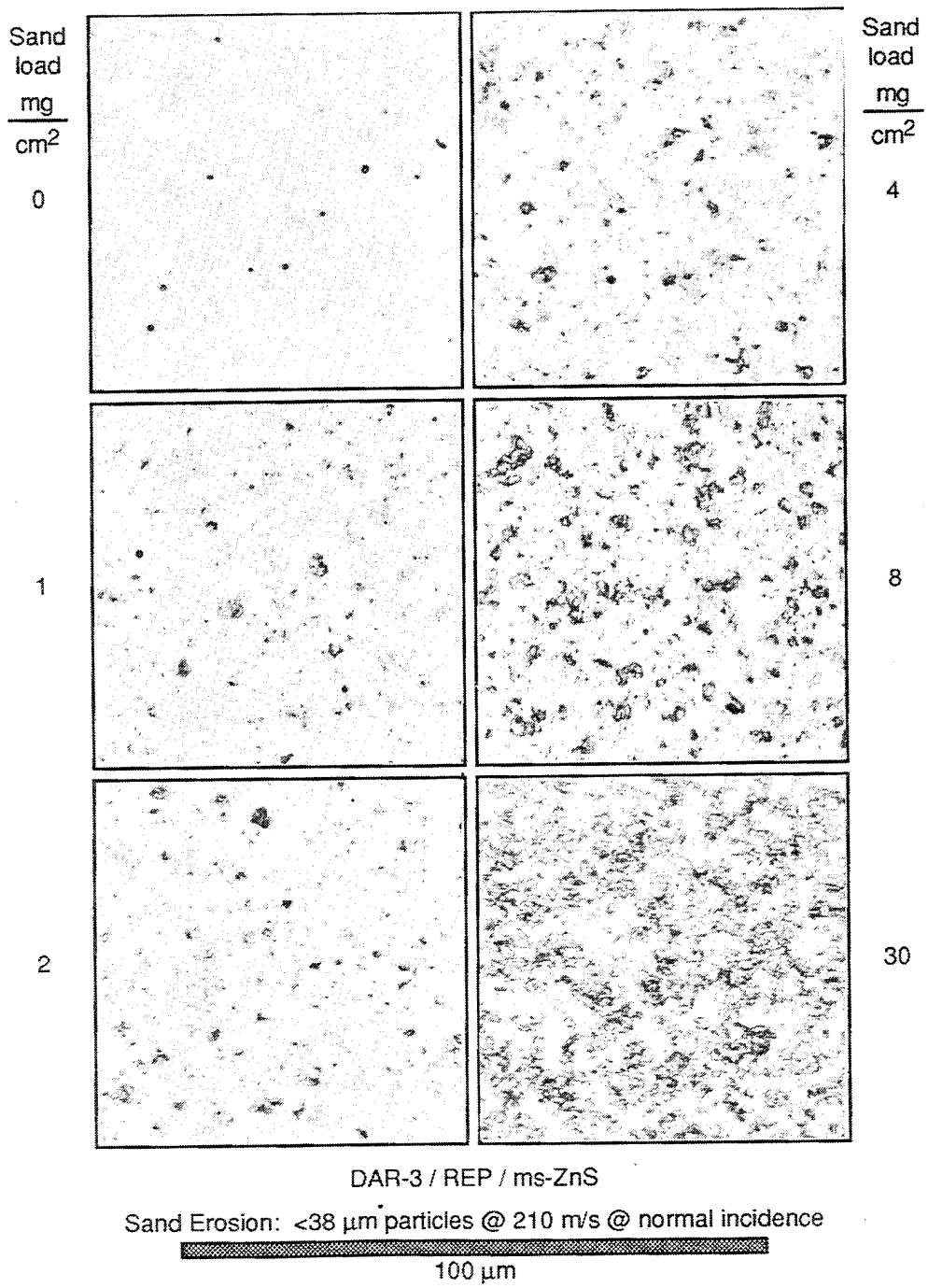

FIGURE 51. Micrographs of ZnS-Coated ms-ZnS (Sample 8) with the Outer Antireflection Coating Designated DAR-3 at Different Stages of Exposure to < 38 µm Sand Particles at 210 m/s at Normal Incidence.

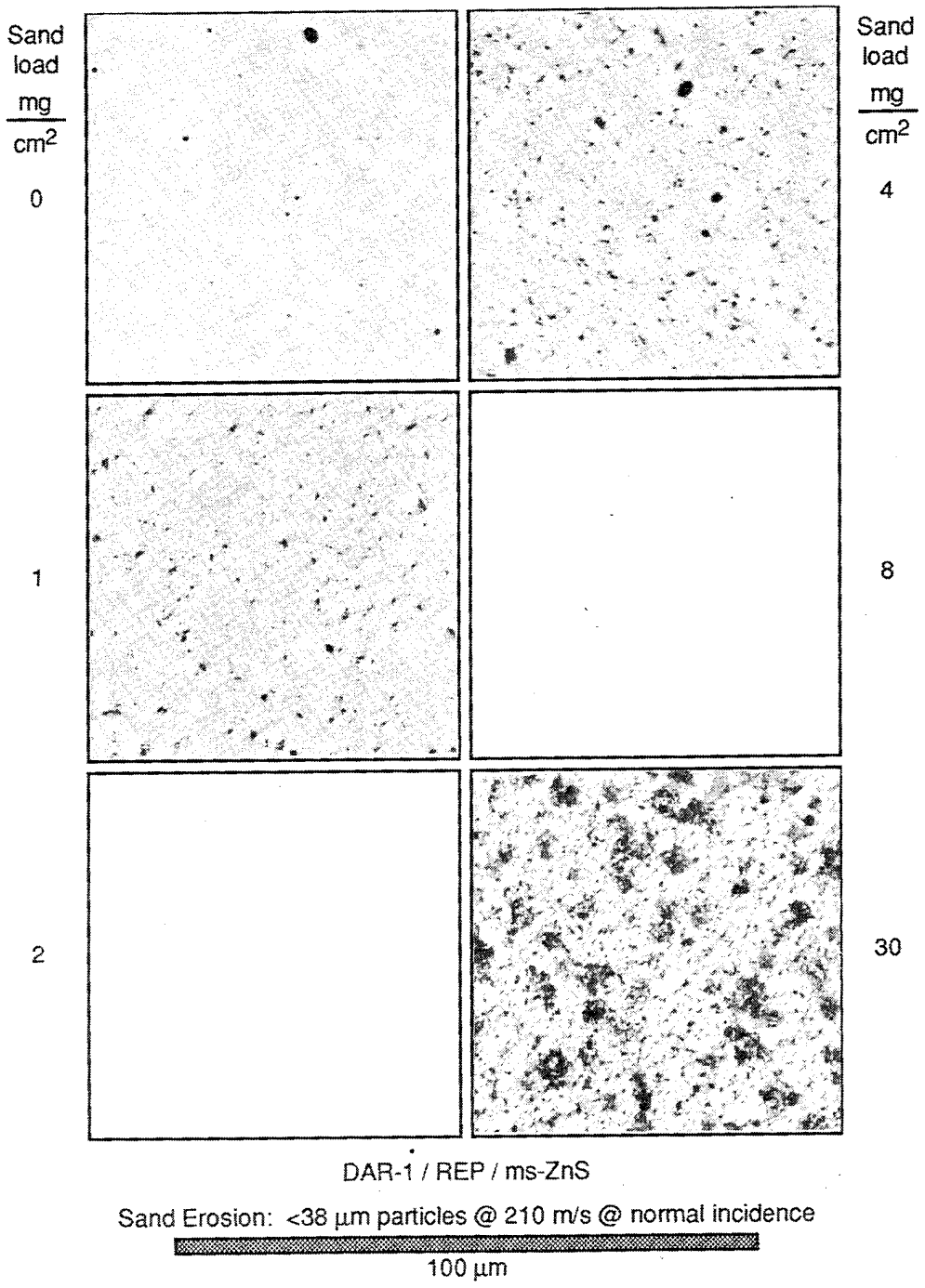

FIGURE 52. Micrographs of ZnS-Coated ms-ZnS (Sample 6) with the Outer Antireflection Coating Designated DAR-1 at Different Stages of Exposure to < 38 µm Sand Particles at 210 m/s at Normal Incidence. This sample had been exposed to 500°C for measuring infrared emission prior to the sand erosion test.

REFERENCES

1. D. R. Gibson, E. M. Waddell, and K. L. Lewis. "Advances in Ultradurable Phosphide-Based Broadband Anti-Reflection Coatings for Sand and Rain Erosion Protection of Infrared Windows and Domes," *Proc. SPIE,* **2286** (1994), p. 335; D. R. Gibson, E. M. Waddell, A. D. Wilson, and K. L. Lewis. "Ultradurable Phosphide-Based Anti-Reflection Coatings for Sand and Rain Erosion Protection," *Opt. Eng.,* 33, 1994, p. 957.

2. P. Klocek, J. T. Hoggins, and M. Wilson. "Broadband IR Transparent Rain Erosion Protection Coating for IR Windows," *Proc. SPIE,* **1760** (1992), p. 211.

3. Naval Air Warfare Center Aircraft Division. *Waterdrop Impact Measurements on GaP Coated Ge Using the Whirling Arm and Cambridge Liquid Jet,* by M. Wilson, M. Thomas, I. Perez, C. Monro, D. Price, and S. Herman. Warminster, Pa., NAWCADWAR, November 1992. 64 pp. (NAWCADWAR-93019-50, publication UNCLASSIFIED.)

4. L. M. Goldman and R. W. Tustison. "High Durability Infrared Transparent Coatings," *Proc. SPIE,* **2286** (1994), p. 316.

5. E. M. Waddell, D. R. Gibson, and J. Meredith. "Sand Impact Testing of Durable Coatings on FLIR ZnS Relevant to the LANTIRN E-O System," *Proc. SPIE,* **2286** (1994), p. 364; E. M. Waddell, D. R. Gibson, and M. Wilson. "Broadband IR Transparent Rain and Sand Erosion Protective Coating for the F-14 Aircraft Infra-Red Search and Track Germanium Dome," *Proc. SPIE,* **2286** (1994), p. 376; Naval Air Warfare Center Aircraft Division. *An Evaluation of Boron Phosphide As a Rain Erosion Protective Coating,* by, M. Wilson, C. Monro, M. Thomas, D. Price, and S. Herman. Warminster, Pa., NAWCADWAR, March 1994. 66 pp. (NAWCADWAR-94068-50, publication UNCLASSIFIED.)

6. Naval Air Warfare Center Aircraft Division. *An Evaluation of Gallium Phosphide As a Rain Erosion Protective, IR Transparent Coating,* by M. Wilson, M. Thomas, I. Perez, D. Price, and S. Herman. Warminster, Pa., NAWCADWAR, June 1994. 56 pp. (NAWCADWAR-94129-50, publication UNCLASSIFIED.)

7. P. C. Archibald and H. E. Bennett. "Scattering from Infrared Missile Domes," *Opt. Eng.,* Vol. 17, 1978, p. 647.

8. P. Klocek, L. E. Stone, M. W. Boucher, and C. DeMilo. "Semiconductor Infrared Optical Materials," *Proc. SPIE,* **929** (1988), p. 65.

9. Naval Air Warfare Center Weapons Division. *Comparative Sand and Rain Erosion Studies of Spinel, Aluminum Oxynitride (ALON), Magnesium Fluoride, and Germanate Glass,* by D. C. Harris. China Lake, Calif., NAWCWPNS, August 1993. 23 pp. (NAWCWPNS TP 8147, publication UNCLASSIFIED.)

INITIAL DISTRIBUTION

1 Naval Air Systems Command, Arlington (AIR-40T3/JP-2, P. Facas)
4 Office of Chief of Naval Research, Arlington
    Code 332
        L. Kabacoff (1)
        B. Pohanka (1)
        L. Sloter (1)
    Code 351, D. Siegel (1)
1 Naval Air Warffare Center Aircraft Division, Warminster (Code 45562, M. Wilson)
1 Naval Surface Warfare Center, Dahlgren Division, Dahlgren (Code R36, C. Blackmon)
2 Naval Surface Warfare Center, Dahlgren Division, White Oak Detachment, Silver Springs
    Code K205, B. Messick (1)
    Code R31, I. Talmy (1)
3 Army Missile Command, Redstone Arsenal
    AMSMI-RD-AS-OG, G. Hutcheson (1)
    AMSMI-RD-MG-IR, R. Passmore (1)
    AMSMI-RD-SE-MT, B. Park (1)
4 Army Strategic Defense Command, Huntsville
    CSSD-KE-E, T. Street (1)
    CSSD-WD-N
        D. Ennis (1)
        G. Jomnes (1)
    SFAE-MD-ARW, PEO (Missile Defense), D. Perry (1)
1 Aberdeen Proving Ground (AMSRL-MA-CA, T. Hynes)
1 Center for Night Vision and Electronic Sensors Directorate, Fort Belvoir (AMSEL-NV-RD-IRT, L. Mizerka)
1 Arnold Engineering Development Center, Arnold Air Force Base (AEDC/IN, M. Amundson)
1 Wright Laboratory, Armament Directorate, Eglin Air Force Base (WL/MNG, E. Boudreaux)
4 Wright Laboratory, Dynamics Directorate, Wright-Patterson Air Force Base
    WL/FIVE, R. Smith (1)
    WL/MLPO
        R. Denison (1)
        R. Ondercin (1)
        R. Susnik (1)
2 Defense Technical Information Center, Alexandria
1 Battelle Pacific Northwest Laboratory, Richland, WA (P. Martin)
1 Crystal Systems, Salem, MA (F. Schmid)
1 Exotic Materials, Murietta, CA (R. Twedt)
1 GRC International, Santa Barbara, CA (B. Adler)
1 Hughes Danbury Optical Systems, Danbury, CT (J. Askinazi)
5 Hughes Missile Systems, Tucson, AZ
    J. Gottlieb (1)
    A. Heller (1)
    T. Jankiewicz (1)
    M. Kevershan (1)
    J. Tingstad (1)
1 Hughes Santa Barbara Research Center, Goleta, CA (R. Hudyma)

2 Johns Hopkins University, Applied Physics Lab, Laurel, MD
K. Frazer (1)
M. Thomas (1)
2 Lockheed Martin Electronics & Missiles, Orlando, FL
A. Fry (1)
J. Meredith (1)
1 Lockheed Missiles & Space Company, Huntsville, AL (C. Wojciechoski)
2 Loral Vought Systems, Dallas, TX
B. Burzlaff (1)
R. C. Knight (1)
1 Materials Systems, Incorporated, Concord, MA (R. Gentilman)
1 Morton/CVD, Woburn, MA (J. Goela)
1 Northrop B-2 Division, Pico Rivera, CA (D. Luippold)
1 Norton Diamond Films, Northboro, MA (K. Gray)
1 Raytheon Electronic Systems, Tewksbury, MA (T. Bailey)
5 Raytheon Electronic Systems, Lexington, MA
S. Bernstein (1)
L. Goldman (1)
T. Hartnett (1)
R. Tustison (1)
C. Willingham (1)
1 Rocketdyne, Canoga Park, CA (S. Holly)
1 Rockwell Science Center, Thousand Oaks, CA (A. Harker)
1 Rockwell Tactical Systems Division, Duluth, GA (E. L. Fleeman)
2 Texas Instruments, Dallas, TX
P. Klocek (1)
W. Weimer (1)
1 University of Dayton Research Institute, Dayton, OH (J. Detrio)
1 Westinghouse Electrooptical Systems, Orlando, FL (B. Cashion)
1 C. Wyman, Huntsville, AL
2 Barr & Stroud, Pilkington Optronics, Scotland
A. Sijan (1)
D. Gibson (1)
1 Defence Research Agency, United Kingdom (J. A. Savage)